12-2021

Impact of PANK1 deletion on mitochondrial acetylation and cardiac function during pressure overload.

Timothy N. Audam
University of Louisville

IMPACT OF PANK1 DELETION ON MITOCHONDRIAL ACETYLATION AND CARDIAC FUNCTION DURING PRESSURE OVERLOAD

By

Timothy N. Audam

B.Sc., University of Abuja, 2012
M.S., East Tennessee State University, 2016
M.S., University of Louisville, 2018

A Dissertation Submitted to the Faculty of the School of Medicine of the University of Louisville in Partial Fulfillment of the Requirements for the Degree of

Doctor of Philosophy in Biochemistry and Molecular Genetics

Department of Biochemistry and Molecular Genetics
University of Louisville
Louisville, Kentucky

December 2021

IMPACT OF PANK1 DELETION ON MITOCHONDRIAL ACETYLATION AND CARDIAC FUNCTION DURING PRESSURE OVERLOAD

By

Timothy N. Audam

B.Sc., University of Abuja, 2012
M.S., East Tennessee State University, 2016
M.S., University of Louisville, 2018

A Dissertation Approved on

August 6th, 2021

By the Following Dissertation Committee

_____
Dissertation Advisor: Steven P. Jones, Ph.D.

_____
Barbara Clark, Ph.D.

_____
Bradford Hill, Ph.D.

_____
Brian Clem, Ph.D.

DEDICATION

I dedicate this work to my awesome parents, Mr. and Mrs. Audam, for their unending

love and support.

ACKNOWLEDGEMENTS

Thanks to the Diabetes and Obesity Center (DOC) Academy. The unique structure of this career training workshop provided me with an opportunity to learn more about various career options and how to position myself for success as a scientist. Thanks to the organizers of this workshop and thanks to the faculty and staff of the DOC for their various support throughout my doctoral training.

ABSTRACT

IMPACT OF PANK1 DELETION ON MITOCHONDRIAL ACETYLATION AND CARDIAC FUNCTION DURING PRESSURE OVERLOAD

Timothy N. Audam

August 6th, 2021

Recent studies have associated elevated protein acetylation levels with heart failure in humans. Although mechanisms promoting elevated acetylation levels are not fully known, excess acetyl-CoA may drive enzyme-independent acetylation of cardiac proteins. Accumulation of acetyl-CoA depends on the availability of sufficient CoA, whose production is regulated by pantothenate kinases in the CoA biosynthetic pathway. We show that cardiac proteins are hyperacetylated during heart failure in humans and tested in mice whether limiting CoA abundance would improve ventricular remodeling during pressure overload-induced hypertrophy. We limited cardiac CoA levels by deleting the rate-limiting enzyme in CoA biosynthesis, *Pank1* (one of three PANK-encoding genes in mice). We reasoned that this strategy would at least partially limit the driving force (excess acetyl-CoA) for acetylation in the failing heart. We found that constitutive, cardiomyocyte-specific *Pank1* deletion (cm*Pank1$^{-/-}$*) significantly reduced PANK1 mRNA, PANK1 protein, and CoA levels compared to *Pank1* sufficient littermates (cm*Pank1$^{+/+}$*) but exerted no obvious deleterious impact on the mice. We then subjected both groups of mice to

pressure overload-induced heart failure. Interestingly, despite limiting acetyl-CoA and acetylation levels in cm$Pank1^{-/-}$ mice, there was more ventricular dilation in cm$Pank1^{-/-}$ during pressure overload. To explore potential mechanisms contributing to this unanticipated result, we performed transcriptomic profiling, which suggested a role for $Pank1$ in regulating fibrotic and metabolic processes during pressure overload. Indeed, $Pank1$ deletion exacerbated cardiac fibrosis following pressure overload. Because we were interested in the possibility of early metabolic impacts in response to pressure overload, we performed untargeted metabolomics, which indicated significant changes to metabolites involved in fatty acid and ketone metabolism, among other pathways.

Lastly, coincident with increased acetylation observed during heart failure, mitochondrial respirasomes (supercomplexes) composition was changed during heart failure and may contribute to reduced mitochondria efficiency; however, it is not known whether acetylation directly affects mitochondrial respirasomes. We showed that reducing mitochondria acetylation alone does not impact mitochondria respirasomes, mitochondria function, or mitochondria dynamics. Furthermore, we did not observe any significant impact in mitochondrial supercomplexes when mitochondria hyperacetylation was induced.

Briefly, our study underscores the role of elevated CoA levels (via $Pank1$) in supporting fatty acid and ketone body oxidation, which may be more important than CoA-driven, enzyme-independent acetylation in the failing heart. We also showed that changing mitochondrial acetylation alone does not impact mitochondria supercomplexes.

TABLE OF CONTENTS

LIST OF TABLES

LIST OF FIGURES

CHAPTER I

BACKGROUND AND LITERATURE REVIEW

According to the Center for Disease Control and Prevention (CDC), cardiovascular diseases (CVD) remain the leading cause of death across most demographics in the United States. In the United States, one person dies every 36 seconds from cardiovascular disease (CVD) related deaths, resulting in about 655,000 deaths each year[1], with racial and ethnic groups disproportionately affected2. CVD is broadly defined as diseases affecting the heart and blood vessels, including, but not limited to, coronary artery disease, stroke, arrhythmia, heart attack, and heart valve problems. Of all the various types of CVD, coronary artery disease (CAD)[3] and heart attack significantly contribute to the overall mortality associated with CVD[4].

Despite sustained efforts to develop new treatments for heart failure, the prognosis remains poor[5]. Over the past three decades, various treatment options, including the use of angiotensin-converting-enzyme (ACE) inhibitors, beta-receptor blockers, aldosterone antagonists, and stem cell therapies, have been utilized to manage heart failure6. Unfortunately, despite the availability of these treatment options, no current treatment cures heart failure but rather delays the progression of the disease. There is, therefore, a need to explore other treatment options for heart failure by exploring the pathological feature of the disease. Considering that metabolic alteration is a major contributor of heart

failure6, treatments geared towards restoring altered metabolic pathways to improve heart failure outcomes may significantly improve HF prognosis.

Metabolic Regulation of Heart failure

The heart requires an enormous amount of energy to sustain its contractile function[6]. To do this, the heart relies on a variety of substrates including, fatty acids, glucose, ketones, lactate, acetate, and branched-chain amino acids (BCAA), to generate ATP through oxidative phosphorylation[7]. In the normal heart, most of the ATP is generated through the oxidation of fatty acids[8]. However, during pathological remodeling, including heart failure (pressure overload and myocardial infarction), the heart undergoes metabolic reprogramming, characterized by increased reliance on glucose as its primary source for ATP generation[9-13]. Although glucose uptake is increased during hypertrophy, capacity of the mitochondria to utilize substrates is also impaired. Hence, both impaired mitochondrial function and alterations in multiple metabolic pathways contribute to the accumulation of various metabolites in the heart[14-17], including C2-carnitine and acetyl-CoA, among others[18, 19]. In addition to reduced capacity to oxidize fatty acids during heart failure, the capacity of the heart to utilize ketones is increased[20]. Increased utilization of ketones can promote accumulation of C2-carnitines[20]. It is speculated that chronic utilization of ketones during heart failure leads to accumulation of acetyl-CoA and C2-carnitines more than the mitochondria can oxidize[20]. Aberrant accumulation of metabolites can promote shunting of these metabolites into other biological processes, including post-translational modification of proteins (PTM). Interestingly, PTM of proteins have been implicated in the pathogenesis of heart failure[21-24].

Post-Translational Modification and Heart failure

Post-translational modification (PTM) of cardiac proteins involves the covalent addition of functional groups onto proteins. The addition of functional groups to proteins can alter their overall tertiary structures, which can profoundly impact protein functions. For instance, PTMs of proteins have been shown to be involved in physiological processes, including protein-protein interactions, protein degradation, and gene expression[25].

One possible way by which the mitochondria proteome is regulated is through PTM. Various studies suggest that mitochondrial function is regulated by various PTMs, including phosphorylation[21], succinylation[22], O-GlcNAcylation[23], and acetylation[24]. Furthermore, PTMs of mitochondrial proteins have been implicated in the progression of CVDs. For example, studies show that phosphorylation of mitochondria complex IV decreases oxidative phosphorylation by promoting destabilization of respirasomes (supercomplexes)[26]. Similarly, multiple proteins and enzymes involved in glucose oxidation, fatty acid oxidation, and respiratory complexes are subjected and regulated by acetylation[27, 28]. Of the multiple types of PTM occurring during heart failure, acetylation plays a major role in the pathophysiology of cardiovascular diseases. Alteration in cardiac acetylation has been implicated in the development and progression of cardiovascular diseases[29]. Interestingly, metabolic changes associated with cardiovascular disease progression are linked to altered acetylation during HF. This dissertation provides an overview of acetylation, and we sought to determine whether limiting aberrant mitochondria acetylation is beneficial in the context of heart failure.

Acetylation

Acetylation is a modification that involved the addition of an acetyl group (CH3CO) on molecules, including proteins. Since acetylation was discovered over 40 years ago[30, 31],

the concept of reversible protein acetylation as it relates to histone modification and transcription of genes has been extensively studied[32, 33]. Although earlier studies on acetylation were focused on histone proteins, evidence of non-histone protein acetylation has been reported[34, 35]. Emergence of high throughput techniques have revealed that a vast number of non-histone proteins are subjected to acetylation, including multiple cytosolic and mitochondrial enzymes[36-38]. Acetylation can occur co-translationally or post-translationally. Co-translational modification usually occurs at the first α-amino group of newly synthesized proteins and its termed N-α-acetylation. Furthermore, post-translational modification occurring at the ε-amino group of lysine residues is termed N-ε-acetylation[39]. Also, acetylation can occur in an enzyme dependent or independently manner[40] (Figure 1). A brief review of N-α-acetylation, N-ε-acetylation, O-acetylation, and enzyme independent acetylation is provided below:
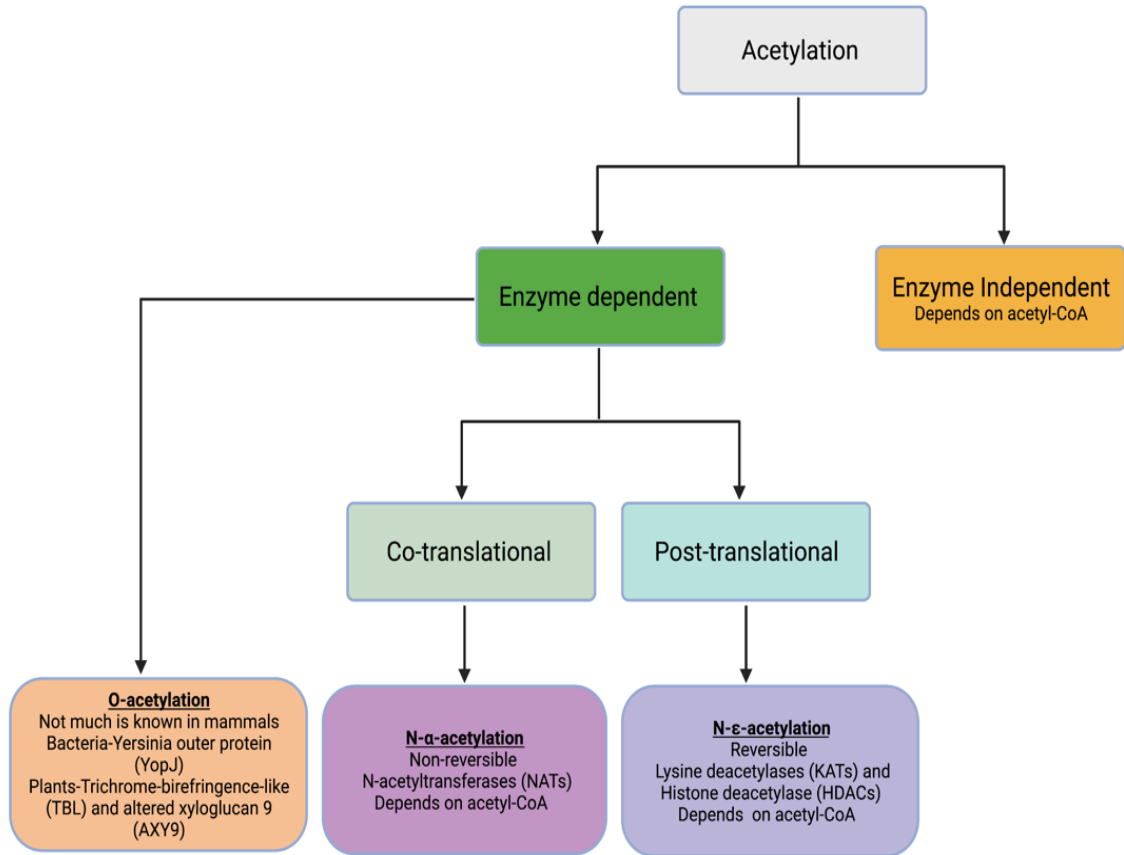
Figure 1: Schematic of the different types of acetylation. Acetylation can occur in an enzyme dependent and independent fashion.

N-α-acetylation

A vast majority of cytoplasmic eukaryotic proteins are subjected to N-α-acetylation. N-α-acetylation is a non-reversible reaction catalyzed by a group of enzyme complexes known as N-terminal acetyltransferases (NATs)[41]. NATs function by transferring an acetyl group from its substrate, acetyl-CoA, to the first amino acid of newly synthesized proteins. The addition of an acetyl group changes the chemical property of the N-terminus by neutralizing its positive charge[41]. In eukaryotes, most of the N-α-acetylation is catalyzed by various NATs, categorized as NatA, NatB, NatC, NatD, and NatE[41]. Although substrate specificity of NATs has been described to be partially conserved in eukaryotes[42-46], various NATs can be differentiated by their subunit compositions[41]. For a detailed review of various NATs, please refer to this review by Starheim et al.[41]. NATs regulate various cellular processes including protein stability[41, 47], protein-protein interaction[41, 48-50], and mediator of protein complex formation[51]. Finally, N-α-acetylation is regulated by the availability of acetyl-CoA[41].

N-ε-acetylation

Unlike N-α-acetylation that is non-reversible, N-ε-acetylation involves a reversible transfer of acetyl group from acetyl-CoA to the ε-amino group of lysine residues. N-ε-acetylation reactions are catalyzed by lysine N-ε-acetyltransferases (KATs), which were previously known as histone acetyltransferases[51]. This reversible reaction is catalyzed by a group of enzymes known as lysine deacetylases (KDACs), which comprises histone deacetylases (HDACS) and sirtuins[52]. Mammalian KATs are generally classified based on their cellular localization. Nuclear KATs are classified as type A, whereas cytoplasmic KATS are classified as type B[53]. KDACs are classified into four major classes, including Class I-III, sirtuins, and class IV HDACs[54]. For a detailed description of various classes of KATs and

KDACs, particularly those involved in the cardiovascular system, please refer to the review by Li et al[53]. Collectively, protein acetylation and deacetylation by KATs and KDACs are crucial for regulating histones to influence gene transcription55.

O-acetylation

O-acetylation is another form of protein acetylation recently identified[56, 57]. In O-acetylation, acetyl groups are transferred from acetyl-CoA to modify serine and threonine residues of proteins[57]. Additionally, the extracellular matrix polysaccharides of plants, algae, bacteria, and fungi are O-acetylated[58]. In bacteria (Yersinia pestis), Yersinia outer protein (YopJ) catalyzes O-acetylation of serine and threonine residues of signaling proteins including, MAPK/ERK kinase and IkappaB Kinase[59]. In plants, O-acetylation of various polysaccharides is catalyzed by three families of proteins including the Trichrome-birefringence-like (TBL), Altered xyloglucan 9 (AXY9), and Reduced wall O-acetylation (RWA) family of proteins[58]. In humans, O-acetylation of sialic acid residue on gangliosides by CAS1 domain-containing protein 1 (CASD1) has been reported[60]. Collectively, protein modification by O-acetylation is thought to act in interplay with other forms of post-translational modification such as phosphorylation to dynamically regulate protein function in different organisms[61]; however, whether and to what extent mammalian cardiac proteins are subjected to O-acetylation remains unknown.

Non-enzymatic acetylation

Unlike the other types of acetylation, non-enzymatic acetylation is not dependent on enzymes. Mitochondrial proteins are particularly susceptible to non-enzymatic acetylation due to their distinctive physiological property compared to other cellular compartments[62]. First, compared to other cellular compartments, the pH of mitochondria is basic and is maintained around 7.9—8.0 due to the extrusion of protons (H+) across the inner

mitochondria membrane to generate proton motive force[63]. Secondly, being the site of ATP generation, mitochondria generate between 0.1—1.5 mM of acetyl-CoA via cellular oxidative phosphorylation[64, 65]. Studies have shown that high concentrations of acetyl-CoA and the basic pH of the mitochondria can drive enzyme independent acetylation of mitochondrial and non-mitochondrial proteins *in vitro*[62, 66, 67]. Additional studies have shown that mitochondria acetylation is primarily through a non-enzymatic mechanism[68]. Thus, levels of acetyl-CoA can dictate mitochondrial acetylation state.

Crucial to sustaining this acetyl-CoA pool in the failing heart is the availability the acyl group carrier, Coenzyme A (CoA)[69]. Synthesis of CoA from pantothenate is catalyzed by pantothenate kinase (PanK), the rate-limiting enzyme in the CoA biosynthetic pathway[70, 71]. CoA is abundant in the liver and heart and interestingly, these tissues have the highest expression of PanK compared to other PanK isoforms—PanK2 and PanK3[72]. Thus, PanK1 is a primary, but not the sole, enzyme regulating CoA biosynthesis in the heart. In summary, because mitochondrial acetylation is mostly enzyme independent and is dependent on the availability of CoA, acetyl-CoA levels can be metabolically regulated by the availability of CoA, creating an avenue to metabolically restrict acetyl-CoA level.

Role of cardiac acetylation

Acetylation in cardiac maturation, differentiation, proliferation, and in cardiac development

During the post-natal stage of cardiac maturation, the ability of the heart to switch from glycolytic metabolism to fatty acid metabolism is crucial to support contractile activity of the heart[73]. Although various factors have been implicated in regulation of cardiac maturation, acetylation of non-histone proteins can regulate cardiac maturation[74]. Fukushima et al.[75] showed that general control of amino acid synthesis 5 like 1 (GCN5L1) enzyme induced acetylation of long-chain acyl-CoA dehydrogenase (LCAD) and β-

8

hydroxyacyl-CoA dehydrogenase (β-HAD) correlates with increased enzymatic activity and fatty acid oxidation in newborns, suggesting a role of acetylation in fatty acid oxidation maturation[75]. Interestingly, inhibition of hyperacetylation during cardiac maturation results in delayed fatty acid oxidation and cardiac dysfunction[76]. Collectively, these studies highlight the important role of acetylation during cardiac metabolic maturation.

Similarly, recent studies have highlighted the role of acetylation in the differentiation of progenitor cells into cardiac cells. For instance, inhibition of histone deacetylase (HDAC) by trichostatin A (TSA) treatment was sufficient to induce an increase in GATA-4 acetylation which promoted the expression of endogenous cardiac beta-myosin heavy chain during embryonic stem (ES) cell differentiation[77]. Similarly, histone acetylation has been shown to regulate islet-1 induced cardiac-specific differentiation of mesenchymal stem cells (MSCs)[78]. In addition to its role in cardiac differentiation, acetylation was shown to be important in cardiomyocyte proliferation. Sirtuin 1 (SIRT1) promotes the deacetylation of p21 resulting in increased cardiomyocyte proliferation[79, 80]. Lastly, the importance of acetylation in cardiac development was demonstrated by the embryonic lethality and cardiac abnormality associated with SIRT1 deficiency in mice[81]. Collectively, these studies emphasized the important role of cardiac acetylation during cardiac maturation, differentiation, proliferation, and cardiac development.

<u>Acetylation in contractile function</u>

Acetylation has also been implicated in cardiac contraction through modulating the activity of sarcomeric proteins. Reversible protein acetylation of cardiomyocyte sarcomeres regulates its myofilament contractile activity[82]. Gupta et al. showed that a complex of histone acetyltransferase, PCAF; and histone deacetylase, HDAC4 associates with the Z-disc and I- and A- band of cardiac sarcomeres and coordinate reversible acetylation of Z-

disc-associated protein, MLP. Furthermore, studies demonstrated that increased acetylation of myosin heavy chain isoform led to its increased enzymatic activity, thereby enhancing its contractile dynamics[83]. Recently, a study demonstrated that acetylation of cardiac troponin I (cTnI) can modulate its myofilament relaxation and sensitivity to calcium[84]. Collectively, these various studies underscore the role of cardiac acetylation on contractile proteins and its effect in regulating cardiac contraction.

Acetylation on mitochondrial function

Acetylation on fatty acid oxidation

Emerging studies utilizing advanced mass spectrometry techniques are revealing the extent to which mitochondrial proteins are acetylated. Many mitochondrial enzymes (about 60%) involved in energy metabolism, including oxidative phosphorylation, electron transport chain, and the TCA cycle, are acetylated[85, 86]. Although mitochondria acetylation is mostly enzyme independent and is dependent on the availability of CoA, mitochondrial acetylation can be regulated to a lesser extent, by some acyl transferases such as GNAT family of acetyltransferases including general control of amino acid synthesis 5 like-1 (GCN5L1)[87, 88] and acetyl-CoA acetyltransferase (ACAT1)[89]. Mitochondria acetylation has been shown to regulate various aspects of fatty acid oxidation. For example, in cardiac myocytes, acetylation was shown to activate the mitochondria fatty acid oxidation enzyme, enoyl-CoA hydratase/3-hydroxyacyl-CoA dehydrogenase[90]. Similarly, acetylation of mitochondrial fatty acid oxidation enzyme, long-chain acyl-CoA dehydrogenase (LCAD), and β-hydroxyacyl-CoA dehydrogenase (β-HAD) is associated with increased enzyme activity and fatty acid oxidation in conditions of excess nutrient[90, 91]. Collectively, acetylation plays important role in regulating fatty acid oxidation.

Acetylation on mitochondria biogenesis, autophagy, and mitophagy

Acetylation of mitochondria proteins has also been implicated in mitochondria biogenesis regulation. Mitochondria biogenesis is the process by which cells increase their mitochondria number through the division of already existing mitochondria. Mitochondria biogenesis is regulated by nuclear-encoded peroxisome proliferator-activated receptor-gamma coactivator 1- alpha (PGC1A)[92]. In the heart and skeletal muscles, PGC1A is highly expressed and transcribes genes encoding mitochondria proteins involved in a variety of processes including oxidative phosphorylation, citric acid cycle (CAC), and fatty acid oxidation[92]. Studies have shown that acetylation regulates PGC1A. SIRT1, a protein deacetylase, can activate PGC1A to regulate exercise-induced mitochondria biogenesis[93, 94]. Collectively, this study suggests the role of acetylation in regulating mitochondria biogenesis. Similarly, studies have shown that acetylation of mitochondria protein regulates autophagy and mitophagy. Studies have shown that in neonatal mouse cardiomyocytes, SIRT3 can regulate mitophagy and autophagy through diacylation of FOXO3a and PARKIN[95]. In summary, acetylation can regulate mitochondria dynamics through the regulation of mitochondria biogenesis and mitophagy.

Acetylation on mitochondria respirasomes (supercomplexes)

Mitochondria are responsible for providing energy for cardiac contraction[96, 97]. A decline in mitochondrial function is a major contributor to the pathogenesis of HF. Mitochondrial electron transport is organized into supercomplexes[98] and supercomplex assembly impacts bioenergetics[99]. Studies have shown that mitochondrial supercomplexes composition is changed during heart failure99, but the mechanism of how this occurs is unknown. Many mitochondrial enzymes in the electron transport chain are acetylated. For instance, studies have shown that complex II hyperacetylation was shown to reduce complex II activity[100]. Similarly, in the failing heart, acetylation of SDHA correlated with

decreased complex II activity and complex II-mediated respiration[101]. In addition, during heart failure, several subunits of Complex III and Complex IV were found to be acetylated in murine model of heart failure. Although studies have shown that phosphorylation of specific subunits of complex IV causes destabilization of supercomplexes[26], the extent to which acetylation promotes destabilization of the supercomplexes has not been elucidated. One of the aims of this dissertation is to address the extent to which changing acetylation levels impact supercomplexes.

Acetylation in cardiovascular disease

Acetylation in cardiac hypertrophy

One way by which the heart adapts to increased workload as a result of a physiological or pathological signal is hypertrophy[102]. Although several studies have investigated the numerous ways by which physiological and pathological cardiac hypertrophy is regulated, there is evidence suggesting that acetylation plays an important role in regulating pathological cardiac hypertrophy. Signatures of pathological hypertrophy include disassembly of sarcomeric structure, increased protein synthesis, increased cardiomyocyte size, reactivation of cardiomyocyte fetal gene expression[103]. Since one of the pathological features of cardiac hypertrophy is fetal gene reprogramming, histone acetyltransferases and deacetylases play an important role in this process. For instance, a histone acetyltransferase (HAT), p300, has been shown to regulate hypertrophy through interacting with transcriptional factors GATA4 and MEF2[104, 105]. Acetylation of GATA4 and MEF2 by P300 can enhance the binding of these transcriptional factors on the DNA to promote the expression of pathological genes associated with cardiac hypertrophy[104, 106]. Also, histone deacetylases were implicated in regulating cardiac hypertrophy. Studies have shown that SIRT3 deletion exacerbates cardiac hypertrophy in response to increased workload[107], suggesting that SIRT3 plays an important role in regulating cardiac

hypertrophy. Similarly, studies showed that SIRT2 expression is downregulated in hypertrophic heart, and SIRT2 knockout promotes cardiac hypertrophy while expression of SIRT2 protects against cardiac hypertrophy[108]. Contrary to the role of SIRT2 and SIRT3 in regulating cardiac hypertrophy, SIRT4 deficiency suppresses prevents hypertrophic growth[109]. Collectively, these data emphasize the differential role of acetyltransferases and deacetylases in regulating cardiac hypertrophy and open questions about specific protein targets of each deacetylase.

Acetylation in cardiac fibrosis

In the injured heart, cardiac fibroblasts become activated into myofibroblasts and are responsible for cardiac fibrosis[110]. Myofibroblasts are characteristically highly proliferative and are involved in synthesizing extracellular matrix (ECM) components. Studies have suggested the role of acetylation in the development of cardiac fibrosis. Cardiac fibroblast isolated from murine fibroblast model of congestive heart failure was shown to have increased expression of HDAC1[111]. Interestingly, the administration of an HDAC inhibitor was sufficient to prevent fibroblast proliferation, activation, and induce apoptosis[112]. Similarly, *HDAC4* knockdown in human cardiac fibroblast was sufficient to inhibit differentiation of naïve fibroblast into myofibroblast[113]. Furthermore, SIRT2 and SIRT3 deletion in mice exacerbated cardiac fibrosis in response to angiotensin II treatment[114, 115]. These studies suggest a role of acetylation in regulating cardiac fibrosis. Further research is warranted to fully understand the mechanisms of how acetylation regulates fibroblast function in the context of heart failure.

Acetylation in ischemia/reperfusion (I/R) injury

Ischemia/reperfusion injury significantly contributes to mortality following myocardial infarction (MI)[116]. Although the pathophysiology of I/R injury is complex and involves

multiple cellular processes, including apoptosis, autophagy, inflammation, and mitochondrial dysfunction [117], studies have implicated the role of acetylation in contributing to I/R injury. Manning *et al.* showed that deletion of GCN5L1, an acyltransferase involved in mitochondrial acetylation, resulted in exacerbated myocardial post-ischemic functions [118], suggesting a protective role of acetylation induced by GCN5L1 in I/R injury. In support of the idea that increasing acetylation is beneficial in the context of I/R injury, Zhao *et al.* reported that suppressing HDACs by trichostatin (TSA) treatment was sufficient to confer cardioprotection partly by reducing myocardial infarct size[119]. Additionally, deletion of SIRT3 exacerbated cardiac response to I/R by affecting mitochondrial function[100, 120]. In summary, regulation of cardiac acetylation plays a significant role in outcomes following I/R injury.

Acetylation in hypertension

Hypertension is a great risk factor for the development of CVD[100]. Studies have shown that acetylation can mediate both mitochondrial and histones to regulate the development of hypertension. For instance, in a model of deoxycorticosterone acetate (DOCA)-salt hypertensive rats, HDAC inhibition increased acetylation of mineralocorticoid receptor and reduced its binding affinity to responsive elements of its hormones, resulting to blunted recruitment of RNA polymerase and significant repression of genes modulating intracellular salt balance[121, 122], suggesting a role of acetylation in regulating hypertension. Similarly, deletion of SIRT3, a mitochondrial-specific deacetylase, promoted the development of hypertension and resulted in increased production of mitochondrial superoxide radicals[123]. Collectively, these studies underscore the role of acetylation in the development of hypertension.

Targeting acetylation as a treatment for HF

Because acetylation can impact the development and progression of CVD, several treatment options have been developed to manage the progression of cardiovascular diseases through targeting acetylation. First, several histone deacylated (HDAC) inhibitors are in the clinical phase to manage cardiovascular diseases[53]. Different classes of histone deacetylases such as hydroxamic acids (trichostatin A, tubastatin A, and vorinostat), benzamines (mocetinostat and entinostat), short-chain fatty acids (valproic acid and sodium butyrate) have been used in animal models of various CVD[53]. Similarly, sirtuin inhibitors have also been used in animal models of CVD, and they include acylamide and β-naphthol. For a full review of acetylation inhibitors used in cardiovascular disease, please refer to a review by Li *et al.*[53]. Lastly, the use of angiotensin-converting-enzyme (ACE) inhibitors, beta-receptor blockers, aldosterone antagonists, and stem cell therapies, have been utilized to manage heart failure[6]. Unfortunately, despite the availability of these treatment options, no current treatment cures heart failure but rather delay the progression of the disease. There is, therefore, a need to explore other treatment options for heart failure by exploring the pathological feature of the disease. Considering that metabolic alteration is a major contributor of heart failure[6], treatments geared towards restoring altered metabolism to improve heart failure outcomes may significantly increase HF prognosis.

Summary and gap in knowledge

Acetylation plays vital role in regulating normal cardiac function and can impact the development and progression of CVD, leading to heart failure related mortality. Although several treatment options targeting acetylation are available to treat heart failure, none of these treatments have made tremendous impact on heart failure prognosis. Although Some of these available therapy targets multiple cellular and molecular cardiac processes,

multiple lines of evidence suggest that metabolic derangement coupled with mitochondrial dysfunction are major contributors of heart failure[6, 14-17]. <u>Considering that metabolic alteration is a major contributor of heart failure, treatments geared towards restoring altered metabolic pathways to improve heart failure outcomes seems like a viable treatment option for heart failure that is currently underexplored</u>. Hence, strategies targeting aberrant metabolic processes in the context of heart failure may significantly improve overall cardiac function and survival.

Additionally, dysregulated metabolism can promote post translational modification of mitochondrial proteins by acetylation. Recent studies have shown that hyperacetylation of mitochondrial proteins is associated with a decline in mitochondrial function. Furthermore, mitochondrial respirasome (supercomplex) composition is changed during HF and may affect mitochondria efficiency. Despite these general, coincidental associations, it is not known whether acetylation directly regulates mitochondrial supercomplexes and bioenergetics. Considering that the heart requires enormous amount of ATP to carry out its contractile activity, studies aimed at identifying additional mechanisms by which mitochondria supercomplexes are regulated may provide a new therapy for repairing mitochondrial dysfunction during heart failure.

In this project, we utilize a metabolic approach to target metabolically driven acetyl-CoA in the failing heart. Because accumulated acetyl-CoA can drive enzyme independent acetylation of mitochondria protein to promote cardiac and mitochondrial dysfunction, we tested the idea that targeting aberrant metabolite accumulation (acetyl-CoA) may be a novel and viable option treating heart failure.

CHAPTER II

HYPOTHESIS AND SPECIFIC AIMS

Significant metabolic changes occur during heart failure (HF). Such metabolic changes are not simply associated with HF; they also likely contribute to the pathophysiology. Among the various metabolic changes, studies have shown that acetyl-CoA levels are elevated in the failing heart. Elevated acetyl-CoA levels may drive enzyme-independent hyperacetylation of proteins (particularly mitochondrial). Recent studies have shown that hyperacetylation of mitochondrial proteins is associated with a decline in mitochondrial function. Furthermore, mitochondrial respirasome (supercomplex) composition is changed during HF and may affect mitochondria efficiency. Despite these general, coincidental associations, it is not known whether limiting mitochondria acetylation will be beneficial in HF and whether such an intervention rescues respirasome assembly after HF. Thus, this project will identify the role of reduced mitochondrial acetylation in HF and will elucidate how changes in mitochondrial acetylation impact mitochondrial function and respirasome assembly. We will limit mitochondrial acetylation in HF by using pantothenate kinase 1 deficient mouse ($Pank1^{-/-}$) which, according to our preliminary data have reduced CoA levels and reduced mitochondrial acetylation. Because recent studies have shown that HF increases acetyl-CoA levels, which drives mitochondrial hyperacetylation and may exacerbate ventricular dysfunction, I predict that reduced mitochondrial acetylation will improve function of the failing heart by rescuing mitochondrial function via restoration of mitochondrial respirasome assembly. This hypothesis will be tested by the following Specific Aims:

Specific Aim 1: Determine whether limiting mitochondria acetylation via restricting CoA affects basal bioenergetics: The effect of limiting acetylation on basal mitochondria and cardiac function will be studied using mitochondria isolated from *Pank1*$^{-/-}$ mice. I will assess total cardiac and mitochondria acetylation levels in *Pank1*$^{-/-}$ mice. I will assess the effect of limiting mitochondria acetylation on mitochondria abundance and cardiac function in *Pank1*$^{-/-}$ mice. Similarly, I will assess mitochondria bioenergetics using extracellular flux analysis (XF). Using mass spectrometry, I will identify mitochondrial proteins differentially acetylated as a result of limiting CoA levels.

Specific Aim 2: Determine whether reduced mitochondrial hyperacetylation is beneficial during HF. *Hypothesis: Limiting CoA biosynthesis will reduce mitochondrial acetylation and improve cardiac function in the failing heart.* The role of reduced mitochondrial acetylation in heart failure will be studied using our established model of HF. Endpoints of ventricular function and cardiac remodeling will be assessed in cardiomyocyte-specific *Pank1* deficient mice (cm*Pank1*$^{-/-}$) post-infarct hearts. I expect to observe improved ventricular function in cm*Pank1*$^{-/-}$ mice compared to WT littermates.

Specific Aim 3: Elucidate the impact of mitochondrial acetylation on mitochondrial bioenergetics in the context of HF. *Hypothesis: Mitochondrial hyperacetylation negatively regulates mitochondrial function and respirasome assembly.* I will characterize cardiac and mitochondrial acetylation status after MI. I will also assess changes and composition of mitochondrial supercomplex after MI using BN-PAGE and mass spectrometry, respectively. Also, I will assess the impact of mitochondrial acetylation on cardiomyocyte bioenergetics (using cardiomyocytes isolated from post-MI, cm*Pank1*$^{-/-}$ mouse hearts). Similarly, I will assess the impact of mitochondrial acetylation on

respirasome assembly using mitochondria isolated from *Pank1*$^{-/-}$ hearts following MI. I expect to rescue mitochondrial function with decreasing acetylation.

We will use a metabolism-centered intervention to generate proof-of-concept observations that limiting CoA biosynthesis will limit the driving force for mitochondrial acetylation. This project will enhance our understanding of the impact of mitochondrial acetylation on bioenergetics in the failing heart and will establish whether reducing mitochondria acetylation will improve mitochondrial function during heart failure. This project could identify a novel target for heart failure.

CHAPTER III

MATERIALS AND METHODS

All animals were used in compliance with the Guide for the Care and Use of Laboratory Animals issued by the National Institutes of Health. The experimental protocols in this study have been reviewed and approved by the University of Louisville Institutional Animal Care and Use Committee. Well-characterized, de-identified human myocardial tissue samples were obtained from the Transplantation Biobank of the Heart and Vascular Center at Semmelweis University, Budapest, Hungary[124]. The procedure of sample procurement was reviewed and approved by the institutional and national ethics committee (ethical permission numbers: ETT TUKEB 7891/2012/EKU (119/PI/12.) and ETT TUKEB IV/10161-1/2020/EKU). Informed consent was obtained from patients in line with the Declaration of Helsinki prior to sample collection. In all cases, myocardial samples were surgically removed and immediately snap-frozen in liquid nitrogen under sterile conditions. Non-failing control left ventricular (LV) myocardial samples were isolated from LV papillary muscles removed from patients undergoing mitral valve replacement. Myocardial LV samples from end-stage heart failure patients were collected during heart transplantation.

Generation of constitutive, cardiac specific Pank1-deficient mice (cm*Pank1*$^{-/-}$): To create cm*Pank1*$^{-/-}$ mice, we crossed *Pank1*-floxed mice[125, 126] with constitutive, cardiomyocyte-specific Cre (*Myh6*-Cre) transgenic mice (Stock #011038, The Jackson Laboratory). Whole body *PanK1* deficient mice (*Pank1*$^{-/-}$) were also used[126]. All animals

used in this study were on a C57BL6/J background. Male and female mice were used in this study.

Transverse aortic constriction surgery: 12-16 wk old cm*Pank1*^{-/-} mice and their wild-type littermates (cm*Pank1*^{+/+}) were subjected to transverse aortic constriction (TAC), as previously described[127, 128, 129, 130]. Briefly, mice were anesthetized intraperitoneally with ketamine (50 mg/kg) and pentobarbital (50 mg/kg). Next, anesthetized mice were then orally intubated with a polyethylene-60 tubing and ventilated (Harvard Apparatus Rodent Ventilator, model 845) with oxygen supplementation. Mice were maintained under anesthesia with an isoflurane vaporizer (1%) supplemented with 100% oxygen. The aorta was visualized through an intercostal incision, and a 7-0 nylon suture was looped around the aorta between the brachiocephalic and left common carotid arteries. The suture was tied around a 27-gauge needle to constrict the aorta to a reproducible diameter. Then the needle was removed, leaving a discrete region of stenosis (TAC mice). Following stenosis, the chest was closed, mice were extubated upon recovery of spontaneous breathing and were allowed to recover in warm, clean cages. Analgesia (ketoprofen, 5 mg/kg, subcutaneous) was given before mice recovered from anesthesia (and by 24 and 48 h later). At the appropriate time point (i.e., 2 and 12 wk post TAC), mice were euthanized, and the hearts were snap-frozen in liquid nitrogen for qPCR, RNA-sequencing, and metabolomics analysis. The surgeon was blinded to the genotype of each mouse.

Echocardiography: Transthoracic echocardiography of the left ventricle was performed similarly to previously described methods[14, 131-135] at 2, 4, 8, and 12 wk post TAC, except that here a VisualSonics Vevo 3100 was used in the present study. The sonographer was blinded to the treatment group.

RNA-sequencing: Total RNA was isolated from cardiac tissue as previously described[136-138]. RNA was quantified and assessed using NanoDrop ONE^C (Thermo Scientific) and at least 10 μg of RNA was sent to Novogene Corporation Inc. for RNA-sequencing. For data analysis, FASTQ files were trimmed using fastp[139] (version 0.20.0) using the following parameters:

--cut_by_quality5 --cut_by_quality3 --detect_adapter_for_pe --overrepresentation_analysis --correction --trim_front1 7 --trim_front2 7. Alignment to the mouse genome (GRCm38.90) was performed using STAR[140] (version 020201) with the following parameters: --runMode alignReads --runThreadN 8 --outSAMstrandField intronMotif --outSAMmode Full --outSAMattributes All[141, 142] --outSAMattrRGline {params.readgroup} [143] --outSAMtype BAM SortedByCoordinat --limitBAMsortRAM 45000000000 --quantMode GeneCounts --outReadsUnmapped Fastx -outSAMunmapped Within {params.keepPairs}.

Differential expression analysis was performed using edgeR[144] (version 3.10). The RLE (relative log expression) method was used to normalize the data. Heat maps were generated using multiviewer (MeV) software as previously described[145]. Finally, volcano plots were generated using OriginPro, version 2020. (OriginLab Corporation, MA, USA). Differentially regulated genes at a threshold of 2-fold change and a p-value <0.05 were considered significant for all RNA-seq analyses used for this study.

Determination of CoA levels: To determine cardiac-specific depletion of CoA levels, heart and skeletal muscle from naïve cm*Pank1*$^{+/+}$ and cm*Pank1*$^{-/-}$ mice were freeze-clamped with Wollenberger forceps and snap-frozen in liquid nitrogen. Samples were stored frozen (–80°C) until CoA extraction was performed. Determination of free CoA and CoA thioesters were performed by HPLC as previously described[146]. Briefly, frozen tissue was homogenized and resuspended in cold water (2 ml). Next, 500 μl of 250mM KOH was

22

added to homogenized cardiac tissue. Next, CoA was derivatized with monobromobimane (mBBr) (Life Technologies) and quantified by reverse-phase HPLC by utilizing a Gemini C18 3 µm column (150 X 4.60 mm) (Phenomenex). For the HPLC run, 50 mM potassium phosphate (pH 4.6) was used as solvent A and 100% acetonitrile was used as solvent B. 20 µl of samples was injected on the column and the flow rate was set at 0.5 ml/min. After the HPLC run, the elution position ofmBBr-CoA, mBBr-dephospho-CoA (deP-CoA), and mBBr-phosphopantrtheine (PPanSH) were compared to known standards.

Metabolomics analysis: Metabolomic analysis was performed as previously described[147, 148]. Briefly, after anesthesia, hearts were snap-frozen in liquid nitrogen, pulverized, and sent to Metabolon Inc. for untargeted metabolite analysis by LC-MS. Analyses of metabolites were performed using MetaboAnalyst 4.0 software (http://www.metaboanalyst.ca/). Differentially regulated metabolites at a threshold of 1.5-fold change and a p-value <0.05 were considered significant for all analyses used for this study.

Reverse transcriptase PCR and real-time PCR: Total cardiac RNA was extracted and used to make cDNA as described previously[136-138]. The relative levels of mRNA transcripts were quantified by real-time PCR using Power SYBR Green (Thermo Fisher Scientific) on a real-time PCR system (ViiA 7, Applied Biosystems). Most primers were made using NCBI Primer Blast except HPRT primers (PPM03559E-200, QIAGEN). The data were normalized to mouse HPRT mRNA threshold cycle (C_T) values by using the $\Delta\Delta C_T$ comparative method.

Protein isolation: Total cardiac protein was isolated as previously described[149]. We determined cardiac lysate protein concentration by the Bradford assay with a protein

assay dye (Bio-Rad, catalog #5000006) using different concentrations (0, 1, 2, 4, and 8 mg/ml) of bovine serum albumin as standards. We measured protein concentrations using a Thermo Multiskan Spectrum spectrophotometer.

Immunoblotting: Total cardiac protein samples were loaded on an SDS-PAGE gel and subjected to electrophoresis at 150 V for 1 h. Next, SDS-PAGE resolved proteins were transferred onto PVDF membrane (Immobilon-P, EMD Millipore, Billerica, MA, USA). For acetylation blots, membranes were blocked for 1 h at room temperature using TBS-T (washed with TBS containing Tween-20) containing 5% BSA. Next, membranes were probed with acetylated-lysine mouse mAb (1:1000, Cell signaling #9681) primary antibody and incubated overnight at 4°C. The next day, membranes were washed three times using TBS-T. Membranes were blocked using 5% BSA for 1 h at room temperature followed by incubation with anti-mouse IgG, HRP-linked (1:1000. Cell signaling #7076S) secondary antibody. Finally, membranes were washed three times at 10 min each time with TBS-T. The membrane was saturated with SuperSignal West Pico Chemiluminescent Substrate (Thermo Fisher Scientific) and imaged on a Fuji LAS-3000 bio-imaging analyzer. To confirm the linear range of the signal, multiple exposures from every experiment were performed. Levels of proteins in each lane were normalized to loading protein content (α-tubulin or to Ponceau stain and expressed as relative to control (set as 100%). All other western blots follow standard protocols as described[130]. *Pank1* expression was determined using a PANK1 antibody (1:1000), which was generated as previously described[150].

Mitochondria Isolation: Mitochondria was isolated from heart tissues as previously described[151]. Briefly, heart tissues from WT C57BL6/J, *cmPanK1$^{+/+}$*, *cmPanK1$^{-/-}$*, *PanK1$^{+/+}$*, *PanK1$^{-/-}$*, or human biopsy were homogenized using a Potter Elvehjem tube and a Teflon

pestle containing 1.2 ml of isolation buffer (Buffer A: 220 mM mannitol, 70 mM sucrose, 5 mM MOPS, 1 mM EGTA, 0.2% fatty acid-free BSA, pH 7.2). Homogenates were transferred to a 1 ml tube and centrifuged at 800g for 10 min at 4°C. After centrifugation, supernatants were collected into a clean 1 ml tube and centrifuged at 10,000g for 15 min at 4°C to obtain mitochondrial pellets. Mitochondrial pellets were then washed twice in 1 ml of isolation buffer and then resuspended in 400 μL respiration buffer (120 mM KCl, 25 mM sucrose, 10 mM HEPES, 1 mM MgCl$_2$, 5 mM KH$_2$PO$_4$, pH 7.2). Protein concentration was assessed using the Lowry DC Protein Assay kit (Biorad), and mitochondrial were used for downstream analysis by extracellular flux analysis, blue native PAGE (BN-PAGE) gel, and western blot analysis.

Measurement of mitochondrial bioenergetics: We assessed mitochondrial respiration using XF24 analyzer (Agilent), as previously described[152-154]. Briefly, 5 μg of mitochondrial protein was suspended in 50 μL of respiration buffer and loaded into 24-well XF culture microplates. Next, loaded microplates were then centrifuged at 500g for 3 min at 4 °C, followed by the addition of 625 μL of warm (37 °C) respiration buffer. Pyruvate (5 mM), malate (2.5 mM) and , ADP (1 mM) (PMA); succinate (5 mM), rotenone (1 μM) and, ADP (1 mM) (SRA); or octanoyl-l-carnitine (100 μM), malate (2.5 mM) and, ADP (1 mM) (PMA) were used to stimulated state 3 respiration in the presence of the following inhibitors: oligomycin (1 μM), FCCP (1 μM), and antimycin A+rotenone (AA/Rot; 10 μM/1 μM).

Blue-native PAGE (BN-PAGE): BN-PAGE was performed as previously described[155]. Briefly, isolated mitochondria pellets were solubilized in digitonin buffer containing 1:100 protease inhibitor cocktail (Sigma). Next, solubilized mitochondria were centrifuged at 16,000g for 15 min at 4°C. The supernatant was collected and separated on BN-PAGE gels. BN-PAGE gels were prepared using polyacrylamide (acrylamide:bis-acrylamide,

37.5:1) at either a 5–15% or a 3–12% gradient. The cathode buffers used contained 50 mM Tricine, 15 mM Bis-Tris, pH 7.0, and 0.02% Coomassie Blue G250 (high blue buffer) or 0.004% Coomassie Blue (low blue buffer). The anode buffer consisted of 50 mM Bis-Tris pH 7.0. Electrophoresis was performed at 4°C using a high blue buffer at 100 V for 1 h, followed by low blue buffer at 250 V for 1.5 h. For assessing supercomplex abundance in Coomassie-stained gels, we loaded 70 µg mitochondrial protein per lane.

Electron Microscopy: Analysis of cardiac ultrastructure by electron microscopy was carried out as previously described with modifications[152]. Briefly, cardiac tissue was dissected into 3-mm^3 pieces and fixed in a solution containing 2% paraformaldehyde and 2% glutaraldehyde for two days. The samples were then post fixed in 1% osmium tetroxide in 0.1 M phosphate buffer, dehydrated in ascending concentrations of ethanol, embedded in Durcopan resin (Sigma-Aldrich), sectioned, and mounted on 100-mesh copper grids. Lastly, mounted sections were doubly stained with uranyl acetate and lead citrate. Ultrastructure was examined by using a Hitachi HT7700 electron microscope operating at 80 kV.

Pathology: Following final echocardiography, hearts were excised and arrested in diastole with 2% KCl. Hearts were then sectioned into 1 mm short-axis sections. A mid-ventricular section was fixed with 10% formalin; the samples were subsequently embedded, cut, and mounted. Later, the slides were deparaffinized and rehydrated as needed for the appropriate stain. All fluorescent and brightfield images were captured using the Keyence BZ-X810, all-in-one fluorescent microscope. Acquired images were analyzed using the hybrid cell count feature (BZ-H4C). For WGA analysis using the Keyence, MATLAB version 9.7.01216025 (R2019b) was used to compile data files

exported from the Keyence analysis software to generate a summary file for data analysis, and the microscopist was blinded to group assignment.

Cardiomyocyte hypertrophy – Cardiac sections were stained with wheat germ agglutinin (WGA; AlexaFluor 555 conjugate; Invitrogen) to identify cell borders and stained with DAPI to detect nuclei. WGA-stained cells were visualized using a fluorescent microscope BZ-X810 (Keyence). Cardiomyocytes were chosen based on a circularity greater than 0.5 and whether they had centrally located nuclei. Circularity was calculated using: $(4*\pi *area)/(perimeter)^2$.

Vascular density – Cardiac sections were stained with isolectin B4 (fluorescein labeled *Griffonia simplicifolia* Lectin I; Vector Labs) as we have described previously[138]. Vascular density was determined as the number of capillaries per area of tissue (number of capillaries per mm^2). A circularity threshold of 0.3 was applied to eliminate all capillaries that are not in cross section and to ensure uniformity.

Cardiac fibrosis – Cardiac sections were stained with Masson's trichrome stain to determine fibrosis and total collagen content according to published protocols[156-158]. Fibrosis was expressed as a percentage of as scar tissue to the total area of short axis LV tissue.

Apoptosis – Cardiac sections were stained using a TUNEL assay (DeadEnd™ Fluorometric TUNEL System, *Promega*) to detect DNA fragments and counterstained with DAPI (VECTASHIELD® PLUS Antifade Mounting Medium with DAPI, *Vector Laboratories*) to identify nuclei. Counted fragmented DNA were compared to the number of nuclei present to determine the percentage of TUNEL positive cells. Signal less than 20 μm^2 and a circularity threshold less than 0.5 were excluded to promote consistency and to ensure that nuclei being counted were in cross-section and the signal being identified was not background. Finally, the counted fragmented DNA were compared to the number

of nuclei present to determine the percentage of cells that are TUNEL positive or considered to be apoptotic.

Statistical analysis: Results are shown as mean ± SD. Statistical analysis was conducted using a one-tailed Student's *t* test to compare two groups. All statistical analyses were performed using GraphPad Prism, version 9 (GraphPad Software, La Jolla, California) and MetaboAnalyst (http://www.metaboanalyst.ca/). Differences were considered statistically significant if $p < 0.05$.

CHAPTER IV

RESULTS

Results for Specific Aim 1

Limiting mitochondrial acetylation does not affect basal mitochondrial dynamics and bioenergetics.

Because both N-α- and N-ε-acetylation depends on availability of acetyl-CoA, and synthesis of acetyl-CoA is partly dependent on the availability of an acyl carrier—coenzyme A (CoA)[39], we sought to reduce CoA levels via *Pank1* deletion—as an intervention to suppress metabolically accumulated acetyl-CoA. First, we assessed the impact of limiting mitochondrial acetylation on basal mitochondrial bioenergetics by utilizing whole body pantothenate kinase 1 deficient mouse (*Pank1*^{-/-}). *Pank1* deletion resulted in a significant reduction in cardiac *Pank1* mRNA (Figure 2B), protein (Figure 2C), and CoA reduction (Figure 2 D). As predicted, mitochondria isolated from whole body KO (*Pank1*^{-/-}) have significantly reduced mitochondrial acetylation compared to their WT littermates (*Pank1*^{+/+}) (Figure 3).
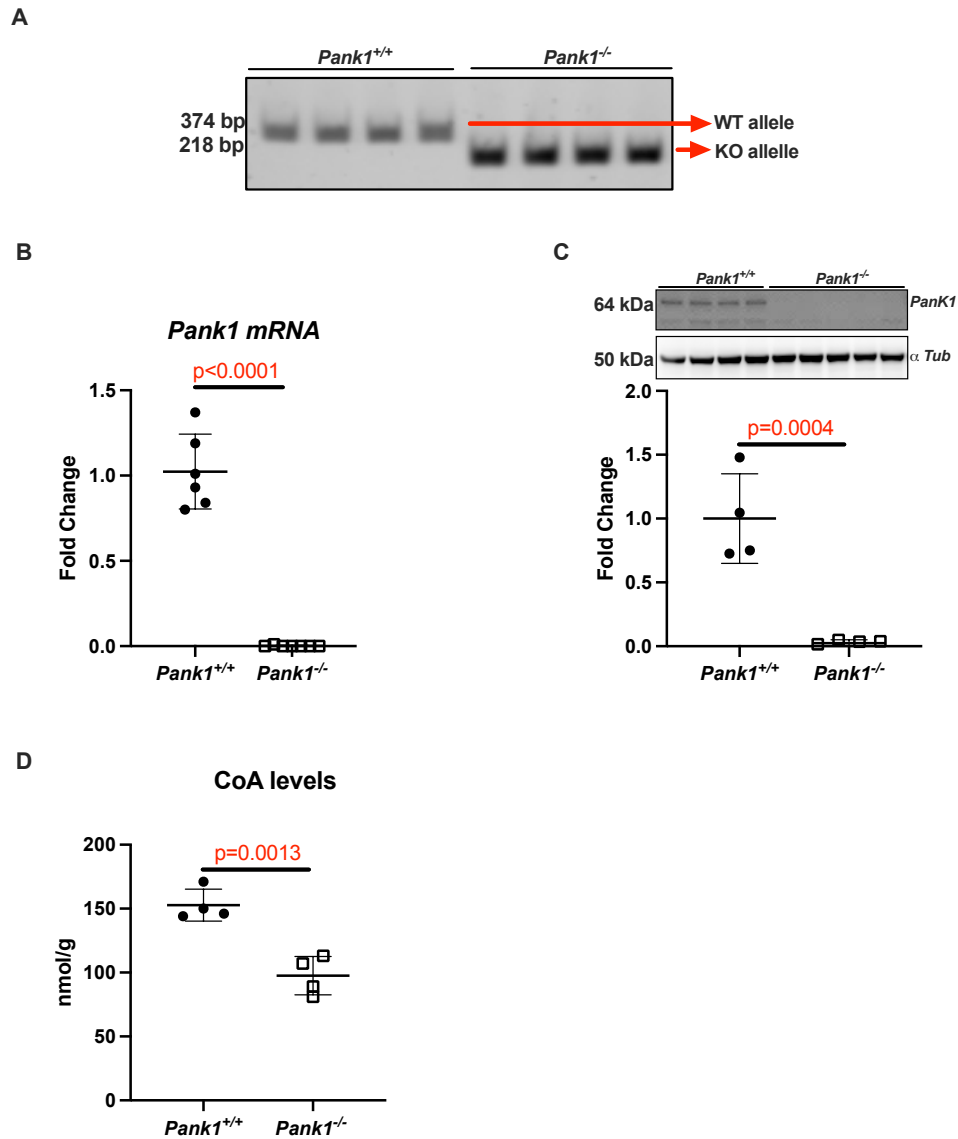
Figure 2: Characterization of pantothenate kinase 1 (Pank1) whole body knockout mice (*Pank1⁻ᐟ⁻*) as a model of limited mitochondrial acetylation. **A)** Genotype for mice with whole body *Pank1* deletion (*Pank1⁻ᐟ⁻*) and littermates (*Pank1⁺ᐟ⁺*) by PCR and agarose gel. A PCR product of 374 bp indicates a wild-type (WT) allele and a PCR product of 218 bp indicates a knockout (KO) allele. **B)** Cardiac *Pank1* mRNA expression. **C)** Cardiac PANK1 protein expression. **D)** Cardiac CoA levels. An unpaired Student's *t* test was used to determine significant differences between *Pank1⁺ᐟ⁺* and *Pank1⁻ᐟ⁻* groups.
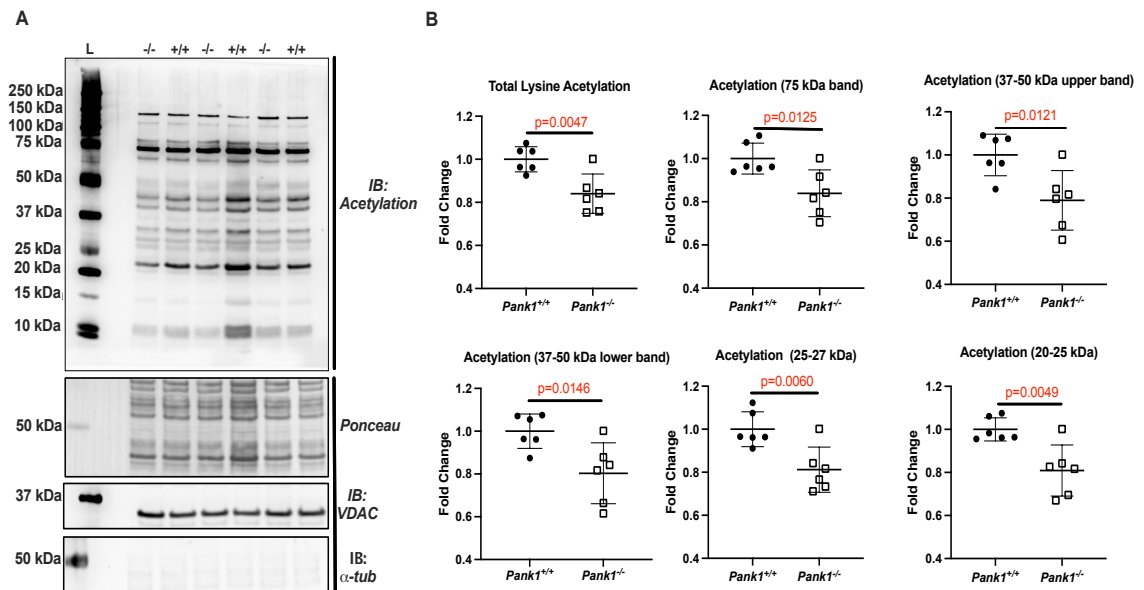
Figure 3: Cardiac CoA depletion partially limits overall mitochondria acetylation. We characterized the impact of partial CoA depletion on overall cardiac mitochondrial acetylation in *Pank1⁻/⁻* and WT littermates *Pank1⁺/⁺*. **A)** Acetylation in *Pank1⁻/⁻* and *Pank1⁺/⁺* isolated mitochondria. **B)** Quantification of acetylation in *Pank1⁻/⁻* and *Pank1⁺/⁺* isolated mitochondria. An unpaired Student's *t* test was used to determine significant differences between *Pank1⁺/⁺* and *Pank1⁻/⁻* groups.

Next, we assessed the impact of limiting mitochondria acetylation on mitochondrial biogenesis and dynamics. We did not observe any significant difference in markers of mitochondrial biogenesis, which includes mRNA expression of *Pgc1b* and *Nrf1* in mitochondria isolated from *Pank1$^{-/-}$* hearts (Figure 4A and B). Furthermore, we did not observe any difference in mitochondrial abundance (Figure 4C). Additionally, we assessed the impact of reducing mitochondrial acetylation on respiratory function by extracellular flux analysis. Compared to *Pank1$^{+/+}$*, limiting mitochondria acetylation does not impact state 3 and 4 respiration in the presence of complex I (pyruvate, malate, and ADP) substrates (Figure 4D). Collectively, these data suggest that limiting mitochondria acetylation does not affect basal mitochondrial biogenesis, dynamics, and mitochondrial function. Given these observations, we then sought to determine whether limiting mitochondrial acetylation will be beneficial during heart failure.
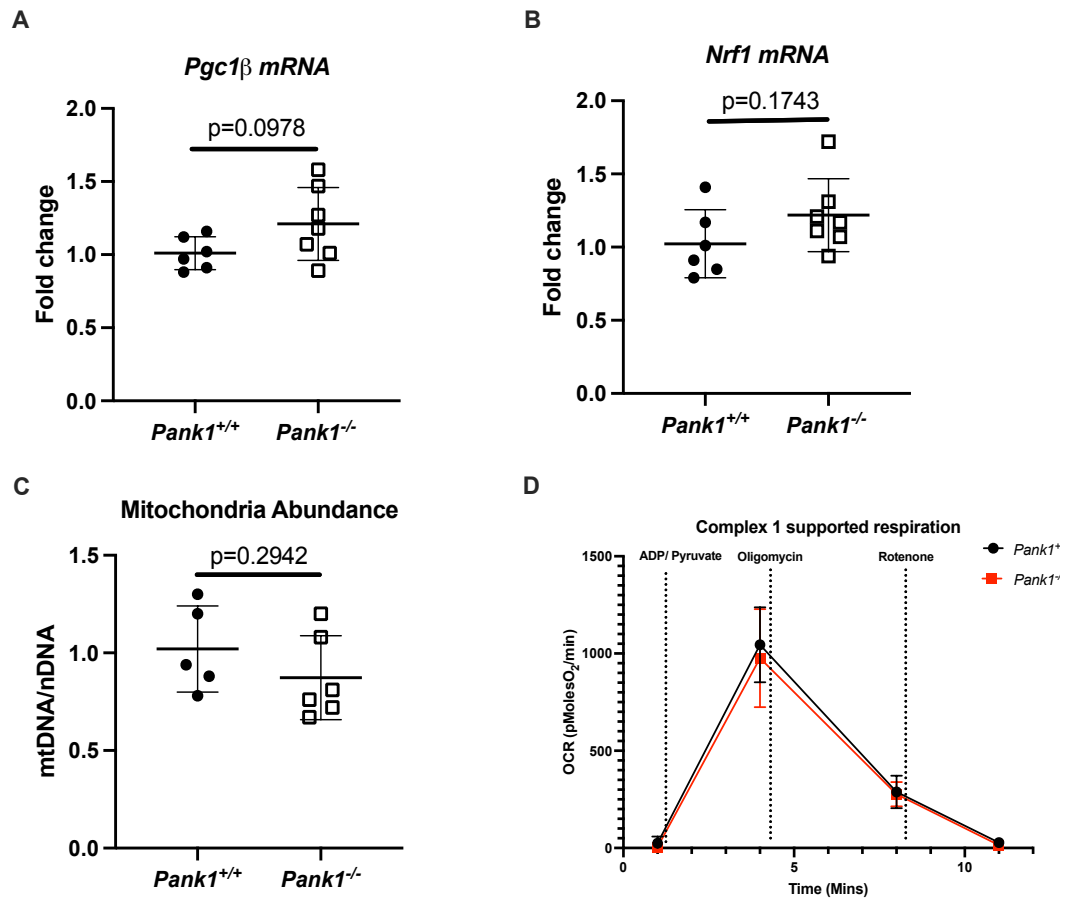
Figure 4: Partially limiting mitochondria acetylation does not impact mitochondrial dynamics and function. A) mRNA expression of *Pgc1*β in *Pank1^-/-^* and *Pank1^+/+^*. **B)** mRNA expression of *Nrf1* in *Pank1^-/-^* and *Pank1^+/+^*. **C)** Mitochondria DNA to nuclear DNA ratio. **D)** State 3 and state 4 respiration in mitochondria isolated from *Pank1^-/-^* and *Pank1^+/+^* hearts. An unpaired Student's *t* test was used to determine significant differences between *PanK1^+/+^* and *PanK1^-/-^* groups.

Specific Aim 2

Cardiac specific pantothenate kinase 1 deletion (cm*Pank1*$^{-/-}$) limited coenzyme A (CoA) availability.

To study whether limiting mitochondria acetylation (through CoA depletion) is beneficial in heart failure, we generated a cardiomyocyte specific Pank1 deficient mice (cm*Pank1*$^{-/-}$). To generate cm*Pank1*$^{-/-}$ mice, we crossed *Pank1*-floxed mice with constitutive, cardiomyocyte-specific Cre (*Myh6*-Cre) transgenic mice, such that control mice (cm*Pank1*$^{+/+}$) were *Myh6*-Cre-negative/*Pank1*$^{fl/fl}$ and our cardiomyocyte-specific *Pank1* deficient mice (cm*Pank1*$^{-/-}$) were *Myh6*-Cre-positive/*Pank1*$^{fl/fl}$. In cm*Pank1*$^{-/-}$ hearts, PANK1 mRNA levels, but not PANK2 or PANK3, were significantly decreased in the hearts compared to WT littermates (lacking the *Myh6*-Cre transgene; cm*Pank1*$^{+/+}$) (Figure 5A). Consistent with decreased mRNA in cm*Pank1*$^{-/-}$ hearts, PANK1 protein was significantly decreased in cm*Pank1*$^{-/-}$ compared to cm*Pank1*$^{+/+}$ hearts (Figure 5B). Furthermore, consistent with changes in PANK1 mRNA and protein, coenzyme A (CoA) levels were significantly lower in cm*Pank1*$^{-/-}$, compared to cm*Pank1*$^{+/+}$ hearts, and not the skeletal muscle (Figure 5C), confirming that CoA depletion is restricted to the heart. Because CoA is abundant in the mitochondria, we examined the impact of *Pank1* deletion on mitochondria acetylation. As expected, PANK1 deletion resulted to significant reduction in mitochondria acetylation at baseline (Figure 5D and 5E).
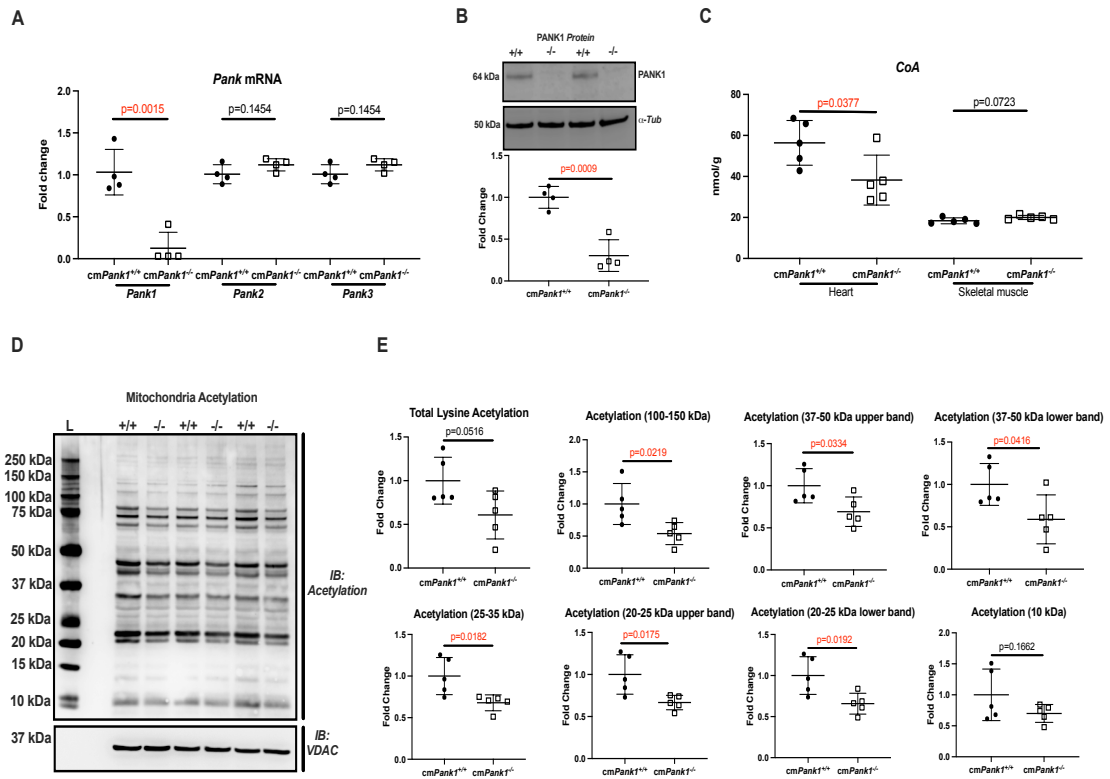
Figure 5: Cardiomyocyte specific *Pank1* deletion limits cardiac mitochondria acetylation. We characterized the impact of cardiomyocyte *Pank1* deletion on cardiac mitochondrial acetylation. **A)** Cardiac *Pank* mRNA expression. **B)** Cardiac PANK1 protein expression. **C)** CoA levels in the heart and skeletal muscle. **D)** Mitochondria acetylation levels via immunoblot. **E)** Quantification of acetylation levels at indicated molecular weights. An unpaired Student's *t* test was used to determine significant differences

cmPank1 deletion minimally affected cardiac function, structure, and global gene expression at baseline.

To determine the impact of *Pank1* deletion on baseline cardiac function, 12-16-week-old cm*Pank1*$^{-/-}$ and cm*Pank1*$^{+/+}$ mice were subjected to echocardiography, and endpoints of cardiac function were assessed. Compared to cm*Pank1*$^{+/+}$, heart rate (HR), stroke volume (SV), left ventricular end-diastolic (EDV) and systolic (ESV) volumes, cardiac output (CO), left ventricular inner diastolic (LVIDd), and systolic (LVIDs) diameter, left ventricular posterior wall thickness at diastole (LVPWd) and systole (LVPWDs), left ventricular anterior wall thickness at systole (LVAWDs) were not significantly changed in cm*Pank1*$^{-/-}$ compared to *cmPank1*$^{+/+}$ (Table 1; Figure 6A and 6B). Ejection fraction (EF) was significantly reduced in cm*Pank1*$^{-/-}$ compared to cm*Pank1*$^{+/+}$ hearts in a sex-dependent manner (Figure 6C; Table 2). Furthermore, left ventricular anterior wall thickness at diastole (LVAWd) was significantly reduced in cm*Pank1*$^{-/-}$ compared to cm*Pank1*$^{+/+}$ hearts (Table 2). Collectively, these data suggest that *Pank1* deletion minimally affected basal cardiac function in naïve mice.

Next, we assessed the impact of *Pank1* deletion on cardiac fibrosis and vascular density at baseline by trichrome staining and isolectin B4 staining. Total fibrosis and vascular density were not changed as a result of *Pank1* deletion (Figure 6D-G).

Table 1: Gravimetric and echocardiographic data from naïve 12-16 wk old mice

*p<0.05 when we compare cm*Pank1*$^{-/-}$ vs cm*Pank1*$^{+/+}$.

	cm*Pank1*$^{+/+}$	cm*Pank1*$^{-/-}$
Total mice (#)	22	25
Body weight (g)	24.0 ± 3.2	24.2 ± 3.8
Sex-Female (%)	40.9%	48.0%
HR (bpm)	518 ± 46	535 ± 43
SV (µL)	27 ± 8	25 ± 7
EDV (µL)	36 ± 11	36 ± 10
ESV (µL)	10 ± 3	11 ± 4
EF (%)	73.5 ± 5.2	70.6 ± 5.9*
CO (mL/min)	13.8 ± 4.0	13.4 ± 3.0
LVIDd (mm)	3.6 ± 0.4	3.5 ± 0.4
LVIDs (mm)	2.0 ± 0.4	2.0 ± 0.4
LVPWd (mm)	0.9 ± 0.2	0.9 ± 0.2
LVPWs (mm)	1.4 ± 0.2	1.3 ± 0.2
LVAWd (mm)	1.1 ± 0.1	1.0 ± 0.1*
LVAWs (mm)	1.6 ± 0.2	1.5 ± 0.1
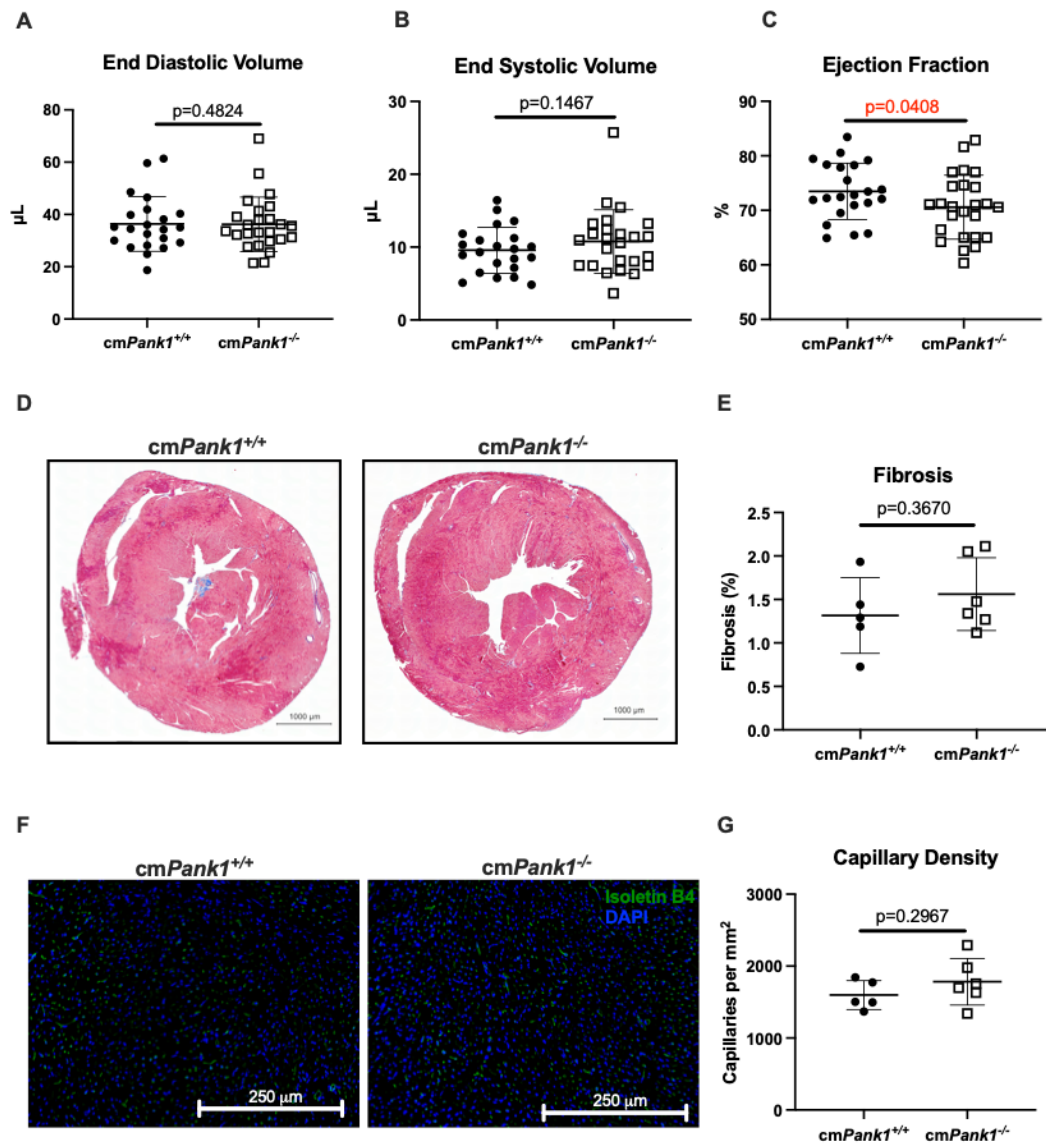
Figure 6: Cardiomyocyte specific *Pank1* deletion does not affect ventricular size, fibrosis, and vascular density in naïve mice hearts. A) End diastolic function (EDV). **B)** End systolic function (ESV). **C)** Ejection fraction (EF). **D)** Trichrome stained hearts. **E)** Quantification of fibrosis in trichrome stained hearts. **F)** Isolectin B4 (green) stained hearts to determine vascular density. **G)** Quantification of vascular density in isolectin B4 stained hearts. An unpaired Student's *t* test was used to determine significant differences between cm*Pank1*^{+/+} and cm*Pank1*^{-/-} groups.

Table 2: Gravimetric and echocardiographic data from naïve 12-16 wk old male and female mice. *p<0.05 when we compare cm*Pank1*$^{-/-}$ vs cm*Pank1*$^{+/+}$.

	Female		Male	
	cm*Pank1*$^{+/+}$	cm*Pank1*$^{-/-}$	cm*Pank1*$^{+/+}$	cm*Pank1*$^{-/-}$
Total mice (#)	9	12	13	13
Body weight (g)	20.8 ± 1.6	21.5 ± 2.0	26.1 ± 1.9	26.7 ± 3.3
HR (bpm)	511 ± 52	532 ± 39	523 ± 44	538 ± 48
SV (µL)	23 ± 6	24 ± 6	30 ± 8	27 ± 7
EDV (µL)	32 ± 8	34 ± 9	40 ± 11	39 ± 11
ESV (µL)	9 ± 3	10 ± 3	10 ± 3	12 ± 6
EF (%)	72.0 ± 6.0	72.0 ± 5.0	74.5 ± 4.5	69.7 ± 6.2*
CO (mL/min)	12.2 ± 2.3	13.0 ± 2.8	15.3 ± 4.0	14.3 ± 3.3
LVIDd (mm)	3.4 ± 0.4	3.4 ± 0.3	3.7 ± 0.4	3.6 ± 0.4
LVIDs (mm)	1.9 ± 0.4	1.9 ± 0.3	2.2 ± 0.5	2.2 ± 0.4
LVPWd (mm)	0.9 ± 0.2	0.6 ± 0.2	0.9 ± 0.2	0.9 ± 0.2
LVPWs (mm)	1.4 ± 0.2	1.4 ± 0.2	1.4 ± 0.2	1.3 ± 0.2
LVAWd (mm)	1.1 ± 0.1	1.0 ± 0.1*	1.1 ± 0.2	1.0 ± 0.1
LVAWs (mm)	1.6 ± 0.2	1.5 ± 0.1	1.7 ± 0.2	1.6 ± 0.2

Next, the impact of *Pank1* deletion on cardiac hypertrophy at baseline was assessed by wheat germ agglutinin (WGA) staining. Consistent with no changes in cardiac fibrosis and vascular density, our results suggest that *Pank1* deletion had no significant impact on cardiac hypertrophy (Figure 7A and 7B), which is consistent with no observable change in heart weights as a result of *Pank1* deletion (Figure 7C).

A

B

Cardiomyocyte CSA

C

HW/TL
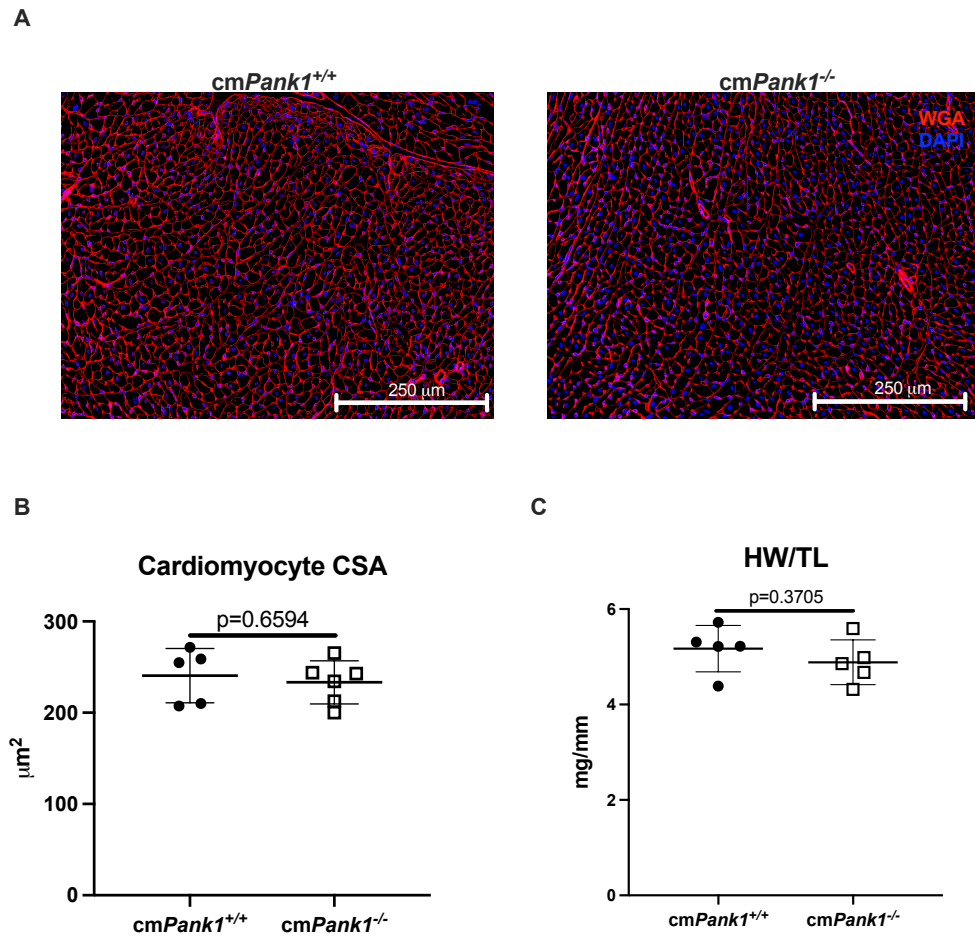
Figure 7: Cardiomyocyte specific *Pank1* deletion does not affect cardiomyocyte size in naïve mice hearts. We assessed the impact of *Pank1* deletion on cardiomyocyte size by wheat germ agglutinin (WGA) and measuring heart weights. **A)** WGA stained (red) cm*Pank1*$^{+/+}$ and cm*Pank1*$^{-/-}$ hearts. **B)** Quantification of WGA stained hearts. **C)** Heart weight/tibia length ratio. An unpaired Student's *t* test was used to determine significant differences between cm*Pank1*$^{+/+}$ and cm*Pank1*$^{-/-}$ groups.

Finally, the impact of *Pank1* deletion on baseline transcriptional changes was assessed by RNA-seq analysis of hearts. 17 protein coding genes were downregulated, and 24 protein coding genes were upregulated as a result of *Pank1* deletion (Figure 8A and 8B). Gene Ontology (GO) enrichment analysis of differentially expressed protein coding genes indicate that *Pank1* deletion upregulates genes significantly involved in cellular oxidant detoxification, erythrocyte development, skeletal muscle contraction, amongst other processes (Figure 8C). Collectively, these data suggest that cardiac *Pank1* deletion minimally affects basal cardiac function without affecting ventricular remodeling as measured by fibrosis, vascular density, and hypertrophy in naïve hearts. Furthermore, despite differences in transcriptional profiles associated with *Pank1* deletion at baseline, cardiac function and structure were minimally affected. The question, however, remained as to whether cardiac *Pank1* deletion, by limiting excessive acetylation, benefits the failing heart.
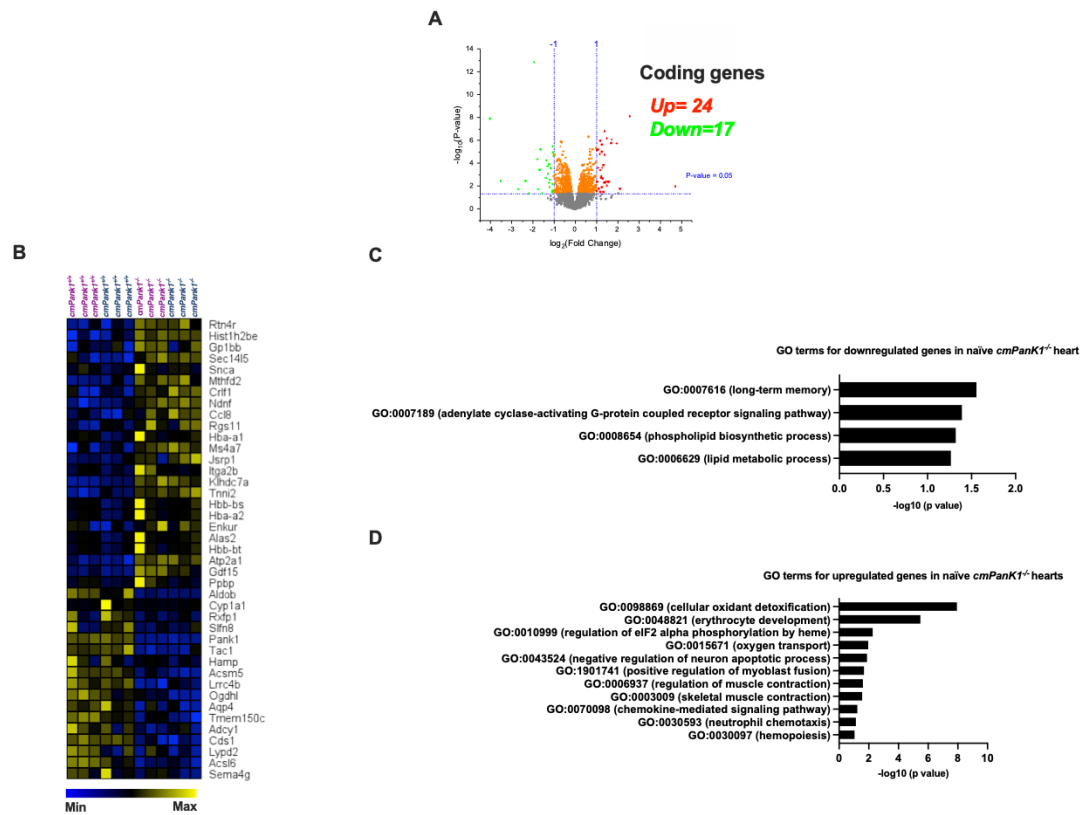
Figure 8: Impact of cardiomyocyte specific *Pank1* deletion on cardiac transcriptional profiles. To study the impact of *Pank1* on cardiac transcriptional profile, total RNA was isolated from naïve male (blue) and female (purple) cm*PanK1*$^{+/+}$ and cm*PanK1*$^{-/-}$ hearts. **A)** Volcano plot of differentially expressed genes in naïve hearts. **B)** Heat map showing differentially regulated genes in cm*Pank1*$^{-/-}$ naïve hearts compared to cm*Pank1*$^{+/+}$. **C)** Gene Ontology (GO) enrichment analysis showing biological processes associated with downregulated genes in cm*Pank1*$^{-/-}$ compared to cm*Pank1*$^{+/+}$ hearts. **D)** Gene Ontology (GO) enrichment analysis showing biological processes associated with upregulated genes in cm*Pank1*$^{-/-}$ compared to cm*Pank1*$^{+/+}$ hearts.

43

cmPank1 deletion exacerbated cardiac dysfunction during pressure overload.

To determine whether cmPank1 deletion benefited cardiac function during pressure overload, 12-16-week-old cm*Pank1*$^{-/-}$ and cm*Pank1*$^{+/+}$ mice were subjected to transverse aortic constriction (TAC) and cardiac function was assessed at 2-12 wk post-TAC by echocardiography. Compared to cm*Pank1*$^{+/+}$, left ventricular end-diastolic (EDV) and systolic (ESV) volumes were significantly increased in cm*Pank1*$^{-/-}$ mice at 2 wk, and continued to significantly dilate until 12 wk post-TAC (Figure 9A and 9B) in a sex independent manner (Figure 10). Consistent with increased EDV and ESV, *Pank1* deletion resulted in significantly reduced ejection fraction (EF) at 2 wk and continued to decrease until 8 wk post-TAC (Figure 9C) in a sex independent manner (Figure 10; Table 4 and 5). Additionally, posterior wall thickness at diastole (LVPWd) and systole (LVPWDs) and left ventricular anterior wall thickness at diastole (LVAWd) and systole (LVAWDs) were significantly reduced as a result of *Pank1* deletion (Table 3). We did not observe any significant difference in body weight, heart rate (HR), stroke volume (SV), and cardiac output (CO) at 2-12 wk post-TAC as a result of *Pank1* deletion (Table 3). Collectively, these data suggest that cardiac *Pank1* deletion exacerbates cardiac dysfunction starting at 2 wk post-TAC. Given these observations, we next sought to investigate how PANK1 deletion contributes to exacerbated cardiac dysfunction during pressure overload.
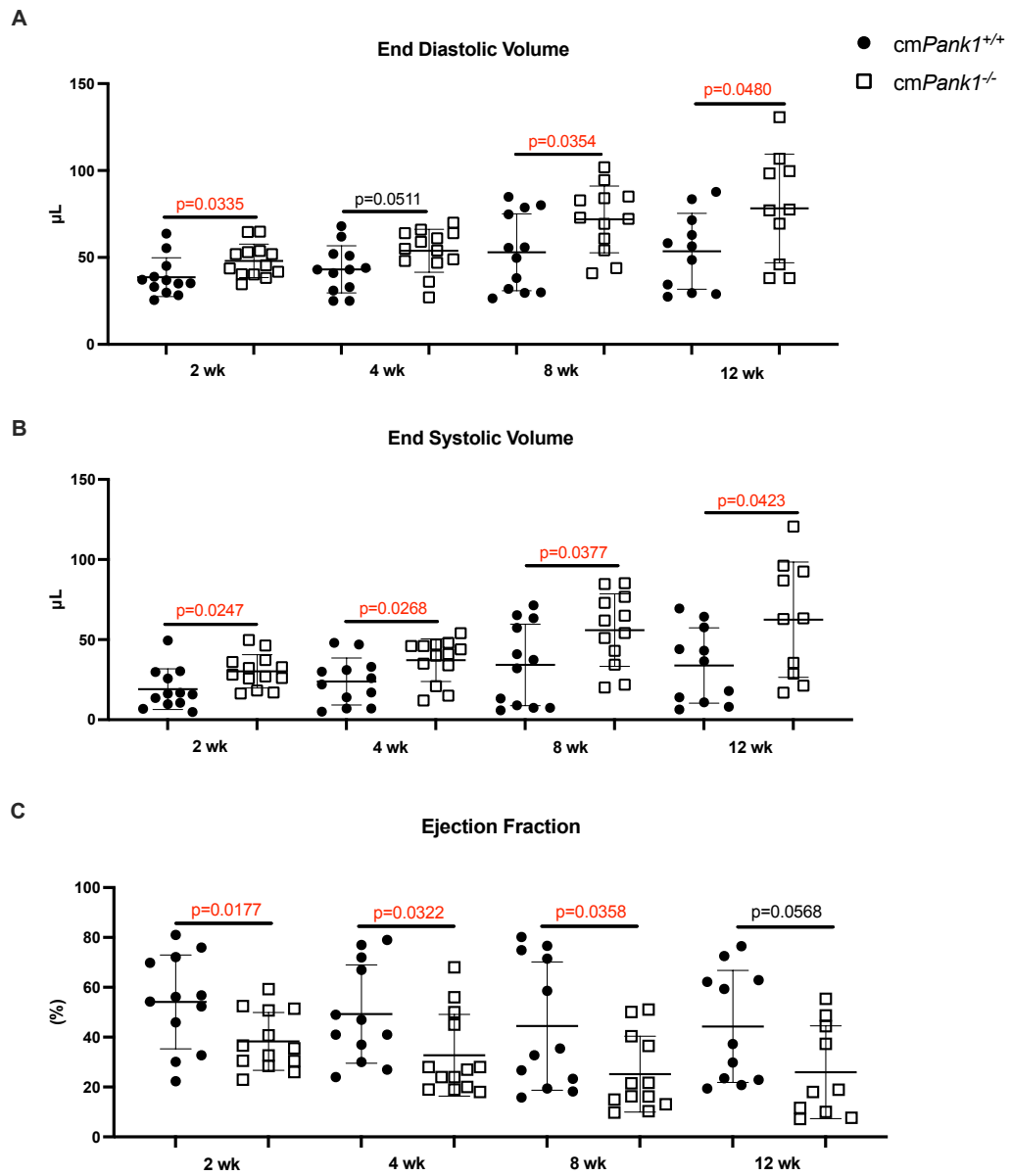
Figure 9: *Pank1* deletion exacerbates ventricular dilation during pressure overload.
Mice were subjected to transverse aortic constriction (TAC) and echocardiography was performed at 2, 4, 8, and 12 wk after TAC. **A)** Left ventricular end diastolic volumes (EDV). **B)** Left ventricular end systolic volumes (ESV). **C)** Ejection fraction (EF). An unpaired Student's *t* test was used to determine significant differences between cm*Pank1*^{+/+} and cm*Pank1*^{-/-} groups at each time point.
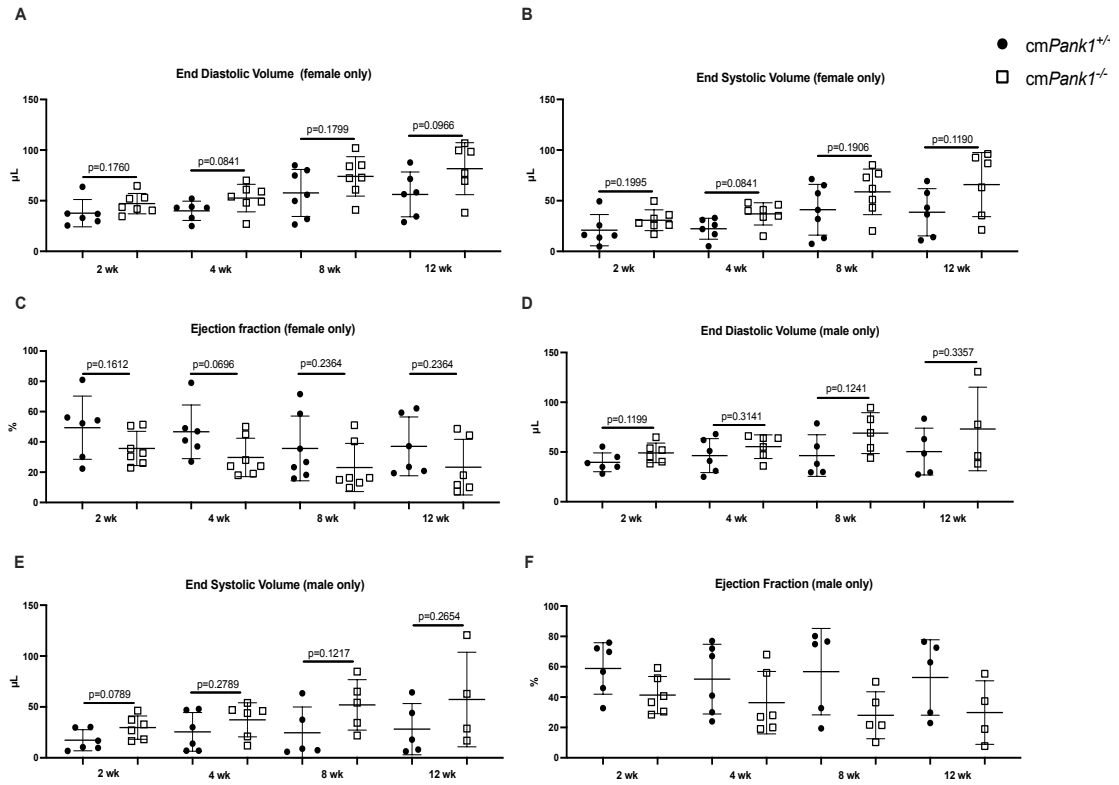
Figure 10: Data from Figure 9 disaggregated by sex. A) Left ventricular end-diastolic volumes (EDV) in female mice. **B)** Left ventricular end-systolic volumes (ESV) in female mice. **C)** Ejection fraction (EF) in female mice. **D)** Left ventricular end diastolic volumes (EDV) in male mice. **E)** Left ventricular end systolic volumes (ESV) in male mice. **F)** Ejection fraction (EF) in male mice. An unpaired Student's t test was used to determine significant differences between cm*Pank1*+/+ and cm*Pank1*-/- groups at each time point.

Table 3: Echocardiography data of mice subjected to TAC. An unpaired Student's *t* test was used to determine significant differences between cm*Pank1*^{+/+} and cm*Pank1*^{-/-} groups. *p<0.05 when we compare cm*Pank1*^{-/-} vs cm*Pank1*^{+/+} at each time point and number of animals at each time point is the same indicated in Figure 9.

	2 wk		4 wk		8 wk		12 wk	
	cm*Pank1*^{+/+}	cm*Pank1*^{-/-}	cm*Pank1*^{+/+}	cm*Pank1*^{-/-}	cm*Pank1*^{+/+}	cm*Pank1*^{-/-}	cm*Pank1*^{+/+}	cm*Pank1*^{-/-}
Weight (g)	23.0 ± 3.4	23.7 ± 2.7	23.4 ± 3.5	23.8 ± 2.3	24.2 ± 3.1	23.3 ± 3.2	25.0 ± 3.4	24.6 ± 3.3
HR (bpm)	533 ± 28	533 ± 44	546 ± 35	549 ± 16	537 ± 38	521 ± 33	543 ± 27	514 ± 54
SV (µL)	20 ± 5	18 ± 4	19 ± 4	17 ± 7	19 ± 5	16 ± 6	20 ± 5	21 ± 17
CO (mL/min)	10.4 ± 2.6	9.5 ± 2.2	10.5 ± 2.4	9.2 ± 4.2	10.0 ± 2.2	8.3 ± 3.3	10.7 ± 2.6	8.2 ± 4.2
LVIDd (mm)	3.6 ± 0.3	3.8 ± 0.3	3.8 ± 0.4	4.0 ± 0.3	4.0 ± 0.6	4.4 ± 0.4*	4.0 ± 0.7	4.6 ± 0.5*
LVIDs (mm)	2.5 ± 0.7	3.0 ± 0.4*	2.8 ± 0.8	3.3 ± 0.5*	3.0 ± 1.0	3.8 ± 0.6*	3.0 ± 1.1	3.9 ± 0.8*
LVPWd (mm)	1.1 ± 0.3	1.1 ± 0.3	1.2 ± 0.3	1.2 ± 0.3	1.3 ± 0.2	1.2 ± 0.3	1.4 ± 0.3	1.1 ± 0.2*
LVPWs (mm)	1.5 ± 0.3	1.3 ± 0.3	1.5 ± 0.3	1.3 ± 0.3*	1.6 ± 0.3	1.2 ± 0.3*	1.7 ± 0.3	1.2 ± 0.2*
LVAWd (mm)	1.2 ± 0.2	1.2 ± 0.2	1.3 ± 0.2	1.3 ± 0.4	1.3 ± 0.3	1.2 ± 0.1*	1.4 ± 0.2	1.1 ± 0.2*
LVAWs (mm)	1.6 ± 0.3	1.5 ± 0.2	1.7 ± 0.2	1.4 ± 0.2*	1.7 ± 0.3	1.4 ± 0.2*	1.7 ± 0.2	1.4 ± 0.3*

Table 4: Data from Table 3 disaggregated by female sex. Echocardiography data of female mice subjected to TAC. An unpaired Student's *t* test was used to determine significant differences between cm*Pank1*$^{+/+}$ and cm*Pank1*$^{-/-}$ groups. *p<0.05 when we compare cm*Pank1*$^{-/-}$ vs cm*Pank1*$^{+/+}$ at each time point and number of animals at each time point is the same indicated in Figure 10.

	2 wk		4 wk		8 wk		12 wk	
	cm*Pank1*$^{+/+}$	cm*Pank1*$^{-/-}$	cm*Pank1*$^{+/+}$	cm*Pank1*$^{-/-}$	cm*Pank1*$^{+/+}$	cm*Pank1*$^{-/-}$	cm*Pank1*$^{+/+}$	cm*Pank1*$^{-/-}$
Weight (g)	20.2 ± 1.4	21.4 ± 1.0	21.5 ± 0.9	22.0 ± 1.0	22.1 ± 0.8	21.6 ± 1.6	22.6 ± 0.7	22.6 ± 1.8
HR (bpm)	534 ± 34	529 ± 49	552 ± 47	544 ± 19	543 ± 29	505 ± 28*	539 ± 24	482 ± 29*
SV (μL)	17 ± 4	16 ± 5	18 ± 3	15 ± 9	17 ± 2	15 ± 8	18 ± 3	30 ± 22
CO (mL/min)	9.0 ± 2.4	8.6 ± 2.3	9.6 ± 1.9	8.4 ± 4.7	9.0 ± 1.4	7.6 ± 3.5	9.5 ± 1.9	7.6 ± 4.8
LVIDd (mm)	3.7 ± 0.4	3.8 ± 0.3	3.8 ± 0.3	4.0 ± 0.4	4.1 ± 0.6	4.3 ± 0.4	4.1 ± 0.7	4.7 ± 0.4
LVIDs (mm)	2.8 ± 0.7	3.1 ± 0.3	2.9 ± 0.6	3.3 ± 0.4	3.3 ± 0.9	3.8 ± 0.6	3.3 ± 1.1	4.0 ± 0.8
LVPWd (mm)	1.1 ± 0.4	1.1 ± 0.2	1.3 ± 0.3	1.2 ± 0.2	1.3 ± 0.2	1.3 ± 0.3	1.4 ± 0.3	1.1 ± 0.2*
LVPWs (mm)	1.4 ± 0.3	1.3 ± 0.2	1.5 ± 0.4	1.3 ± 0.2	1.6 ± 0.3	1.4 ± 0.3	1.6 ± 0.4	1.3 ± 0.2*
LVAWd (mm)	1.2 ± 0.2	1.2 ± 0.2	1.3 ± 0.3	1.1 ± 0.1	1.4 ± 0.2	1.2 ± 0.1*	1.4 ± 0.1	1.1 ± 0.2*
LVAWs (mm)	1.5 ± 0.3	1.5 ± 0.1	1.6 ± 0.2	1.4 ± 0.1*	1.7 ± 0.3	1.4 ± 0.1*	1.7 ± 0.3	1.3 ± 0.3*

Table 5: Data from Table 3 disaggregated by male sex. Echocardiography data of male mice subjected to TAC. An unpaired Student's *t* test was used to determine significant differences between cm*Pank1*$^{+/+}$ and cm*Pank1*$^{-/-}$ groups. *p<0.05 when we compare cm*Pank1*$^{-/-}$ vs cm*Pank1*$^{+/+}$ at each time point and number of animals at each time point is the same indicated in Figure 10.

	2 wk		4 wk		8 wk		12 wk	
	cm*Pank1*$^{+/+}$	cm*Pank1*$^{-/-}$	cm*Pank1*$^{+/+}$	cm*Pank1*$^{-/-}$	cm*Pank1*$^{+/+}$	cm*Pank1*$^{-/-}$	cm*Pank1*$^{+/+}$	cm*Pank1*$^{-/-}$
Weight (g)	25.8 ± 2.5	26.3 ±1.3	25.2 ± 3.4	26.0 ± 1.3	27.0 ± 2.9	25.8 ± 3.4	28.0 ± 2.8	27.3 ± 3.1
HR (bpm)	533 ± 24	538 ± 42	540 ± 20	554 ± 11	529 ± 51	543 ± 27	549 ± 33	563 ± 46
SV (µL)	22 ± 4	19 ± 3	21 ± 4	18 ± 6	22 ± 5	17 ± 5	22 ± 5	16 ± 5*
CO (mL/min)	11.9 ± 2.2	10.5 ± 1.8	11.3 ± 2.4	10.2 ± 3.5	11.4 ± 2.4	9.3 ± 2.9*	12.2 ± 2.7	9.0 ± 3.4
LVIDd (mm)	3.5 ± 0.5	3.8 ± 0.3	3.8 ± 0.5	4.0 ± 0.3	3.7 ± 0.7	4.5 ± 0.3*	3.9 ± 0.8	4.5 ± 0.6
LVIDs (mm)	2.2 ± 0.6	3.0 ± 0.6*	2.6 ± 0.9	3.4 ± 0.6	2.6 ± 1.1	3.8 ± 0.6*	2.7 ± 1.2	3.8 ± 0.9
LVPWd (mm)	1.1 ± 0.2	1.1 ± 0.3	1.1 ± 0.2	1.1 ± 0.4	1.3 ± 0.3	1.1 ± 0.3	1.3 ± 0.3	1.0 ± 0.3
LVPWs (mm)	1.6 ± 0.2	1.4 ± 0.4	1.6 ± 0.2	1.3 ± 0.3*	1.7 ± 0.3	1.3 ± 0.1*	1.7 ± 0.3	1.2 ± 0.3*
LVAWd (mm)	1.2 ± 0.2	1.1 ± 0.2	1.3 ± 0.2	1.3 ± 0.2	1.3 ± 0.3	1.2 ± 0.2	1.3 ± 0.1	1.2 ± 0.3
LVAWs (mm)	1.7 ± 0.3	1.5 ± 0.2	1.7 ± 0.3	1.5 ± 0.3	1.8 ± 0.4	1.5 ± 0.2	1.7 ± 0.2	1.5 ± 0.4

cmPank1 deletion impacted transcriptional landscape related to fibrotic and metabolic processes during pressure overload.

To investigate how *Pank1* deletion contributes to exacerbated cardiac dysfunction during pressure overload, total RNA was isolated from cm*Pank1*$^{-/-}$ and cm*Pank1*$^{+/+}$ male and female hearts at 12 wk post-TAC and subjected to unbiased bulk RNA-seq analysis. 50 protein coding genes were downregulated, and 75 protein coding genes were upregulated as a result of *Pank1* deletion (Figure 11A-C). Gene Ontology (GO) enrichment analysis of differentially expressed genes indicate that *Pank1* deletion downregulates genes significantly involved in cellular oxidant detoxification, muscle contraction, circadian rhythm, fatty acid metabolic process, and regulation of slow-twitch skeletal muscle fiber contraction amongst other processes (Figure 11D) in *cmPank1*$^{-/-}$ hearts. Genes involved in cell cycle, cycle division, response to mechanical stimulus, positive regulation of fibroblast proliferation, and SMAD protein signal transduction amongst other processes were upregulated (Figure 11D). Taken together, these data suggest a role of *Pank1* in regulating fibrotic and metabolic processes during pressure overload. We then sought to determine how PANK1 regulates remodeling and metabolic processes during TAC.
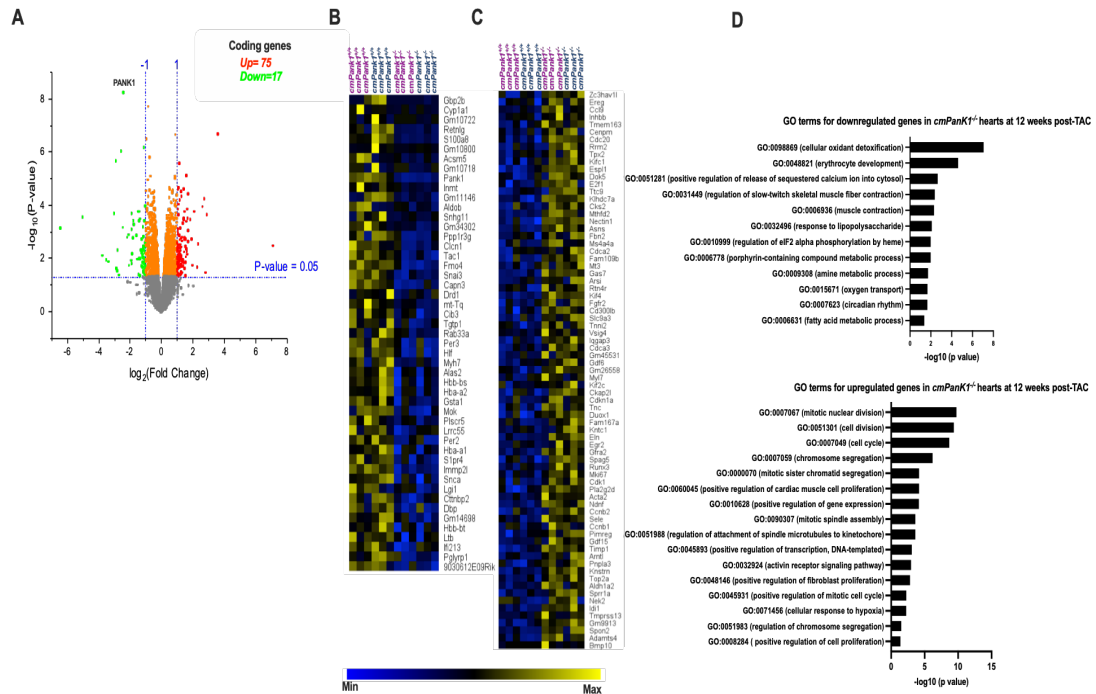
Figure 11: Cardiomyocyte *Pank1* deletion impacts transcriptional profile of fibrotic and metabolic processes at 12 wk post pressure overload. Total RNA was isolated from hearts 12 wk post TAC and RNA-Seq was performed. **A)** Volcano plot of differentially expressed genes. **B)** Heat map showing upregulated genes in male (blue) and female (purple) hearts. **C)** Heat map showing downregulated genes in male (blue) and female (purple) hearts. **D)** Gene Ontology (GO) enrichment analysis showing biological processes associated with downregulated and upregulated genes in *cmPank1*$^{-/-}$ compared to *cmPank1*$^{+/+}$ hearts.

Next, to determine whether cmPank1 deletion contributes to adverse ventricular remodeling, we assessed the impact of partial CoA depletion on several indices of ventricular remodeling like hypertrophy, fibrosis, vascular density, and apoptosis by wheat germ agglutinin (WGA), trichrome, isolectin B4, and TUNEL staining after final echocardiography at 12 wk post-TAC. Cardiac hypertrophy was not significantly changed as a result of *Pank1* deletion (Figure 12A and 12B). Consistent with WGA staining, we did not observe significant differences in normalized heart weights (HW) as a result of *Pank1* deletion (Figure 12C).
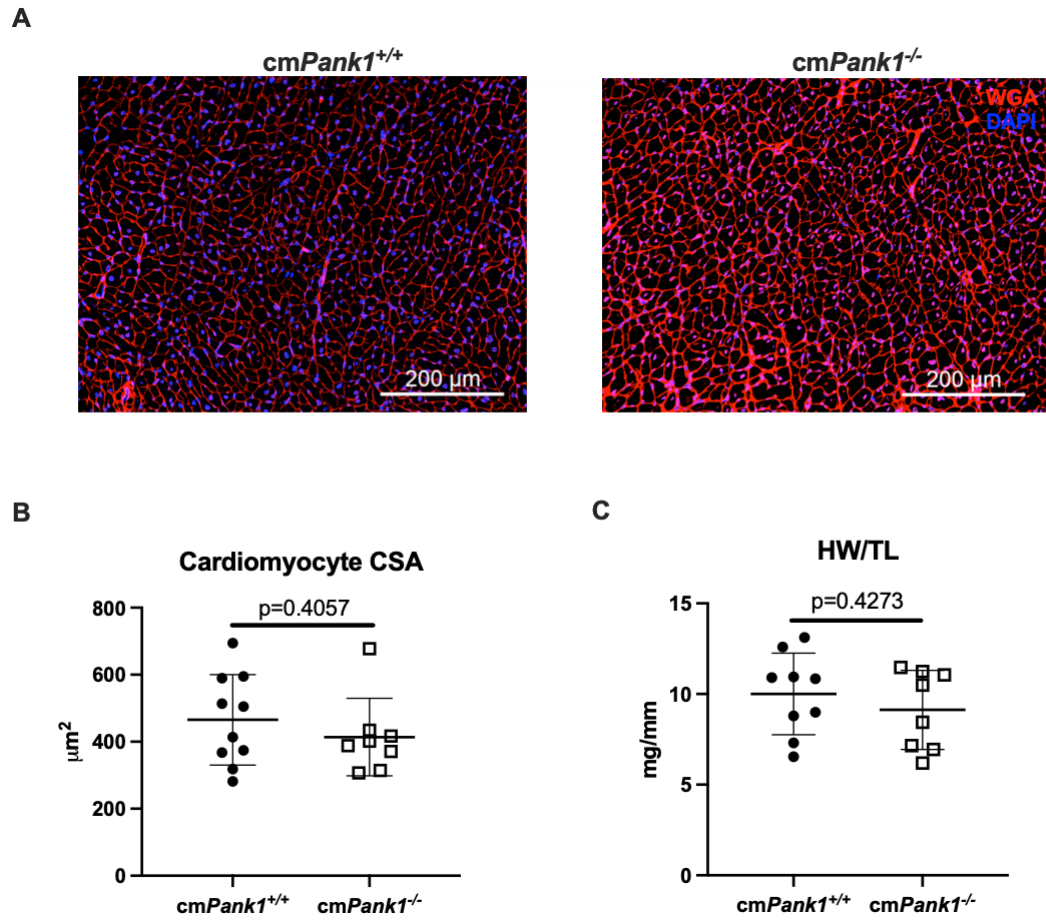
Figure 12: Cardiomyocyte specific *Pank1* deletion does not affect cardiomyocyte size 12 wk post TAC. We assessed cardiomyocyte size by wheat germ agglutinin (WGA) and measuring heart weights. **A)** WGA stained (red) hearts. **B)** Quantification of WGA stained hearts. **C)** Heart weight/tibia length ratio. An unpaired Student's *t* test was used to determine significant differences between cm*Pank1*+/+ and cm*Pank1*-/- groups.

Next, the impact of *Pank1* deletion on cardiac fibrosis was assessed at 12 wk post-TAC. Interestingly, cardiac fibrosis was significantly increased as a result of *Pank1* deletion (Figure 13A and B). This is further supported by our RNAseq data that showed upregulation of genes involved in fibrotic and ECM remodeling, including *Acta2*, *Inhhb*, *Gdf15*, *Gdf6*, *Fbn2*, *Tnc*, and *Timp1* amongst others (Figure 13C-F).
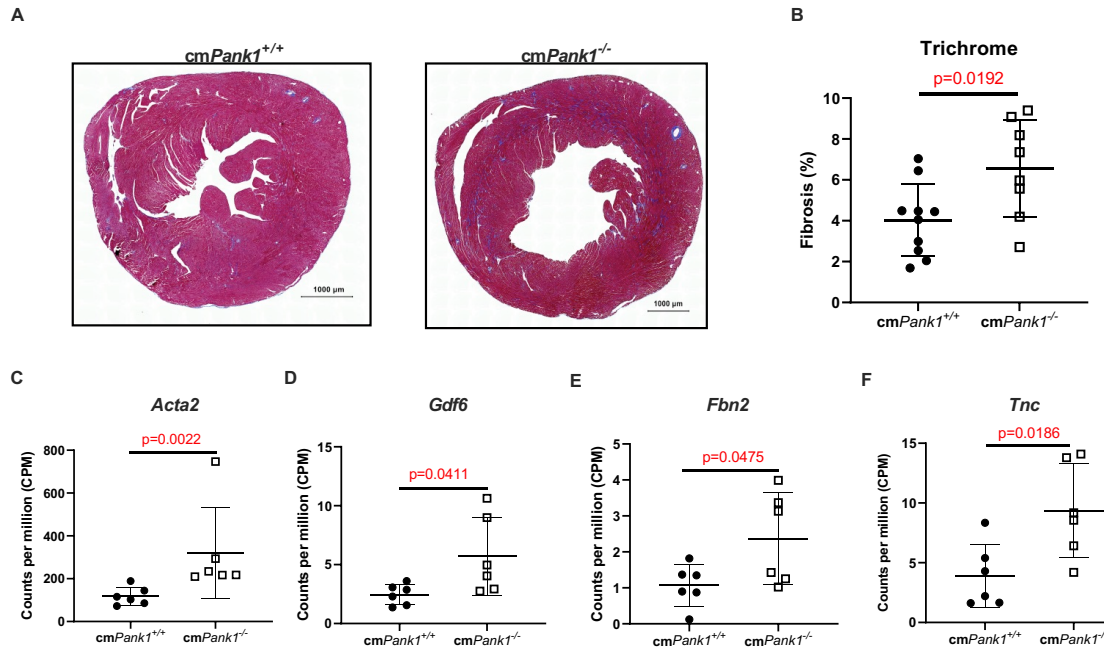
Figure 13: Cardiomyocyte *Pank1* deletion increases cardiac fibrosis 12 wk post TAC. A) Trichrome stained cm*Pank1*$^{+/+}$ and cm*Pank1*$^{-/-}$ hearts 12 wk post TAC. **B)** Quantification of fibrosis in trichrome stained hearts 12 wk post-TAC. **B)** Quantification of fibrosis in trichrome stained hearts. RNA-seq data showing **C)** Cardiac *Acta2* mRNA expression 12 wk post-TAC. **D)** Cardiac *Gdf6* mRNA expression 12 wk post-TAC. **E)** Cardiac *Fbn2* mRNA expression 12 wk post-TAC. **F)** Cardiac *Tnc* mRNA expression 12 wk post-TAC. An unpaired Student's *t* test was used to determine significant differences between cm*Pank1*$^{+/+}$ and cm*Pank1*$^{-/-}$ groups.

Furthermore, our results indicate no significant changes in vascular density as a result of *Pank1* deletion (Figure 14A and 14B). Finally, we assessed the impact of *Pank1* deletion on cardiac apoptosis. Our results indicate no significant changes in apoptosis as a result of *Pank1* deletion (Figure 14C and 14D). Collectively, these data suggest that cardiac PANK1 deletion exacerbates cardiac fibrosis without affecting vascular density, hypertrophy, and apoptosis at 12 wk post pressure overload.
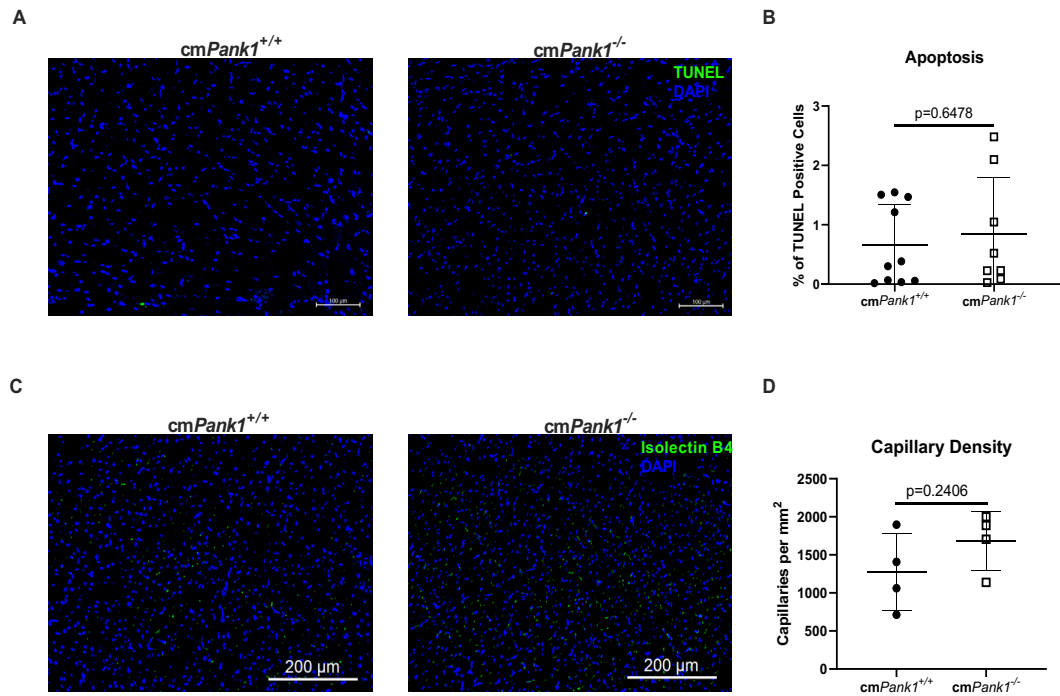
Figure 14: Cardiomyocyte *Pank1* deletion does not affect cardiac apoptosis and capillary density 12 wk post TAC. **A)** TUNEL (Green) stained hearts 12 wk post TAC. **B)** Quantification of TUNEL (green) stained hearts 12 wk post TAC. **C)** Isolectin B4 (Green) stained hearts 12 wk post TAC. **D)** Quantification of isolectin B4 stained hearts 12 wk post TAC. An unpaired Student's *t* test was used to determine significant differences between cm*Pank1*+/+ and cm*Pank1*-/- groups.

cmPank1 deletion altered metabolites involved in substrate utilization early during pressure overload.

To determine how *Pank1* deletion alters cardiac metabolism in naïve animals and during pressure overload, cm*Pank1*$^{-/-}$ and cm*Pank1*$^{+/+}$ male and female mice were subjected to TAC (Table 6) and cardiac metabolism was assessed by LC-MS at 2 wk post-TAC. Principal component analysis (PCA) of global metabolic profiles reveals clear separations as a result and *Pank1* deletion (Figure 15A). Although both female and male mice were included in this study, clustering pattern was not widely affected as a result of sex (Figure 15A). In naïve mice, 36 metabolites were significantly changed as a result of *Pank1* deletion. Pathway enrichment analysis of significantly changed metabolites suggests that *Pank1* deletion significantly impacts metabolites involved in the pantothenate and CoA biosynthetic pathway, ketone body metabolism, pentose phosphate pathway, amino sugar metabolism, and fatty acid biosynthesis among other pathways (Figure 15B). Interestingly, during TAC, 71 metabolites were significantly changed as a result of *Pank1* deletion. Pathway analysis of significantly changed metabolites suggests that during TAC, *Pank1* deletion significantly impacts metabolites involved in butyrate metabolism, pantothenate and CoA biosynthesis, ketone body metabolism, mitochondria beta-oxidation of short, medium, long, and very long chain saturated fatty acids, aspartate metabolism and arginine and proline metabolism among other metabolic processes (Figure 15D). Because ketone body consumption increases during heart failure, we further examined metabolites involved in ketone oxidation as a result of *Pank1* deletion.

58

Table 6*: Gravimetric and echocardiographic data from a separate cohort of mice subjected to TAC for 2 wk for metabolomics analysis. *p<0.05 when we compare cm*Pank1*^{−/−} (n=6) vs cm*Pank1*^{+/+} (n=6).

	cm*Pank1*^{+/+}	cm*Pank1*^{−/−}
Body weight (g)	23.78 ± 5.4	22.6 ± 3.4
HR (BPM)	531 ± 43	501 ± 38
SV (µL)	20 ± 8	15 ± 3
EDV (µL)	45 ± 8	60 ± 13 *
ESV (µL)	25 ± 10	46 ± 11 *
EF (%)	46.0 ± 19.6	24.0 ± 4. 3 *
CO (mL/min)	10.8 ± 4.6	7.2 ± 1.4
LVIDd (mm)	3.8 ± 0.4	4.0 ± 0.4
LVIDs (mm)	2.9 ± 0.5	3.6 ± 0.4 *
LVPWd (mm)	1.2 ± 0.2	1.3 ± 0.3
LVPWs (mm)	1.5 ± 0.2	1.5 ± 0.3
LVAWd (mm)	1.3 ± 0.1	1.2 ± 0.4
LVAWs (mm)	1.7 ± 0.1	1.4 ± 0.1 *
FS (%)	22.4 ± 8.6	10.0 ± 2.0 *
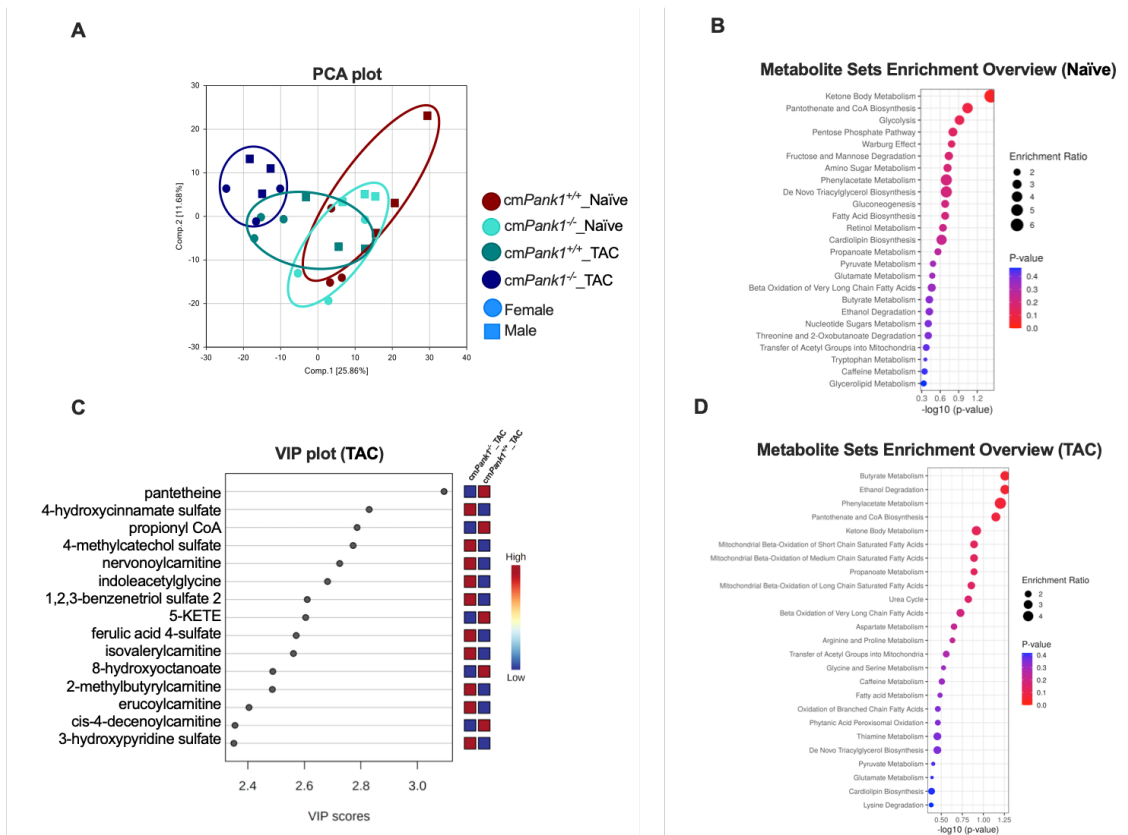
Figure 15: Cardiomyocyte *Pank1* deletion alters metabolites involved in substrate utilization after 2 wk of pressure overload. A) Principal component analysis (PCA) plot. **B)** Metabolite set enrichment analysis in naïve animals. **C)** Variable of importance (VIP) plot of animals subjected to TAC. **D)** Metabolite set enrichment analysis in animals subjected to TAC.

Interestingly, levels of 3-hydroxybutyrate were significantly increased in naïve mice as a result of *Pank1* deletion (Figure 16A). Similarly, during TAC, we observed an elevated (but not significant p=0.0649) 3-hydroxybutyrate level (Figure 16B).

A

3-hydroxybutyrate (Naïve)

p=0.0031

Scaled Intensity

1.5
1.0
0.5
0.0

cm*Pank1*$^{+/+}$ cm*Pank1*$^{-/-}$

B

3-hydroxybutyrate (TAC)

p=0.0649

Scaled Intensity

1.5
1.0
0.5
0.0

cm*Pank1*$^{+/+}$ cm*Pank1*$^{-/-}$
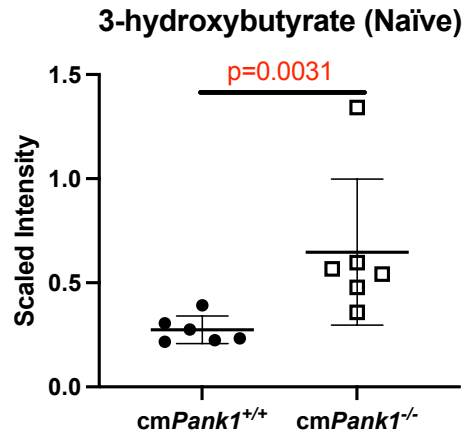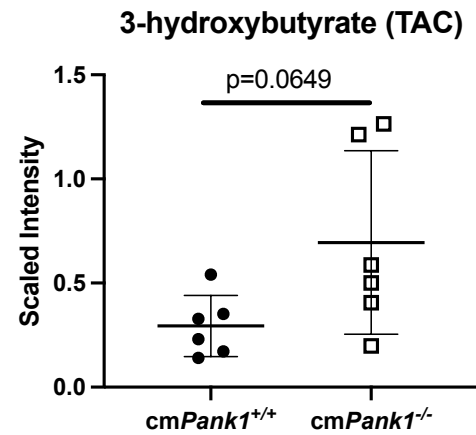
Figure 16: Cardiac ketone body metabolite 3-hydroxybutyrate accumulates as a result of *Pank1* deletion. We assessed cardiac metabolites in hearts from naïve mice or from 2 wk post-TAC. **A)** 3-hydroxybutyrate levels in naïve animals. **B)** 3-hydroxybutyrate levels in post-TAC hearts. An unpaired Student's *t* test was used to determine significant differences between cm*Pank1*$^{+/+}$ and cm*Pank1*$^{-/-}$ hearts.

Furthermore, *Pank1* deletion resulted in significant reduction in precursors required for succinyl-CoA synthesis such as propionyl-CoA, acetyl-CoA, and methylmalonyl-carnitine during TAC (Figure 17). Because succinyl-CoA is required for the transfer of CoA during ketone body oxidation (during the conversion of acetoacetate to acetoacetate-CoA by SCOT1), our data suggest that *Pank1* deletion may limit succinyl-CoA levels and that may impinge on ketone body oxidation in the heart—hence elevated levels of 3-hydroxybutyrate level.
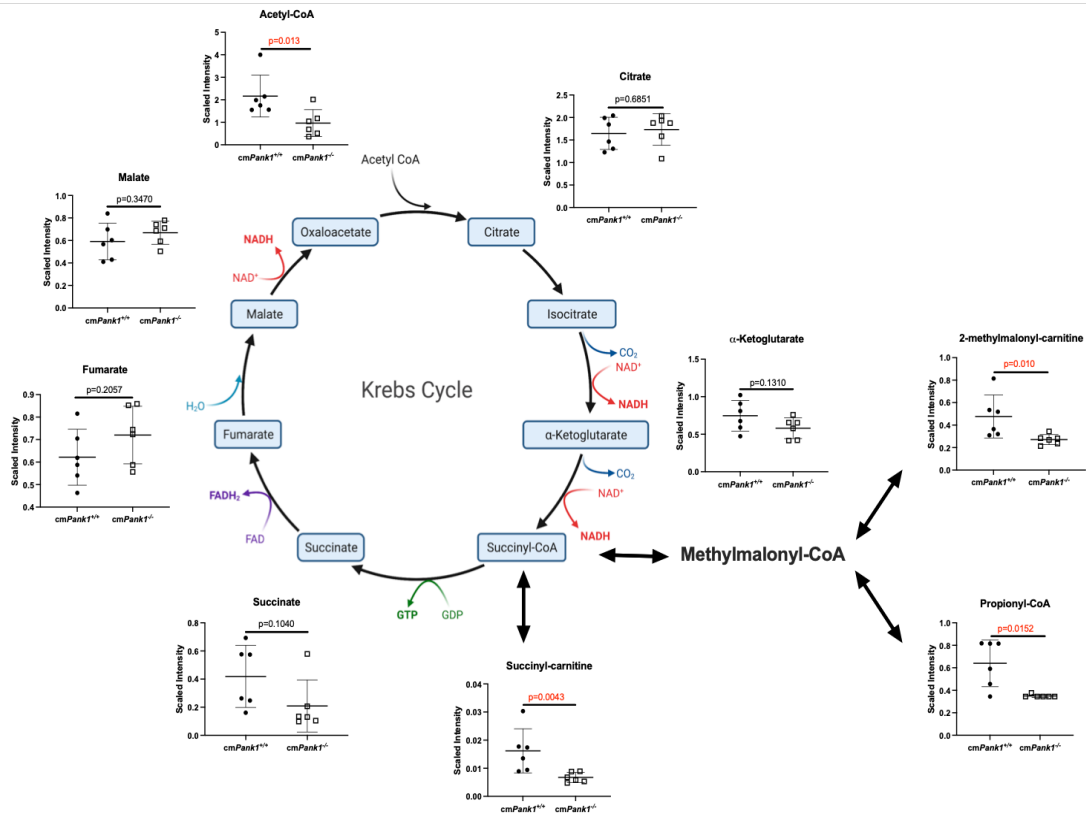
Figure 17: Succinyl-CoA precursors are decreased 2 wk post-TAC. Unbiased metabolomics analysis of metabolites involved in the citric acid cycle. An unpaired Student's t test was used to determine significant differences between cm$Pank1^{+/+}$ and cm$Pank1^{-/-}$ hearts.

We next examined the impact of *Pank1* deletion on acyl-carnitines. Interestingly, beta-hydroxyisovaleroyl-carnitine, 2-methylbutyryl-carnitine, and lignoceroyl-carnitine were significantly elevated while methylsuccinoyl-carnitine, succinyl-carnitine, and 2 methylmalonyl-carnitine were significantly downregulated in naïve hearts (Figure 18).
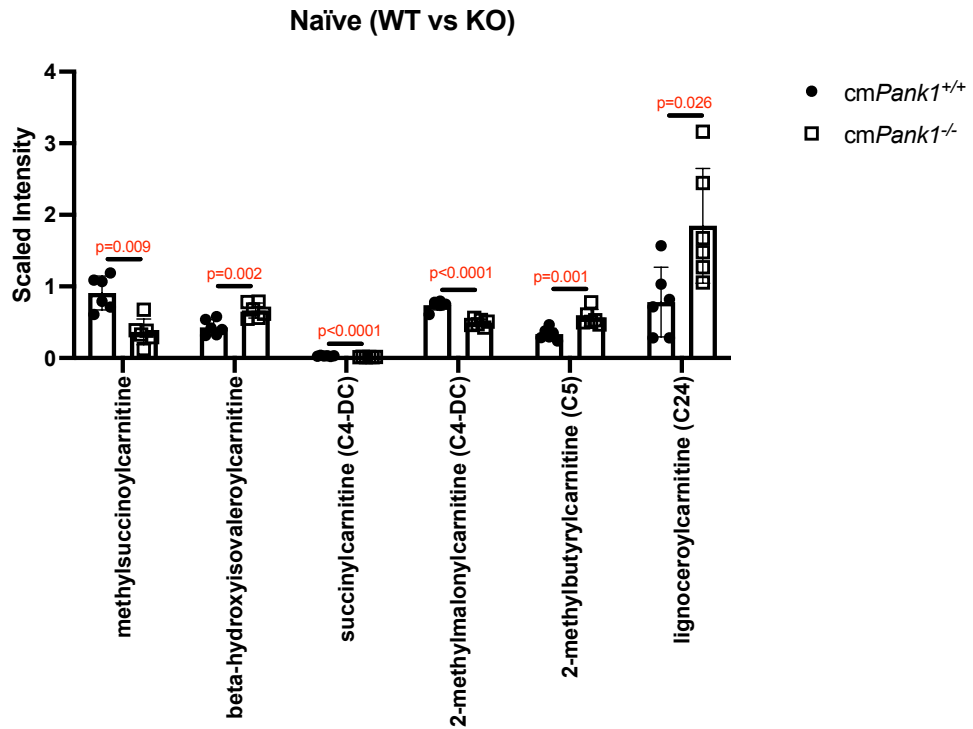
Figure 18: Acyl-carnitines levels as a result of *Pank1* deletion in naïve cm*Pank1*^{+/+} and cm*Pank1*^{-/-} hearts. We plotted acyl-carnitine levels in naïve cm*Pank1*^{+/+} and cm*Pank1*^{-/-} hearts from our metabolomics data. An unpaired Student's *t* test was used to determine significant differences between cm*Pank1*^{+/+} and cm*Pank1*^{-/-} hearts.

However, during TAC, *Pank1* deletion resulted in significant accumulation of acyl-carnitines, including, isobutyryl-carnitine, butenoyl-carnitine, isovaleryl-carnitine, tigly-carnitine, 2-methylbutyryl-carnitine, arachidoyl-carnitine, eicosenoyl-carnitine, behenoyl-carnitine, erucoyl-carnitine, lignoceroyl-carnitine, and nervonoyl-carnitine. Interestingly, consistent with our naïve data, succinyl-carnitine and 2-methylmalonyl-carnitine were significantly downregulated (Figure 19).
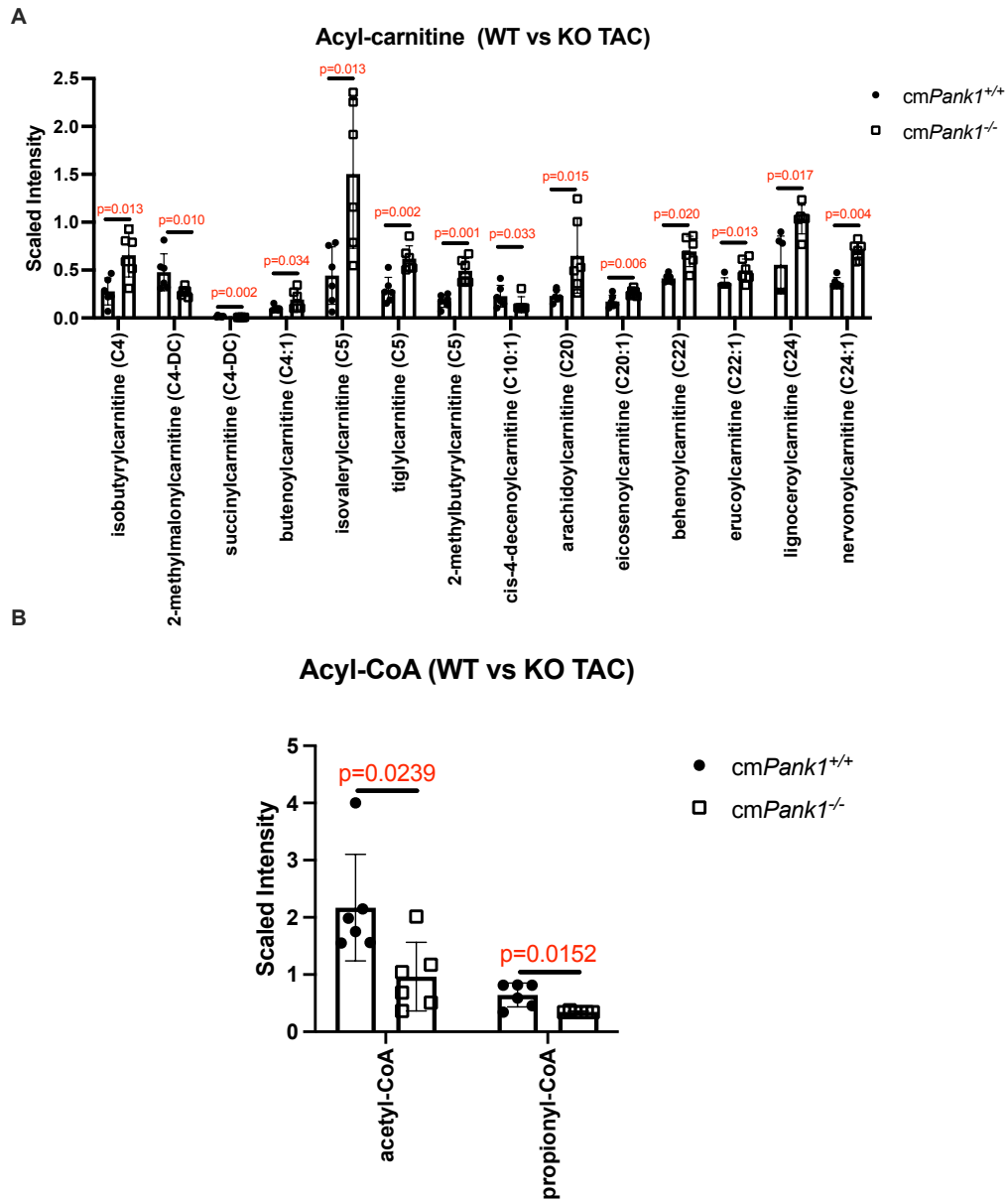
Figure 19: Acyl-carnitines accumulate in *Pank1* deficient hearts 2 wk post-TAC. We plotted acyl-carnitine and acyl-CoA levels in cm*Pank1*^+/+^ and cm*Pank1*^-/-^ hearts subjected to TAC from metabolomics data. **A)** Acyl-carnitine levels. **B)** Acyl-CoA levels. An unpaired Student's *t* test was used to determine significant differences between cm*Pank1*^+/+^ and cm*Pank1*^-/-^ hearts.

Finally, during TAC, *Pank1* deletion led to significant elevation of metabolites involved in tissue remodeling including 4-hydroxycinnamate sulfate, 4-methylcatechol sulfate, proline, ornithine, arginosuccinate, and 2'-AMP were significantly elevated during TAC as a result of *Pank1* deletion among other metabolites (Table 7). Collectively, these data suggest that *Pank1* deletion results to significant changes to metabolites associated with energy metabolism, substrate utilization and tissue remodeling early during pressure overload.

Table 7: Changes in metabolites in cm*Pank1*^{-/-} hearts subjected to TAC for 2 wk compared to cm*Pank1*^{+/+} hearts.

SN	Metabolites	FC	log2(FC)	raw.pval	-LOG10(p)
1	1-carboxyethylisoleucine	2.0414	1.0295	0.00828	2.082
2	1-carboxyethylleucine	2.3944	1.2596	0.006948	2.1582
3	1-carboxyethylphenylalanine	2.3854	1.2542	0.027289	1.564
4	1-carboxyethyltyrosine	2.6304	1.3953	0.034159	1.4665
5	1-carboxyethylvaline	2.029	1.0208	0.007955	2.0993
6	1,2,3-benzenetriol sulfate 2	4.0938	2.0334	0.0299	1.5243
7	12-HETE	2.5856	1.3705	0.023747	1.6244
8	2-aminophenol sulfate	2.1402	1.0977	0.014811	1.8294
9	2-methylbutyrylcarnitine C5	2.7862	1.4783	0.000524	3.2809
10	2-methylmalonylcarnitine C4-DC	0.57466	-0.79922	0.010226	1.9903
11	2-myristoylglycerol 140	0.63426	-0.65685	0.043635	1.3602
12	2-palmitoleoylglycerol 161	0.59709	-0.74397	0.023014	1.638
13	2-stearoyl-GPE 180	1.7086	0.77284	0.032673	1.4858
14	2'-AMP	2.1172	1.0821	0.041532	1.3816
15	3-hydroxyisobutyrate	1.794	0.84316	0.018749	1.727
16	3-hydroxypyridine sulfate	2.5197	1.3333	0.01192	1.9237
17	4-ethylcatechol sulfate	2.0958	1.0675	0.025339	1.5962
18	4-hydroxycinnamate sulfate	3.3515	1.7448	0.01444	1.8404
19	4-methylcatechol sulfate	5.4835	2.4551	0.023925	1.6211
20	4-vinylcatechol sulfate	2.4886	1.3154	0.007228	2.141
21	5-KETE	0.16576	-2.5928	0.044077	1.3558
22	5-methyluridine ribothymidine	1.914	0.93663	0.045319	1.3437
23	6-oxopiperidine-2-carboxylate	1.5423	0.62509	0.029281	1.5334
24	8-hydroxyoctanoate	0.41793	-1.2587	0.030929	1.5096
25	9,10-DiHOME	2.0503	1.0359	0.004046	2.393
26	acetyl-CoA	0.44301	-1.1746	0.012633	1.8985
27	arachidoylcarnitine C20	3.1064	1.6352	0.015598	1.8069
28	argininosuccinate	1.9047	0.92958	0.014225	1.8469
29	behenoylcarnitine C22	2.2536	1.1722	0.020207	1.6945
30	beta-hydroxyisovaleroylcarnitine	1.6245	0.69996	0.006692	2.1745
31	butenoylcarnitine C41	2.4825	1.3118	0.034265	1.4652
32	catechol sulfate	1.7994	0.84753	0.02936	1.5322
33	cis-4-decenoylcarnitine C101	0.35269	-1.5035	0.033558	1.4742
34	CoA-glutathione	0.52296	-0.93523	0.000251	3.6006
35	eicosenoylcarnitine C201	1.5531	0.63519	0.00611	2.214
36	erucoylcarnitine C221	3.0025	1.5862	0.012851	1.891
37	erythronate	1.5403	0.6232	0.010343	1.9854
38	ferulic acid 4-sulfate	3.1054	1.6348	0.022199	1.6537
39	gamma-glutamyl-epsilon-lysine	2.09	1.0635	0.021983	1.6579
40	gamma-glutamyltyrosine	1.5961	0.67453	0.041342	1.3836
41	hippurate	2.3923	1.2584	0.004624	2.335
42	indoleacetylglycine	2.9985	1.5842	0.013157	1.8809
43	isobutyrylcarnitine C4	2.3765	1.2488	0.013018	1.8855
44	isovalerylcarnitine C5	3.4936	1.8047	0.013188	1.8798
45	kynurenate	1.9006	0.92644	0.002092	2.6794
46	lignoceroylcarnitine C24	2.1429	1.0996	0.017797	1.7496
47	N-acetylmethionine	1.5539	0.63586	0.004569	2.3402
48	N-ADP-ribosyl-arginine 1	0.48371	-1.0478	0.029098	1.5361
49	N-ADP-ribosyl-arginine 2	0.44708	-1.1614	0.023794	1.6235
50	N-carbamoylaspartate	1.8454	0.88396	0.014717	1.8322
51	N-palmitoyl-sphinganine d180/160	2.1357	1.0947	0.039042	1.4085
52	N-palmitoylglycine	0.65397	-0.6127	0.021714	1.6633
53	N2-acetyllysine	1.5218	0.60574	0.020353	1.6914
54	nervonoylcarnitine C241	2.998	1.584	0.004229	2.3738
55	O-sulfo-L-tyrosine	1.5558	0.6377	0.002179	2.6617
56	ornithine	1.702	0.76725	0.007365	2.1328
57	orotate	2.2234	1.1527	0.031294	1.5045
58	pantetheine	0.24844	-2.009	0.000668	3.1755
59	phenylpropionylglycine	2.617	1.3879	0.035383	1.4512
60	proline	1.5682	0.64911	0.001213	2.9161
61	propionyl CoA	0.21282	-2.2323	0.006837	2.1651
62	R-3-hydroxybutyrylcarnitine	2.4765	1.3083	0.005883	2.2304
63	sphinganine	1.7126	0.77619	0.017329	1.7612
64	sphingosine	1.5045	0.58926	0.031209	1.5057
65	stachydrine	1.6119	0.68876	0.009102	2.0408
66	succinoyltaurine	0.6254	-0.67715	0.026363	1.579
67	succinylcarnitine C4-DC	0.41977	-1.2523	0.002602	2.5847
68	tiglyl carnitine C5	2.1321	1.0922	0.001894	2.7227
69	trans-urocanate	1.9511	0.96426	0.027943	1.5537
70	urate	1.7872	0.83771	0.016934	1.7712
71	xanthosine	1.5768	0.65697	0.018349	1.7364

Specific Aim 3

Mitochondria isolated from failing hearts have increased acetylation and reduced respirasome.

To assess changes in mitochondrial acetylation and respirasome during HF, mitochondria isolated from failing and non-failing human hearts were assessed by immunoblotting. Compared to non-failing heart (NF), mitochondrial acetylation was significantly increased in failing hearts (HF) (Figure 20A and 20B). This finding is consistent with a previously published study[101]. Several studies suggest an alteration in mitochondria electron transport chain (ETC) during heart failure[159]. To assess the changes in mitochondria respirasome during heart failure, mitochondria isolated from failing and non-failing human hearts were assessed by BN-PAGE analysis. Consistent with increased mitochondria acetylation observed in the failing hearts, mitochondria respirasome were decreased in HF mitochondria compared to non-failing heart mitochondria (Figure 20C and 20D). Collectively, this data suggests that mitochondria isolated from the failing hearts have increased acetylation and reduced respirasomes. Given these observations, we next sought to determine whether acetylation levels directly affect mitochondria bioenergetics and respirasomes.
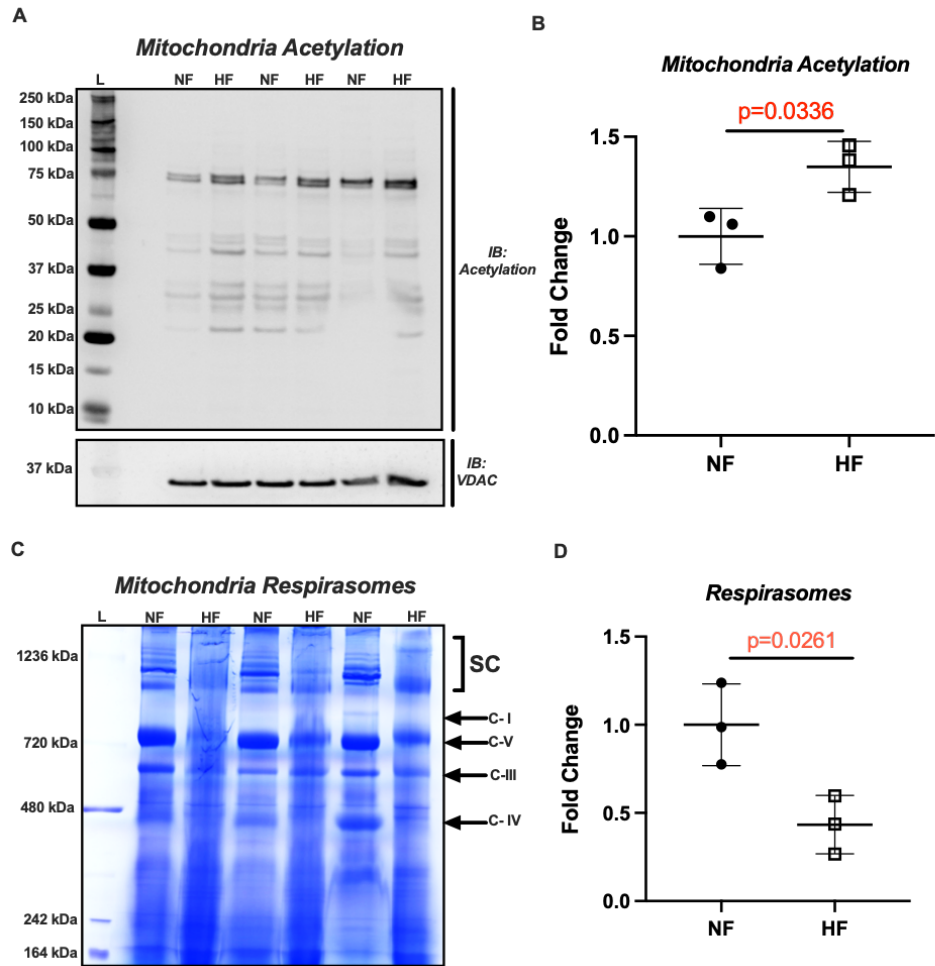
Figure 20: Mitochondria isolated from failing hearts have increased acetylation and reduced respirasomes. **A)** Mitochondrial acetylation in non-failing (NF) and heart failure (HF) hearts. **B)** Quantification of mitochondrial acetylation in non-failing (NF) and heart failure (HF) hearts. **C)** BN-PAGE analysis of mitochondrial respirasome assembly isolated from non-failing (NF) and heart failure (HF) mitochondria. **D)** Quantification of BN-PAGE analysis of mitochondrial respirasome assembly isolated from non-failing (NF) and heart failure (HF) mitochondria. An unpaired Student's *t* test was used to determine significant differences between NF and HF groups.

Mitochondria hyperacetylation suppresses state 3 supported respiration in the presence of complex II and fatty acid oxidation substrates, without affecting state 3 respiration in the presence of complex I substrates.

To determine whether changing mitochondria acetylation directly regulates mitochondria bioenergetics, we induced mitochondria hyperacetylation in isolated mitochondria by acetic anhydride treatment as previously described[160]. Increasing concentration of acetic anhydride induced a concentration dependent increase in mitochondria acetylation (Figure 21A and 21B). Next, to determine whether mitochondrial hyperacetylation affect mitochondria respiratory functions, we measured state 3 respiration in the presence of C-I (pyruvate/malate/ADP), C-II (succinate/rotenone/ADP), and fatty acid oxidation (octanoylcarnithine/malate/ADP) substrates in mitochondria treated with 50 μM of acetic anhydride—to induce hyperacetylation. Compared to vehicle control, we did not observe significant difference in state 3 respiration in the presence of C-I substrates in mitochondria treated with 50 μM of acetic anhydride (Figure 21C). Interestingly, compared to vehicle control, state 3 respiration was suppressed in the presence of complex II and fatty acid oxidation substrates in mitochondria treated with 50 μM of acetic anhydride (Figure 21D-21E). Suggesting that mitochondria hyperacetylation may directly impact C-II respiration and fatty acid oxidation, but not C-I respiration.
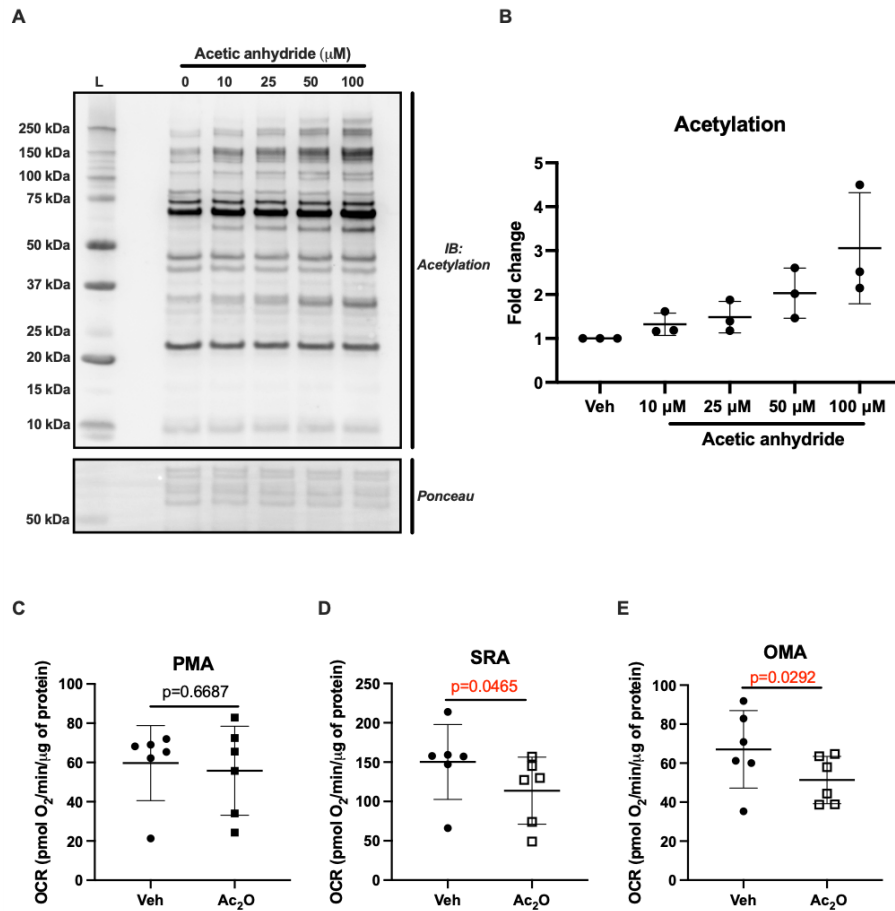
Figure 21: Mitochondrial hyperacetylation suppresses state 3 respiration in the presence of complex II and fatty acid oxidation substrates. Mitochondria hyperacetylation was induced by treating isolated mitochondria with increasing concentrations of Ac_2O and mitochondria function was assessed by extracellular flux analysis. **A)** Concentration dependent induction of mitochondrial hyperacetylation by Ac_2O treatment. **B)** Quantification of mitochondrial acetylation by Ac_2O treatment. **C)** Assessing state 3 respiration using pyruvate, malate and ADP (PMA) as complex I substrates. **D)** Assessing state 3 respiration using succinate, rotenone and ADP (SRA) as complex II substrates. **E)** Assessing medium chain fatty acid oxidation supported state 3 respiration using octanoylcarnitine, malate and ADP (OMA) as substrate. An unpaired Student's *t* test was used to determine significant differences between vehicle and Ac_2O treated groups.

Mitochondrial acetylation alone does not affect supercomplexes.

To determine whether changing mitochondria acetylation directly regulates mitochondria bioenergetics, mitochondria from cm*Pank1*$^{-/-}$—which have reduced mitochondrial acetylation—were isolated and analyzed BN-PAGE. We did not observe any significant changes to mitochondria supercomplexes when we limit mitochondria acetylation (Figure 22A and 22B). Furthermore, to assess the impact of mitochondria hyperacetylation on respirasome, isolated mitochondria were treated with 50 μM of acetic anhydride to induce mitochondria hyperacetylation and respirasome was assessed by BN-PAGE. Compared to vehicle treated hearts, mitochondrial hyperacetylation alone does not appear to impair mitochondrial respirasome (Figure 22C).
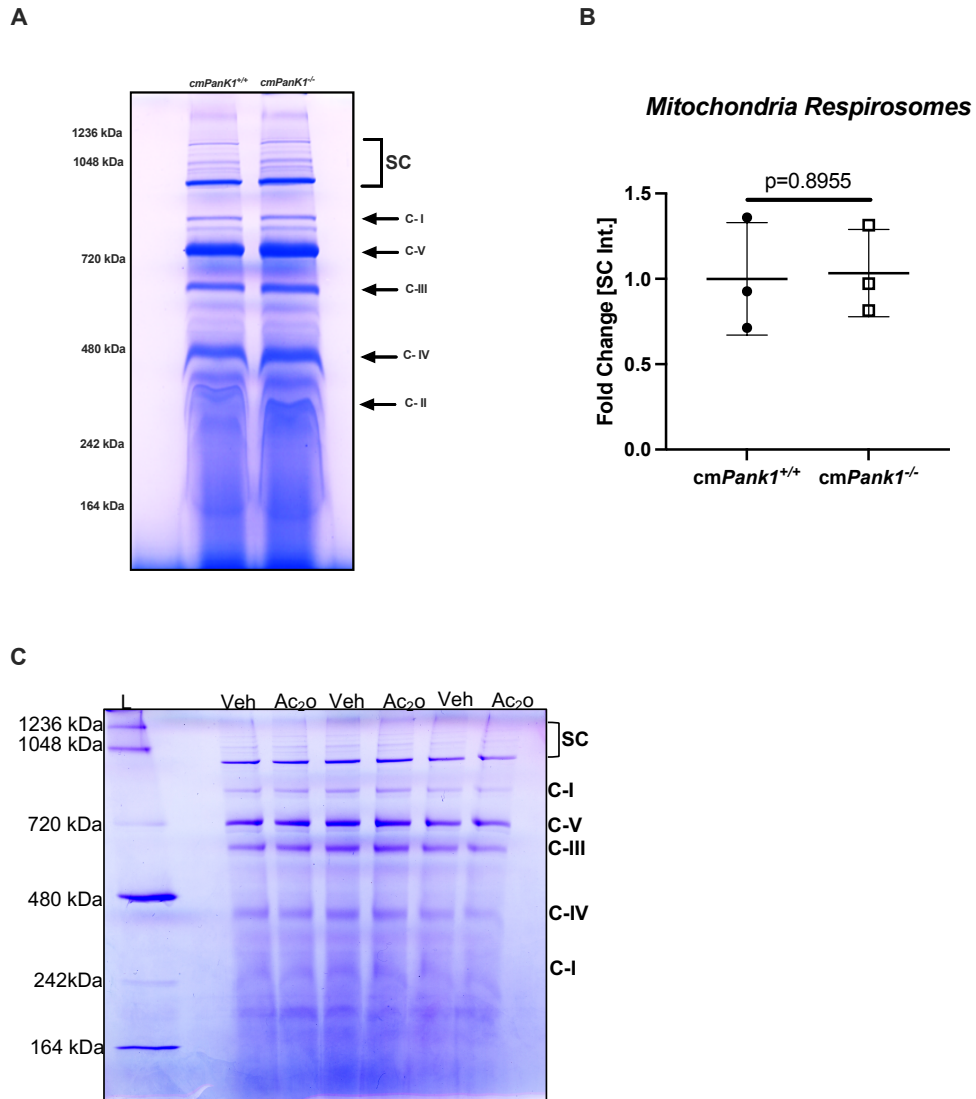
Figure 22: Changing acetylation alone does not impact mitochondrial respirasomes. A) BN-PAGE analysis of mitochondrial proteins isolated from cm*Pank1*^{-/-} hearts. **B)** Quantification BN-PAGE analysis of mitochondrial proteins isolated from cm*Pank1*^{-/-} hearts. **C)** BN-PAGE analysis of mitochondrial proteins isubjected to hyperacetylation. An unpaired Student's *t* test was used to determine significant differences when comparing groups.

CHAPTER V

DISCUSSION

Recent studies have associated elevated acetyl-CoA levels with heart failure in humans[19]. This association, in part, may involve enhanced acetylation, which is thought to promote pathology. Several studies suggest that elevated acetyl-CoA may promote enzyme independent acetylation of cardiac and mitochondrial proteins[161, 162], contributing to mitochondria dysfunction[67, 163-165]. Here, we sought to limit CoA levels to curb excessive acetylation during heart failure. We hypothesized that deleting *Pank1* will limit available CoA pools, which would limit acetylation and thereby attenuate ventricular remodeling during pressure overload. Our results show that although constitutive, cardiomyocyte restricted *Pank1* deletion decreased acetyl-CoA levels during TAC, this intervention exacerbated ventricular remodeling during pressure overload. Lastly, our results suggest that metabolic alterations, rather than structural alterations associated with *Pank1* deletion, may underlie the exacerbated cardiac phenotype during pressure overload.

Acetylation of cardiac proteins has been associated with a decline in mitochondria function[67, 163-166]; however, recent studies have challenged the deleterious nature of mitochondrial hyperacetylation[167]. Although we hypothesized that targeting enzyme independent acetylation would be beneficial, our data suggest that metabolic changes, rather than CoA-driven enzyme independent acetylation, may be more important in the context of heart failure. It is, therefore, possible that hyperacetylation may not be deleterious because our attempt to limit acetylation did not improve cardiac function. More

77

importantly, the intervention of deleting *Pank1* did not impact only acetylation; it likely impacted other metabolic events following TAC.

Additionally, although studies have linked other enzyme dependent mechanisms, such as sirtuins and NAD^+ to protein hyperacetylation[101, 143], others suggest that mitochondrial acetylation is largely enzyme independent and depends on the availability of substrates such as acetyl-CoA[161, 162]—hence our rationale to limit acetyl-CoA. Yet, we did not observe significant transcriptional changes in SIRT3 or NAD^+, suggesting that our method of limiting mitochondrial acetylation may be independent of SIRT3 and NAD^+ pathway.

To explore more proximal metabolic relationships to explain why *Pank1* deletion may have exacerbated heart failure, we focused on potential impacts at the level of intermediary metabolism. One prominent observation from our studies is the dysregulation of metabolites in the ketone body pathway because of *Pank1* deletion. The failing heart may at least partially rely on ketones for energy[168, 169]. Our metabolomics data suggest suppressed oxidation of ketones as indicated by elevated 3-hydroxybutyrate at baseline and during TAC, and significant reduction in precursors required for succinyl-CoA synthesis such as propionyl-CoA, acetyl-CoA, succinyl-carnitine, and methylmalonyl-carnitine. Although our metabolomics data did not detect levels of succinyl-CoA during TAC, we can speculate from our data that succinyl-CoA may be limiting. Because succinyl-CoA is required for the transfer of CoA during ketone body oxidation (during the conversion of acetoacetate to acetoacetate-CoA by SCOT1), an intervention potentially limiting succinyl-CoA levels may be suppressing a shift to ketones as a source of energy during heart failure. In other words, it is possible that limiting CoA pools impinged on the ability of cardiomyocyte to utilize ketone bodies for fuel, due to shortfall of metabolites required

to oxidize ketones. Thus, given that ketone body utilization is inadequate in the failing heart, it is possible that *Pank1* deletion further exacerbated this energetic crisis.

The impact of *Pank1* deletion on acyl-carnitine levels was also assessed. Interestingly, *Pank1* deletion resulted in significant accumulation of short, medium, and long chain acyl-carnitine in naïve and TAC animals. Succinyl-carnitine and 2-methylmalonyl-carnitine were significantly downregulated in naïve and TAC animals, strongly suggesting a potential role of CoA in regulating succinyl-carnitine and 2-methylmalonyl-carnitine levels. Additionally, we did not observe any changes in mitochondria structure during TAC as a result of *Pank1* deletion (Figure 23). Suggesting that suppressed substrate utilization, rather than mitochondria dysfunction may be promoting the accumulation of acyl-carnitines as a result of *Pank1* deletion. Our data is consistent with previously published work that suggests that liver CoA depletion resulted in reduced fatty acid oxidation as evident by the accumulation of acyl-carnitines[126]. In summary, our data indicates a role of cardiac CoA in regulation fatty acid oxidation.

A

cm*Pank1*^{+/+}

cm*Pank1*^{-/-}

B
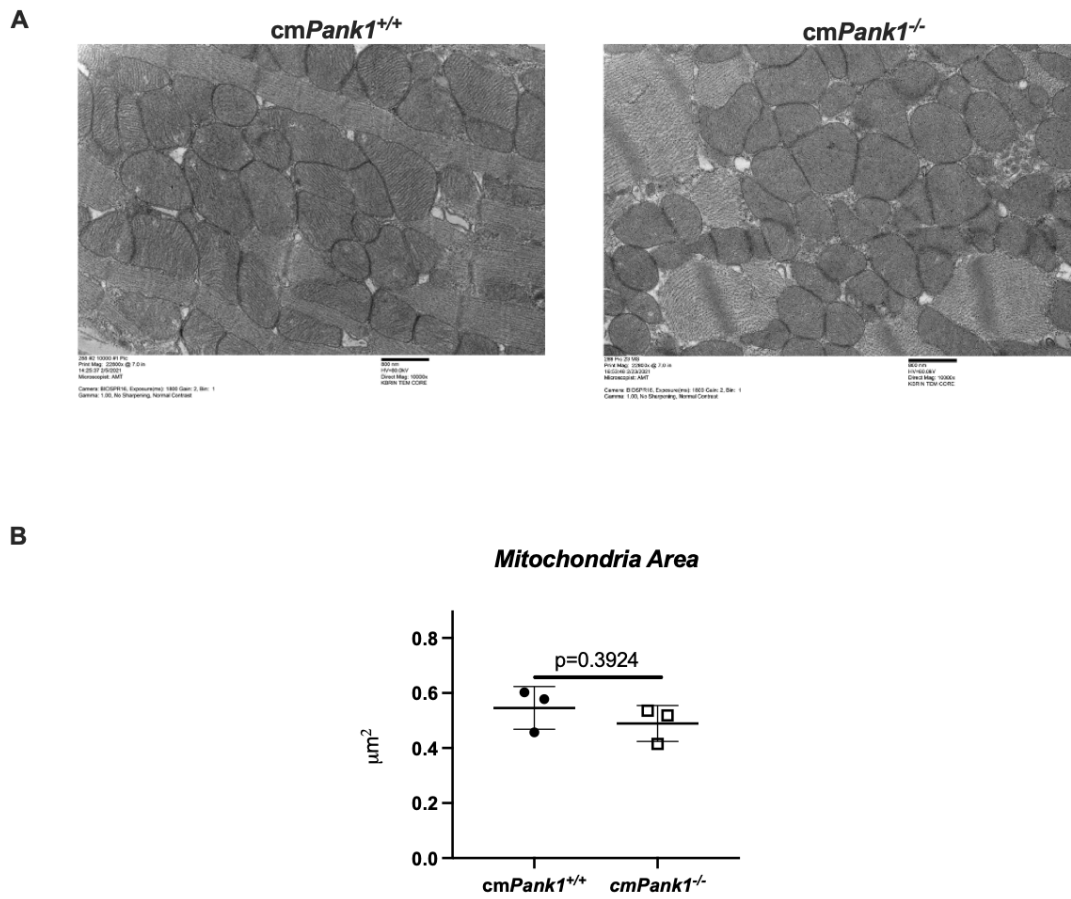
Mitochondria Area

Figure 23: Mitochondria size is not affected as a result of *Pank1* deletion. A) TEM images of mitochondria. **B)** Quantification of mitochondria area. An unpaired Student's *t* test was used to determine significant differences between cm*Pank1*^{+/+} and cm*Pank1*^{-/-} hearts.

Furthermore, studies have shown that acyl-CoA pools are decreased, and that preserving acyl-CoA availability attenuates pathological and metabolic remodeling[170]. Unfortunately, our platform did not provide broad coverage of significantly changed acyl-carnitine and acyl-CoA metabolites in WT mice. Nevertheless, our intervention to limit acetyl-CoA in cardiomyocytes by *Pank1* deletion minimally impacted the overall cardiac acyl-CoA pool (of those for which we had coverage) at baseline and following TAC—with the exception of acetyl-CoA.

The group differences in ventricular dimensions prompted us to query a potential impact at the level of fibrosis. Indeed, our pathology data indicated that loss of PANK1 resulted in increased fibrosis during pressure overload. This observation was further corroborated by our unbiased RNA-seq data, which showed upregulation of α-smooth muscle actin (*Acta2*), a marker of myofibroblast activation, indicating that *Pank1* deletion promotes a myofibroblast phenotype in the heart during pressure overload. Furthermore, *Pank1* deletion also resulted in increased mRNA expression of TGF-β family of proteins, including inhibin beta B (*Inhhb*), growth differentiation factor 15 (*Gdf15*), growth differentiation factor 6 (*Gdf6*), and bone morphogenic peptide 10 (*Bmp10*)—some of which have been shown to be involved in fibroblast proliferation, myofibroblast differentiation, myocardial fibrosis, and extracellular matrix protein deposition[171-173]. Interestingly, these data are further supported by GO analyses, which suggest that *Pank1* deletion upregulates genes involved in positive regulation of fibroblast proliferation. Additionally, *Pank1* deletion also upregulated genes of extracellular matrix (ECM) remodeling proteins, including, fibrilin-2 (*Fbn2*), arylsulfatase I (*Arsi*), tenascin C (*Tnc*), elastin (*Eln*), neuron derived neurotrophic factor (*Ndnf*), tissue inhibitor of metalloproteinases 1 (*Timp1*), and ADAM metallopeptidase with thrombospondin type 1 motif 4 (*Adamts4*). Upregulation of these

enzymes has been implicated in a variety of cardiac fibrotic and inflammatory responses [174-177]. These data were further supported by our metabolomics data indicating differential abundances in metabolites involved in collagen metabolism, including proline and arginosuccinate—a precursor for arginine. Collectively, these data suggest a role of CoA metabolism in regulating fibrosis and collagen turnover in the heart. However, it is possible that other changes occurred upstream of this enhanced fibrotic response to contribute to this observed fibrotic phenotype. Nevertheless, whether a more direct relationship exists between intracellular CoA metabolism and the fibrotic response in the heart is intriguing and will be pursued in future studies.

Coincident with changes in acetylation levels during heart failure, the stoichiometry of the mitochondrial respirasome is changed[99]; these changes are associated with a decline in mitochondrial energetics[99, 178]. Nevertheless, the question of whether changes in mitochondrial acetylation levels directly affect respirasome and mitochondrial function was one of the questions we asked. Our results suggest that limiting mitochondria acetylation does not affect mitochondrial dynamics, function, and respirasomes. Additionally, although we did not observe changes to mitochondrial respirasomes when we induced mitochondrial hyperacetylation, our data suggest that hyperacetylation may suppress complex II and fatty acid supported respiration. This is consistent with previously published studies[101, 179]. Horton et al.[15] recently showed that succinate dehydrogenase (SDHA)—a key in both the TCA cycle and respiratory C-II—is acetylated at multiple sites with heart failure in human and mice. Furthermore, Horton et al.[15] also showed that directly increasing acetylation of SDHA—using an acetyl-mimetic point mutation—was sufficient to suppress C-II respiratory functions. Consistent with suppressed state 3 respiration with hyperacetylation in the presence of C-II substrates, our data also suggest that state 3 respiration in the presence of fatty acid is also suppressed. However, we did not observe

any significant difference in state 3 respiration in the presence of C-I substrates. Conversely, limiting mitochondria acetylation does not impact overall mitochondria energetics and dynamics. Collectively, our data suggest that acetylation of mitochondrial proteins may play a minimal role in the assembly of respirasomes. Also, our results suggest that hyperacetylation of mitochondria proteins alone may be sufficient to impact mitochondria respiratory functions.

In terms of rigor and reproducibility, this study was planned, blinded, and appropriately controlled. Furthermore, this study used both male and female mice, both of which responded similarly to *Pank1* deletion in response to pressure overload. We have frequently used the TAC model of heart failure and are able to create consistent stenoses in adult mice. Our approach of using cell type-specific ablation of *Pank1* has several issues worthy of consideration. In terms of advantages, our approach avoids the broad, systemic effects of administering a PANK inhibitor. Such an inhibitor would impact other organs, including the liver, and, if sufficiently potent, would completely eliminate CoA levels; this, of course, would be incompatible with life. Deleting only one of the PANK isoforms partially limited CoA pools allowing us to test our hypothesis. Although there are two other PANK isoforms, we did not observe compensation at the level of mRNA of *Pank2* or *Pank3*.

CHAPTER VI

SUMMARY AND FUTURE DIRECTION

Heart failure is characterized by hyperacetylation of mitochondrial proteins[101]. Because studies have shown that increased acetylation levels in tissues such as the heart, liver, and skeletal muscle correlate with a decline in oxidative phosphorylation[67, 163-165], we tested the question of whether limiting mitochondrial acetylation will be beneficial during heart failure. Because both N-α-acetylation and N-ε-acetylation depends on the availability of acetyl-CoA, and synthesis of acetyl-CoA is partly dependent on the availability of an acyl carrier—Coenzyme A (CoA)[39], we sought to restrict cardiac mitochondria acetylation by limiting CoA levels (via *Pank1* deletion). Our results show that CoA depletion limited overall mitochondrial acetylation compared to controls. Furthermore, results show that although limiting mitochondria acetylation minimally affects cardiac function at baseline, cardiac dysfunction was exacerbated during pressure overload compared to the control.

Because limiting mitochondrial acetylation exacerbated cardiac function, we next assessed the impact of *Pank1* deletion on other endpoints of ventricular remodeling. At baseline, limiting mitochondrial acetylation did not affect fibrosis, hypertrophy, and vascular density. However, our data suggest that limiting mitochondria acetylation exacerbates cardiac fibrosis without affecting myocyte hypertrophy and vascular density during TAC. To identify possible mechanisms contributing to increased fibrosis and exacerbated cardiac function associated with limiting mitochondrial acetylation during TAC, we performed RNA-seq analysis during TAC. Interestingly, limiting mitochondria

acetylation via *Pank1* deletion resulted in the downregulation of genes involved in various metabolic and fibrotic processes, including metabolites involved in ketone body, fatty acid, and tissue remodeling.

We also investigated whether changing mitochondrial acetylation alone—i.e., increasing or decreasing acetylation—was sufficient to induce mitochondrial dysfunction. Our results suggest that mitochondrial hyperacetylation suppresses state 3 respiration in the presence of C-II substrates and fatty acids compared to vehicle controls. Collectively, our results suggest that hyperacetylation of mitochondria proteins alone may be sufficient to impact mitochondria respiratory functions.

Coincident with elevated mitochondria acetylation levels during heart failure, the stoichiometry of the mitochondrial respirasome is changed[99]; these changes are associated with a decline in mitochondrial energetics[99, 178]. We then sought to determine whether changing mitochondria acetylation alone was sufficient to impact respirasomes. Although our results show that mitochondrial respirasome is destabilized in human failing hearts, inducing hyperacetylations by acetic anhydride treatment did not sufficiently impact respirasomes. Similarly, limiting mitochondrial acetylation did not impact respirasomes. Suggesting that changing acetylation alone does not influence respirasome assembly.

To briefly summarize, we decreased acetylation by limiting cardiac CoA levels via cardiomyocyte-restricted deletion of *Pank1*, which is the rate-limiting enzyme in CoA biosynthesis. Contrary to our predictions, *Pank1* deletion exacerbated ventricular remodeling. This created a serendipitous opportunity for us to explore why this may have been the case. The results of our exploration suggest that CoA availability may be more

beneficial in terms of sustaining cardiac ketone body metabolism and substrate utilization

(Figure 24A and B). Also, we showed that acetylation alone does not impact mitochondrial

respirasomes.
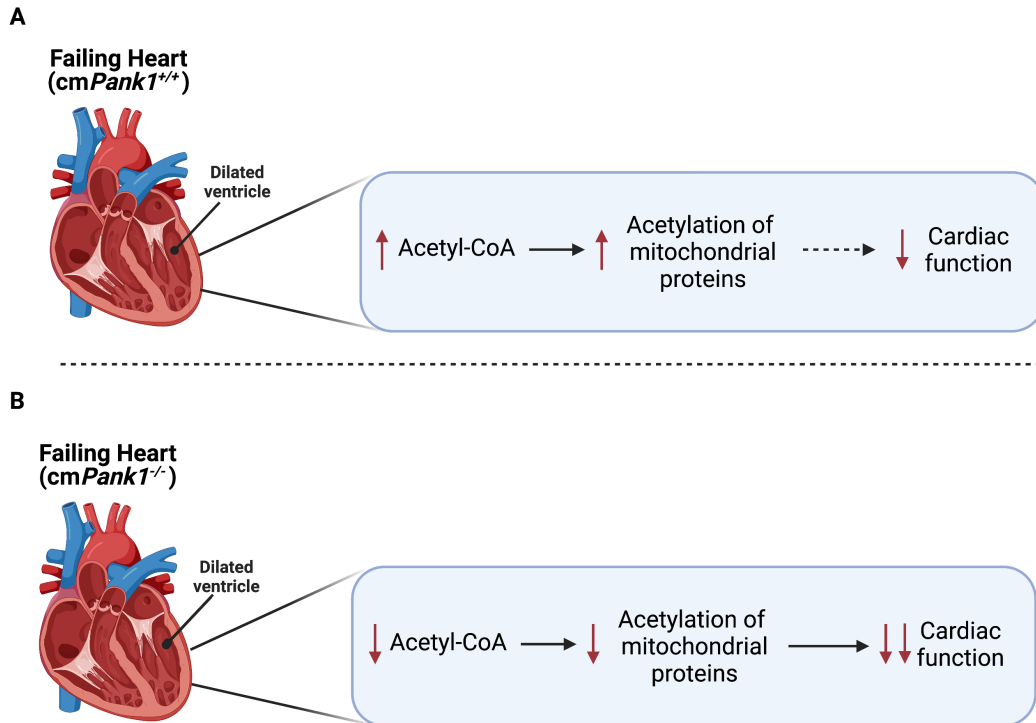
Figure 24: Summary of Findings. Metabolic dysregulation occurring in heart failure promotes accumulation of acetyl-CoA. Acetyl-CoA accumulation can drive enzyme independent acetylation of mitochondrial function and is associated with a decline in cardiac function (Figure 24A). We hypothesized that limiting acetyl-CoA can reduce mitochondrial acetylation and be pro-adaptive during heart failure. We generated a cardiomyocyte-specific *Pank1* deficient mice (cm*Pank1*-/-) as a model of reduced acetyl-CoA. We showed that even though cm*Pank1*-/- have reduced Acetyl-CoA and reduced mitochondrial acetylation, cardiac dysfunction was exacerbated as a result of *Pank1* deletion (Figure 24B).

In terms of potentially translating the present insights, our data argue against a strategy of limiting CoA to limit acetylation. Future studies will investigate the impact of CoA levels on ketone body and fatty acid oxidation during heart failure. We will utilize the *ex vivo* working heart model to investigate the direct impact of increasing or decreasing CoA levels on ketone body and fatty acid oxidation. To deplete cardiac CoA levels, we will utilize or cardiomyocyte specific *Pank1* knockout model (cm*Pank1*$^{-/-}$). Furthermore, we will activate PANK (to increase CoA levels) using a feeding diet containing 75 ppm of pantazine (PZ-3022)—this concentration has been shown to sufficiently activate cardiac PANK and CoA levels[146]. Similarly, we will assess the impact of increasing CoA on cardiac function and remodeling during pressure overload. Given the important role of CoA in regulating intermediary metabolism and substrate utilization in the failing heart as indicated by our data, this study will answer the question of whether increasing CoA is sufficient to improve cardiac function by improving utilization of fatty acid and ketones during pressure overload.

Also, because another pathological feature associated with *Pank1* deletion during heart failure was increased fibrosis, future studies will investigate the link between CoA and fibrosis in the context of heart failure. During heart failure, activated fibroblasts are primarily responsible for initiating fibrotic responses. Because we observed significantly increased fibrosis as a result of cardiomyocyte specific *Pank1* knockout model (cm*Pank1*$^{-/-}$), we speculate that a paracrine mechanism between cardiomyocyte and fibroblast may be regulating this increased fibrosis phenotype. To test this, we will utilize a co-culture technique to test the question of whether secretory factors produced from cardiomyocyte lacking *Pank1* is sufficient to activate fibroblast *in vitro* using co-culture techniques. This future experiment will assess mechanisms by which cardiomyocyte specific *Pank1* deletion contributes to cardiac fibrosis.

Finally, although our data suggest that changing acetylation levels minimally impacts mitochondria supercomplexes, several questions remain unanswered. First, although we successfully depleted acetyl-CoA (which is the driving force for enzyme dependent mitochondrial acetylation), we did not assess mitochondria acetylation during pressure overload. Assessing acetylation levels in cm$Pank1^{-/-}$ may provide additional insight on the extent to which $Pank1$ deletion may be impacting mitochondrial acetylation compared to its role in regulating cardiac metabolism.

REFERENCES

1.   Virani SS, Alonso A, Benjamin EJ, Bittencourt MS, Callaway CW, Carson AP, Chamberlain AM, Chang AR, Cheng S, Delling FN, Djousse L, Elkind MSV, Ferguson JF, Fornage M, Khan SS, Kissela BM, Knutson KL, Kwan TW, Lackland DT, Lewis TT, Lichtman JH, Longenecker CT, Loop MS, Lutsey PL, Martin SS, Matsushita K, Moran AE, Mussolino ME, Perak AM, Rosamond WD, Roth GA, Sampson UKA, Satou GM, Schroeder EB, Shah SH, Shay CM, Spartano NL, Stokes A, Tirschwell DL, VanWagner LB and Tsao CW. Heart Disease and Stroke Statistics-2020 Update: A Report From the American Heart Association. *Circulation*. 2020;141:e139-e596.
2.   Mensah GA, Mokdad AH, Ford ES, Greenlund KJ and Croft JB. State of disparities in cardiovascular health in the United States. *Circulation*. 2005;111:1233-41.
3.   Benjamin EJ, Muntner P, Alonso A, Bittencourt MS, Callaway CW, Carson AP, Chamberlain AM, Chang AR, Cheng S, Das SR, Delling FN, Djousse L, Elkind MSV, Ferguson JF, Fornage M, Jordan LC, Khan SS, Kissela BM, Knutson KL, Kwan TW, Lackland DT, Lewis TT, Lichtman JH, Longenecker CT, Loop MS, Lutsey PL, Martin SS, Matsushita K, Moran AE, Mussolino ME, O'Flaherty M, Pandey A, Perak AM, Rosamond WD, Roth GA, Sampson UKA, Satou GM, Schroeder EB, Shah SH, Spartano NL, Stokes A, Tirschwell DL, Tsao CW, Turakhia MP, VanWagner LB, Wilkins JT, Wong SS and Virani SS. Heart Disease and Stroke Statistics-2019 Update: A Report From the American Heart Association. *Circulation*. 2019;139:e56-e528.
4.   Fryar CD, Chen TC and Li X. Prevalence of uncontrolled risk factors for cardiovascular disease: United States, 1999-2010. *NCHS Data Brief*. 2012:1-8.
5.   Mosterd A, Cost B, Hoes AW, de Bruijne MC, Deckers JW, Hofman A and Grobbee DE. The prognosis of heart failure in the general population: The Rotterdam Study. *European heart journal*. 2001;22:1318-27.
6.   Neubauer S. The failing heart--an engine out of fuel. *N Engl J Med*. 2007;356:1140-51.
7.   Gibb AA and Hill BG. Metabolic Coordination of Physiological and Pathological Cardiac Remodeling. *Circulation research*. 2018;123:107-128.
8.   Taegtmeyer H, Lam T and Davogustto G. Cardiac Metabolism in Perspective *Comprehensive Physiology*: 1675-1699.
9.   Allard MF, Schönekess BO, Henning SL, English DR and Lopaschuk GD. Contribution of oxidative metabolism and glycolysis to ATP production in hypertrophied hearts. *Am J Physiol*. 1994;267:H742-50.
10.   Akki A, Smith K and Seymour A-ML. Compensated cardiac hypertrophy is characterised by a decline in palmitate oxidation. *Molecular and Cellular Biochemistry*. 2008;311:215-224.
11.   Barger PM and Kelly DP. Fatty Acid Utilization in the Hypertrophied and Failing Heart: Molecular Regulatory Mechanisms. *The American Journal of the Medical Sciences*. 1999;318:36-42.
12.   Taegtmeyer H, Sen S and Vela D. Return to the fetal gene program: a suggested metabolic link to gene expression in the heart. *Ann N Y Acad Sci*. 2010;1188:191-198.
13.   Sorokina N, O'Donnell JM, McKinney RD, Pound KM, Woldegiorgis G, LaNoue KF, Ballal K, Taegtmeyer H, Buttrick PM and Lewandowski ED. Recruitment of compensatory pathways to sustain oxidative flux with reduced carnitine palmitoyltransferase I activity characterizes inefficiency in energy metabolism in hypertrophied hearts. *Circulation*. 2007;115:2033-41.

14.   Sansbury BE, DeMartino AM, Xie Z, Brooks AC, Brainard RE, Watson LJ, DeFilippis AP, Cummins TD, Harbeson MA, Brittian KR, Prabhu SD, Bhatnagar A, Jones SP and Hill BG. Metabolomic analysis of pressure-overloaded and infarcted mouse hearts. *Circ Heart Fail*. 2014;7:634-42.

15.   Sun H, Olson KC, Gao C, Prosdocimo DA, Zhou M, Wang Z, Jeyaraj D, Youn JY, Ren S, Liu Y, Rau CD, Shah S, Ilkayeva O, Gui WJ, William NS, Wynn RM, Newgard CB, Cai H, Xiao X, Chuang DT, Schulze PC, Lynch C, Jain MK and Wang Y. Catabolic Defect of Branched-Chain Amino Acids Promotes Heart Failure. *Circulation*. 2016;133:2038-49.

16.   Wang W, Zhang F, Xia Y, Zhao S, Yan W, Wang H, Lee Y, Li C, Zhang L, Lian K, Gao E, Cheng H and Tao L. Defective branched chain amino acid catabolism contributes to cardiac dysfunction and remodeling following myocardial infarction. *Am J Physiol Heart Circ Physiol*. 2016;311:H1160-h1169.

17.   Lewis GD, Wei R, Liu E, Yang E, Shi X, Martinovic M, Farrell L, Asnani A, Cyrille M, Ramanathan A, Shaham O, Berriz G, Lowry PA, Palacios IF, Taşan M, Roth FP, Min J, Baumgartner C, Keshishian H, Addona T, Mootha VK, Rosenzweig A, Carr SA, Fifer MA, Sabatine MS and Gerszten RE. Metabolite profiling of blood from individuals undergoing planned myocardial infarction reveals early markers of myocardial injury. *J Clin Invest*. 2008;118:3503-3512.

18.   Lai L, Leone TC, Keller MP, Martin OJ, Broman AT, Nigro J, Kapoor K, Koves TR, Stevens R, Ilkayeva OR, Vega RB, Attie AD, Muoio DM and Kelly DP. Energy metabolic reprogramming in the hypertrophied and early stage failing heart: a multisystems approach. *Circ Heart Fail*. 2014;7:1022-31.

19.   Bedi KC, Jr., Snyder NW, Brandimarto J, Aziz M, Mesaros C, Worth AJ, Wang LL, Javaheri A, Blair IA, Margulies KB and Rame JE. Evidence for Intramyocardial Disruption of Lipid Metabolism and Increased Myocardial Ketone Utilization in Advanced Human Heart Failure. *Circulation*. 2016;133:706-16.

20.   Aubert G, Martin OJ, Horton JL, Lai L, Vega RB, Leone TC, Koves T, Gardell SJ, Krüger M, Hoppel CL, Lewandowski ED, Crawford PA, Muoio DM and Kelly DP. The Failing Heart Relies on Ketone Bodies as a Fuel. *Circulation*. 2016;133:698-705.

21.   Deng N, Zhang J, Zong C, Wang Y, Lu H, Yang P, Wang W, Young GW, Wang Y, Korge P, Lotz C, Doran P, Liem DA, Apweiler R, Weiss JN, Duan H and Ping P. Phosphoproteome analysis reveals regulatory sites in major pathways of cardiac mitochondria. *Mol Cell Proteomics*. 2011;10:M110.000117.

22.   Zhang Z, Tan M, Xie Z, Dai L, Chen Y and Zhao Y. Identification of lysine succinylation as a new post-translational modification. *Nat Chem Biol*. 2011;7:58-63.

23.   Hart GW, Slawson C, Ramirez-Correa G and Lagerlof O. Cross talk between O-GlcNAcylation and phosphorylation: roles in signaling, transcription, and chronic disease. *Annu Rev Biochem*. 2011;80:825-58.

24.   Papanicolaou KN, O'Rourke B and Foster DB. Metabolism leaves its mark on the powerhouse: recent progress in post-translational modifications of lysine in mitochondria. *Front Physiol*. 2014;5:301.

25.   Fukuda H, Sano N, Muto S and Horikoshi M. Simple histone acetylation plays a complex role in the regulation of gene expression. *Brief Funct Genomic Proteomic*. 2006;5:190-208.

26.   Rosca M, Minkler P and Hoppel CL. Cardiac mitochondria in heart failure: normal cardiolipin profile and increased threonine phosphorylation of complex IV. *Biochim Biophys Acta*. 2011;1807:1373-82.

27.   Kim SC, Sprung R, Chen Y, Xu Y, Ball H, Pei J, Cheng T, Kho Y, Xiao H, Xiao L, Grishin NV, White M, Yang XJ and Zhao Y. Substrate and functional diversity of lysine acetylation revealed by a proteomics survey. *Mol Cell*. 2006;23:607-18.

28.	Choudhary C, Kumar C, Gnad F, Nielsen ML, Rehman M, Walther TC, Olsen JV and Mann M. Lysine acetylation targets protein complexes and co-regulates major cellular functions. *Science*. 2009;325:834-40.

29.	Li P, Ge J and Li H. Lysine acetyltransferases and lysine deacetylases as targets for cardiovascular disease. *Nature reviews Cardiology*. 2019.

30.	Gershey EL, Vidali G and Allfrey VG. Chemical studies of histone acetylation. The occurrence of epsilon-N-acetyllysine in the f2a1 histone. *J Biol Chem*. 1968;243:5018-22.

31.	Norris KL, Lee J-Y and Yao T-P. Acetylation goes global: the emergence of acetylation biology. *Sci Signal*. 2009;2:pe76-pe76.

32.	Jenuwein T and Allis CD. Translating the histone code. *Science*. 2001;293:1074-80.

33.	Xu L, Glass CK and Rosenfeld MG. Coactivator and corepressor complexes in nuclear receptor function. *Curr Opin Genet Dev*. 1999;9:140-7.

34.	Piperno G and Fuller MT. Monoclonal antibodies specific for an acetylated form of alpha-tubulin recognize the antigen in cilia and flagella from a variety of organisms. *J Cell Biol*. 1985;101:2085-2094.

35.	L'Hernault SW and Rosenbaum JL. Chlamydomonas alpha-tubulin is posttranslationally modified by acetylation on the epsilon-amino group of a lysine. *Biochemistry*. 1985;24:473-8.

36.	Ringel AE, Tucker SA and Haigis MC. Chemical and Physiological Features of Mitochondrial Acylation. *Molecular cell*. 2018;72:610-624.

37.	Dittenhafer-Reed Kristin E, Richards Alicia L, Fan J, Smallegan Michael J, Fotuhi Siahpirani A, Kemmerer Zachary A, Prolla Tomas A, Roy S, Coon Joshua J and Denu John M. SIRT3 Mediates Multi-Tissue Coupling for Metabolic Fuel Switching. *Cell Metabolism*. 2015;21:637-646.

38.	Svinkina T, Gu H, Silva JC, Mertins P, Qiao J, Fereshetian S, Jaffe JD, Kuhn E, Udeshi ND and Carr SA. Deep, Quantitative Coverage of the Lysine Acetylome Using Novel Anti-acetyl-lysine Antibodies and an Optimized Proteomic Workflow*[S]. *Molecular & Cellular Proteomics*. 2015;14:2429-2440.

39.	Menzies KJ, Zhang H, Katsyuba E and Auwerx J. Protein acetylation in metabolism — metabolites and cofactors. *Nature Reviews Endocrinology*. 2016;12:43-60.

40.	Weinert BT, Iesmantavicius V, Moustafa T, Schölz C, Wagner SA, Magnes C, Zechner R and Choudhary C. Acetylation dynamics and stoichiometry in Saccharomyces cerevisiae. *Mol Syst Biol*. 2014;10:716-716.

41.	Starheim KK, Gevaert K and Arnesen T. Protein N-terminal acetyltransferases: when the start matters. *Trends in Biochemical Sciences*. 2012;37:152-161.

42.	Arnesen T, Van Damme P, Polevoda B, Helsens K, Evjenth R, Colaert N, Varhaug JE, Vandekerckhove J, Lillehaug JR, Sherman F and Gevaert K. Proteomics analyses reveal the evolutionary conservation and divergence of N-terminal acetyltransferases from yeast and humans. *Proceedings of the National Academy of Sciences*. 2009;106:8157.

43.	Bienvenut WV, Sumpton D, Martinez A, Lilla S, Espagne C, Meinnel T and Giglione C. Comparative Large Scale Characterization of Plant versus Mammal Proteins Reveals Similar and Idiosyncratic N-α-Acetylation Features*. *Molecular & Cellular Proteomics*. 2012;11:M111.015131.

44.	Starheim Kristian K, Arnesen T, Gromyko D, Ryningen A, Varhaug Jan E and Lillehaug Johan R. Identification of the human Nα-acetyltransferase complex B (hNatB): a complex important for cell-cycle progression. *Biochemical Journal*. 2008;415:325-331.

45.	Starheim KK, Gromyko D, Evjenth R, Ryningen A, Varhaug JE, Lillehaug JR and Arnesen T. Knockdown of Human N<sup>α</sup>-Terminal Acetyltransferase Complex C Leads to p53-Dependent Apoptosis and Aberrant Human Arl8b Localization. *Molecular and Cellular Biology*. 2009;29:3569.

46.   Evjenth R, Hole K, Karlsen OA, Ziegler M, Arnesen T and Lillehaug JR. Human Naa50p (Nat5/San) Displays Both Protein Nα- and Nε-Acetyltransferase Activity*. *Journal of Biological Chemistry*. 2009;284:31122-31129.

47.   Ciechanover A and Ben-Saadon R. N-terminal ubiquitination: more protein substrates join in. *Trends Cell Biol*. 2004;14:103-6.

48.   Behnia R, Panic B, Whyte JR and Munro S. Targeting of the Arf-like GTPase Arl3p to the Golgi requires N-terminal acetylation and the membrane protein Sys1p. *Nat Cell Biol*. 2004;6:405-13.

49.   Behnia R, Barr FA, Flanagan JJ, Barlowe C and Munro S. The yeast orthologue of GRASP65 forms a complex with a coiled-coil protein that contributes to ER to Golgi traffic. *J Cell Biol*. 2007;176:255-61.

50.   Murthi A and Hopper AK. Genome-wide screen for inner nuclear membrane protein targeting in Saccharomyces cerevisiae: roles for N-acetylation and an integral membrane protein. *Genetics*. 2005;170:1553-60.

51.   Scott DC, Monda JK, Bennett EJ, Harper JW and Schulman BA. N-terminal acetylation acts as an avidity enhancer within an interconnected multiprotein complex. *Science*. 2011;334:674-8.

52.   Sadoul K, Wang J, Diagouraga B and Khochbin S. The Tale of Protein Lysine Acetylation in the Cytoplasm. *Journal of Biomedicine and Biotechnology*. 2011;2011:970382.

53.   Li P, Ge J and Li H. Lysine acetyltransferases and lysine deacetylases as targets for cardiovascular disease. *Nature Reviews Cardiology*. 2020;17:96-115.

54.   Menzies KJ, Zhang H, Katsyuba E and Auwerx J. Protein acetylation in metabolism - metabolites and cofactors. *Nat Rev Endocrinol*. 2016;12:43-60.

55.   Kaelin WG, Jr. and McKnight SL. Influence of metabolism on epigenetics and disease. *Cell*. 2013;153:56-69.

56.   Mittal R, Peak-Chew SY and McMahon HT. Acetylation of MEK2 and I kappa B kinase (IKK) activation loop residues by YopJ inhibits signaling. *Proc Natl Acad Sci U S A*. 2006;103:18574-9.

57.   Mukherjee S, Keitany G, Li Y, Wang Y, Ball HL, Goldsmith EJ and Orth K. Yersinia YopJ acetylates and inhibits kinase activation by blocking phosphorylation. *Science*. 2006;312:1211-4.

58.   Pauly M and Ramírez V. New Insights Into Wall Polysaccharide O-Acetylation. *Frontiers in Plant Science*. 2018;9.

59.   Yang XJ and Grégoire S. Metabolism, cytoskeleton and cellular signalling in the grip of protein Nepsilon - and O-acetylation. *EMBO Rep*. 2007;8:556-62.

60.   Cavdarli S, Delannoy P and Groux-Degroote S. O-acetylated Gangliosides as Targets for Cancer Immunotherapy. *Cells*. 2020;9:741.

61.   Yang X-J and Grégoire S. Metabolism, cytoskeleton and cellular signalling in the grip of protein Nepsilon - and O-acetylation. *EMBO reports*. 2007;8:556-562.

62.   Wagner GR and Payne RM. Widespread and enzyme-independent Nε-acetylation and Nε-succinylation of proteins in the chemical conditions of the mitochondrial matrix. *The Journal of biological chemistry*. 2013;288:29036-29045.

63.   Casey JR, Grinstein S and Orlowski J. Sensors and regulators of intracellular pH. *Nat Rev Mol Cell Biol*. 2010;11:50-61.

64.   Hansford RG and Johnson RN. The steady state concentrations of coenzyme A-SH and coenzyme A thioester, citrate, and isocitrate during tricarboxylate cycle oxidations in rabbit heart mitochondria. *J Biol Chem*. 1975;250:8361-75.

65.   Cai L, Sutter BM, Li B and Tu BP. Acetyl-CoA induces cell growth and proliferation by promoting the acetylation of histones at growth genes. *Mol Cell*. 2011;42:426-37.

66.   Wagner Gregory R and Hirschey Matthew D. Nonenzymatic Protein Acylation as a Carbon Stress Regulated by Sirtuin Deacylases. *Molecular Cell*. 2014;54:5-16.

67.   Davies MN, Kjalarsdottir L, Thompson JW, Dubois LG, Stevens RD, Ilkayeva OR, Brosnan MJ, Rolph TP, Grimsrud PA and Muoio DM. The Acetyl Group Buffering Action of Carnitine Acetyltransferase Offsets Macronutrient-Induced Lysine Acetylation of Mitochondrial Proteins. *Cell Reports*. 2016;14:243-254.

68.   Baeza J, Smallegan MJ and Denu JM. Site-Specific Reactivity of Nonenzymatic Lysine Acetylation. *ACS Chemical Biology*. 2015;10:122-128.

69.   Rock CO, Karim MA, Zhang Y-M and Jackowski S. The murine pantothenate kinase (Pank1) gene encodes two differentially regulated pantothenate kinase isozymes. *Gene*. 2002;291:35-43.

70.   Leonardi R, Zhang YM, Rock CO and Jackowski S. Coenzyme A: back in action. *Prog Lipid Res*. 2005;44:125-53.

71.   Robishaw JD, Berkich D and Neely JR. Rate-limiting step and control of coenzyme A synthesis in cardiac muscle. *J Biol Chem*. 1982;257:10967-72.

72.   Dansie LE, Reeves S, Miller K, Zano SP, Frank M, Pate C, Wang J and Jackowski S. Physiological roles of the pantothenate kinases. *Biochem Soc Trans*. 2014;42:1033-6.

73.   Porter GA, Jr., Hom J, Hoffman D, Quintanilla R, de Mesy Bentley K and Sheu SS. Bioenergetics, mitochondria, and cardiac myocyte differentiation. *Prog Pediatr Cardiol*. 2011;31:75-81.

74.   Yang M, Zhang Y and Ren J. Acetylation in cardiovascular diseases: Molecular mechanisms and clinical implications. *Biochimica et Biophysica Acta (BBA) - Molecular Basis of Disease*. 2020;1866:165836.

75.   Fukushima A, Alrob OA, Zhang L, Wagg CS, Altamimi T, Rawat S, Rebeyka IM, Kantor PF and Lopaschuk GD. Acetylation and succinylation contribute to maturational alterations in energy metabolism in the newborn heart. *Am J Physiol Heart Circ Physiol*. 2016;311:H347-63.

76.   Fukushima A, Zhang L, Huqi A, Lam VH, Rawat S, Altamimi T, Wagg CS, Dhaliwal KK, Hornberger LK, Kantor PF, Rebeyka IM and Lopaschuk GD. Acetylation contributes to hypertrophy-caused maturational delay of cardiac energy metabolism. *JCI Insight*. 2018;3:e99239.

77.   Kawamura T, Ono K, Morimoto T, Wada H, Hirai M, Hidaka K, Morisaki T, Heike T, Nakahata T, Kita T and Hasegawa K. Acetylation of GATA-4 is involved in the differentiation of embryonic stem cells into cardiac myocytes. *J Biol Chem*. 2005;280:19682-8.

78.   Yin N, Lu R, Lin J, Zhi S, Tian J and Zhu J. Islet-1 promotes the cardiac-specific differentiation of mesenchymal stem cells through the regulation of histone acetylation. *Int J Mol Med*. 2014;33:1075-82.

79.   Li B, Li M, Li X, Li H, Lai Y, Huang S, He X, Si X, Zheng H, Liao W, Liao Y and Bin J. Sirt1-inducible deacetylation of p21 promotes cardiomyocyte proliferation. *Aging*. 2019;11:12546-12567.

80.   Li B, Hu Y, Li X, Jin G, Chen X, Chen G, Chen Y, Huang S, Liao W, Liao Y, Teng Z and Bin J. Sirt1 Antisense Long Noncoding RNA Promotes Cardiomyocyte Proliferation by Enhancing the Stability of Sirt1. *J Am Heart Assoc*. 2018;7:e009700.

81.   McBurney MW, Yang X, Jardine K, Hixon M, Boekelheide K, Webb JR, Lansdorp PM and Lemieux M. The mammalian SIR2alpha protein has a role in embryogenesis and gametogenesis. *Mol Cell Biol*. 2003;23:38-54.

82.   Main A, Fuller W and Baillie GS. Post-translational regulation of cardiac myosin binding protein-C: A graphical review. *Cellular Signalling*. 2020;76:109788.

83.   Samant SA, Pillai VB, Sundaresan NR, Shroff SG and Gupta MP. Histone Deacetylase 3 (HDAC3)-dependent Reversible Lysine Acetylation of Cardiac Myosin

Heavy Chain Isoforms Modulates Their Enzymatic and Motor Activity*. *Journal of Biological Chemistry*. 2015;290:15559-15569.

84.   Lin YH, Schmidt W, Fritz KS, Jeong MY, Cammarato A, Foster DB, Biesiadecki BJ, McKinsey TA and Woulfe KC. Site-specific acetyl-mimetic modification of cardiac troponin I modulates myofilament relaxation and calcium sensitivity. *J Mol Cell Cardiol*. 2020;139:135-147.

85.   Baeza J, Smallegan MJ and Denu JM. Mechanisms and Dynamics of Protein Acetylation in Mitochondria. *Trends in Biochemical Sciences*. 2016;41:231-244.

86.   Hebert Alexander S, Dittenhafer-Reed Kristin E, Yu W, Bailey Derek J, Selen Ebru S, Boersma Melissa D, Carson Joshua J, Tonelli M, Balloon Allison J, Higbee Alan J, Westphall Michael S, Pagliarini David J, Prolla Tomas A, Assadi-Porter F, Roy S, Denu John M and Coon Joshua J. Calorie Restriction and SIRT3 Trigger Global Reprogramming of the Mitochondrial Protein Acetylome. *Molecular Cell*. 2013;49:186-199.

87.   Scott I, Webster Bradley R, Li Jian H and Sack Michael N. Identification of a molecular component of the mitochondrial acetyltransferase programme: a novel role for GCN5L1. *Biochemical Journal*. 2012;443:655-661.

88.   Thapa D, Zhang M, Manning JR, Guimarães DA, Stoner MW, O'Doherty RM, Shiva S and Scott I. Acetylation of mitochondrial proteins by GCN5L1 promotes enhanced fatty acid oxidation in the heart. *Am J Physiol Heart Circ Physiol*. 2017;313:H265-h274.

89.   Fan J, Shan C, Kang H-B, Elf S, Xie J, Tucker M, Gu T-L, Aguiar M, Lonning S, Chen H, Mohammadi M, Britton L-Mae P, Garcia Benjamin A, Alečković M, Kang Y, Kaluz S, Devi N, Van Meir Erwin G, Hitosugi T, Seo Jae H, Lonial S, Gaddh M, Arellano M, Khoury Hanna J, Khuri Fadlo R, Boggon Titus J, Kang S and Chen J. Tyr Phosphorylation of PDP1 Toggles Recruitment between ACAT1 and SIRT3 to Regulate the Pyruvate Dehydrogenase Complex. *Molecular Cell*. 2014;53:534-548.

90.   Zhao S, Xu W, Jiang W, Yu W, Lin Y, Zhang T, Yao J, Zhou L, Zeng Y, Li H, Li Y, Shi J, An W, Hancock SM, He F, Qin L, Chin J, Yang P, Chen X, Lei Q, Xiong Y and Guan KL. Regulation of cellular metabolism by protein lysine acetylation. *Science*. 2010;327:1000-4.

91.   Abo Alrob O and Lopaschuk Gary D. Role of CoA and acetyl-CoA in regulating cardiac fatty acid and glucose oxidation. *Biochemical Society Transactions*. 2014;42:1043-1051.

92.   Fan W and Evans R. PPARs and ERRs: molecular mediators of mitochondrial metabolism. *Current Opinion in Cell Biology*. 2015;33:49-54.

93.   Cantó C, Jiang LQ, Deshmukh AS, Mataki C, Coste A, Lagouge M, Zierath JR and Auwerx J. Interdependence of AMPK and SIRT1 for metabolic adaptation to fasting and exercise in skeletal muscle. *Cell Metab*. 2010;11:213-9.

94.   Cantó C, Jiang LQ, Deshmukh AS, Mataki C, Coste A, Lagouge M, Zierath JR and Auwerx J. Interdependence of AMPK and SIRT1 for metabolic adaptation to fasting and exercise in skeletal muscle. *Cell metabolism*. 2010;11:213-219.

95.   Yu W, Gao B, Li N, Wang J, Qiu C, Zhang G, Liu M, Zhang R, Li C, Ji G and Zhang Y. Sirt3 deficiency exacerbates diabetic cardiac dysfunction: Role of Foxo3A-Parkin-mediated mitophagy. *Biochimica et Biophysica Acta (BBA) - Molecular Basis of Disease*. 2017;1863:1973-1983.

96.   Ventura-Clapier R, Garnier A and Veksler V. Energy metabolism in heart failure. *The Journal of physiology*. 2004;555:1-13.

97.   Doenst T, Nguyen TD and Abel ED. Cardiac metabolism in heart failure: implications beyond ATP production. *Circ Res*. 2013;113:709-24.

98.   Dudkina NV, Kouřil R, Peters K, Braun H-P and Boekema EJ. Structure and function of mitochondrial supercomplexes. *Biochimica et Biophysica Acta (BBA) - Bioenergetics*. 2010;1797:664-670.

99.   Rosca MG, Vazquez EJ, Kerner J, Parland W, Chandler MP, Stanley W, Sabbah HN and Hoppel CL. Cardiac mitochondria in heart failure: decrease in respirasomes and oxidative phosphorylation. *Cardiovasc Res*. 2008;80:30-9.

100.   Parodi-Rullán RM, Chapa-Dubocq X, Rullán PJ, Jang S and Javadov S. High Sensitivity of SIRT3 Deficient Hearts to Ischemia-Reperfusion Is Associated with Mitochondrial Abnormalities. *Front Pharmacol*. 2017;8:275.

101.   Horton JL, Martin OJ, Lai L, Riley NM, Richards AL, Vega RB, Leone TC, Pagliarini DJ, Muoio DM, Bedi KC, Jr., Margulies KB, Coon JJ and Kelly DP. Mitochondrial protein hyperacetylation in the failing heart. *JCI Insight*. 2016;2.

102.   Qin J, Guo N, Tong J and Wang Z. Function of histone methylation and acetylation modifiers in cardiac hypertrophy. *J Mol Cell Cardiol*. 2021;159:120-129.

103.   Dadson K, Hauck L and Billia F. Molecular mechanisms in cardiomyopathy. *Clinical Science*. 2017;131:1375-1392.

104.   Yanazume T, Hasegawa K, Morimoto T, Kawamura T, Wada H, Matsumori A, Kawase Y, Hirai M and Kita T. Cardiac p300 Is Involved in Myocyte Growth with Decompensated Heart Failure. *Molecular and Cellular Biology*. 2003;23:3593-3606.

105.   Yanazume T, Morimoto T, Wada H, Kawamura T and Hasegawa K. Biological role of p300 in cardiac myocytes. *Molecular and Cellular Biochemistry*. 2003;248:115-119.

106.   Wei JQ, Shehadeh LA, Mitrani JM, Pessanha M, Slepak TI, Webster KA and Bishopric NH. Quantitative control of adaptive cardiac hypertrophy by acetyltransferase p300. *Circulation*. 2008;118:934-46.

107.   Koentges C, Pfeil K, Schnick T, Wiese S, Dahlbock R, Cimolai MC, Meyer-Steenbuck M, Cenkerova K, Hoffmann MM, Jaeger C, Odening KE, Kammerer B, Hein L, Bode C and Bugger H. SIRT3 deficiency impairs mitochondrial and contractile function in the heart. *Basic Res Cardiol*. 2015;110:36.

108.   Tang X, Chen XF, Wang NY, Wang XM, Liang ST, Zheng W, Lu YB, Zhao X, Hao DL, Zhang ZQ, Zou MH, Liu DP and Chen HZ. SIRT2 Acts as a Cardioprotective Deacetylase in Pathological Cardiac Hypertrophy. *Circulation*. 2017;136:2051-2067.

109.   Luo Y-X, Tang X, An X-Z, Xie X-M, Chen X-F, Zhao X, Hao D-L, Chen H-Z and Liu D-P. SIRT4 accelerates Ang II-induced pathological cardiac hypertrophy by inhibiting manganese superoxide dismutase activity. *European Heart Journal*. 2017;38:1389-1398.

110.   Papait R, Serio S and Condorelli G. Role of the Epigenome in Heart Failure. *Physiol Rev*. 2020;100:1753-1777.

111.   Nural-Guvener HF, Zakharova L, Nimlos J, Popovic S, Mastroeni D and Gaballa MA. HDAC class I inhibitor, Mocetinostat, reverses cardiac fibrosis in heart failure and diminishes CD90+ cardiac myofibroblast activation. *Fibrogenesis Tissue Repair*. 2014;7:10.

112.   Williams SM, Golden-Mason L, Ferguson BS, Schuetze KB, Cavasin MA, Demos-Davies K, Yeager ME, Stenmark KR and McKinsey TA. Class I HDACs regulate angiotensin II-dependent cardiac fibrosis via fibroblasts and circulating fibrocytes. *J Mol Cell Cardiol*. 2014;67:112-25.

113.   Guo W, Shan B, Klingsberg RC, Qin X and Lasky JA. Abrogation of TGF-β1-induced fibroblast-myofibroblast differentiation by histone deacetylase inhibition. *American Journal of Physiology-Lung Cellular and Molecular Physiology*. 2009;297:L864-L870.

114.   Wei T, Huang G, Gao J, Huang C, Sun M, Wu J, Bu J and Shen W. Sirtuin 3 Deficiency Accelerates Hypertensive Cardiac Remodeling by Impairing Angiogenesis. *Journal of the American Heart Association*. 6:e006114.

115. Tang X, Chen X-F, Wang N-Y, Wang X-M, Liang S-T, Zheng W, Lu Y-B, Zhao X, Hao D-L, Zhang Z-Q, Zou M-H, Liu D-P and Chen H-Z. SIRT2 Acts as a Cardioprotective Deacetylase in Pathological Cardiac Hypertrophy. *Circulation*. 2017;136:2051-2067.

116. Benjamin EJ, Blaha MJ, Chiuve SE, Cushman M, Das SR, Deo R, de Ferranti SD, Floyd J, Fornage M, Gillespie C, Isasi CR, Jiménez MC, Jordan LC, Judd SE, Lackland D, Lichtman JH, Lisabeth L, Liu S, Longenecker CT, Mackey RH, Matsushita K, Mozaffarian D, Mussolino ME, Nasir K, Neumar RW, Palaniappan L, Pandey DK, Thiagarajan RR, Reeves MJ, Ritchey M, Rodriguez CJ, Roth GA, Rosamond WD, Sasson C, Towfighi A, Tsao CW, Turner MB, Virani SS, Voeks JH, Willey JZ, Wilkins JT, Wu JH, Alger HM, Wong SS and Muntner P. Heart Disease and Stroke Statistics-2017 Update: A Report From the American Heart Association. *Circulation*. 2017;135:e146-e603.

117. Kalogeris T, Baines CP, Krenz M and Korthuis RJ. Ischemia/Reperfusion. *Compr Physiol*. 2016;7:113-170.

118. Manning JR, Thapa D, Zhang M, Stoner MW, Traba J, McTiernan CF, Corey C, Shiva S, Sack MN and Scott I. Cardiac-specific deletion of GCN5L1 restricts recovery from ischemia-reperfusion injury. *J Mol Cell Cardiol*. 2019;129:69-78.

119. Zhao TC, Du J, Zhuang S, Liu P and Zhang LX. HDAC inhibition elicits myocardial protective effect through modulation of MKK3/Akt-1. *PLoS One*. 2013;8:e65474-e65474.

120. Porter GA, Urciuoli WR, Brookes PS and Nadtochiy SM. SIRT3 deficiency exacerbates ischemia-reperfusion injury: implication for aged hearts. *Am J Physiol Heart Circ Physiol*. 2014;306:H1602-9.

121. Lee HA, Lee DY, Cho HM, Kim SY, Iwasaki Y and Kim IK. Histone deacetylase inhibition attenuates transcriptional activity of mineralocorticoid receptor through its acetylation and prevents development of hypertension. *Circ Res*. 2013;112:1004-12.

122. Iyer A, Fenning A, Lim J, Le GT, Reid RC, Halili MA, Fairlie DP and Brown L. Antifibrotic activity of an inhibitor of histone deacetylases in DOCA-salt hypertensive rats. *British Journal of Pharmacology*. 2010;159:1408-1417.

123. Dikalova AE, Itani HA, Nazarewicz RR, McMaster WG, Flynn CR, Uzhachenko R, Fessel JP, Gamboa JL, Harrison DG and Dikalov SI. Sirt3 Impairment and SOD2 Hyperacetylation in Vascular Oxidative Stress and Hypertension. *Circ Res*. 2017;121:564-574.

124. Sayour AA, Oláh A, Ruppert M, Barta BA, Horváth EM, Benke K, Pólos M, Hartyánszky I, Merkely B and Radovits T. Characterization of left ventricular myocardial sodium-glucose cotransporter 1 expression in patients with end-stage heart failure. *Cardiovascular Diabetology*. 2020;19:159.

125. Garcia M, Leonardi R, Zhang YM, Rehg JE and Jackowski S. Germline deletion of pantothenate kinases 1 and 2 reveals the key roles for CoA in postnatal metabolism. *PLoS One*. 2012;7:e40871.

126. Leonardi R, Rehg JE, Rock CO and Jackowski S. Pantothenate Kinase 1 Is Required to Support the Metabolic Transition from the Fed to the Fasted State. *PLOS ONE*. 2010;5:e11107.

127. Dassanayaka S, Zheng Y, Gibb AA, Cummins TD, McNally LA, Brittian KR, Jagatheesan G, Audam TN, Long BW, Brainard RE, Jones SP and Hill BG. Cardiac-specific overexpression of aldehyde dehydrogenase 2 exacerbates cardiac remodeling in response to pressure overload. *Redox Biol*. 2018;17:440-449.

128. Facundo HT, Brainard RE, Watson LJ, Ngoh GA, Hamid T, Prabhu SD and Jones SP. O-GlcNAc signaling is essential for NFAT-mediated transcriptional reprogramming during cardiomyocyte hypertrophy. *Am J Physiol Heart Circ Physiol*. 2012;302:H2122-H2130.

129. Baba SP, Zhang D, Singh M, Dassanayaka S, Xie Z, Jagatheesan G, Zhao J, Schmidtke VK, Brittian KR, Merchant ML, Conklin DJ, Jones SP and Bhatnagar A.

Deficiency of aldose reductase exacerbates early pressure overload-induced cardiac dysfunction and autophagy in mice. *J Mol Cell Cardiol*. 2018;118:183-192.

130.   Dassanayaka S, Brainard RE, Watson LJ, Long BW, Brittian KR, DeMartino AM, Aird AL, Gumpert AM, Audam TN, Kilfoil PJ, Muthusamy S, Hamid T, Prabhu SD and Jones SP. Cardiomyocyte Ogt limits ventricular dysfunction in mice following pressure overload without affecting hypertrophy. *Basic Res Cardiol*. 2017;112:23-23.

131.   Brainard RE, Watson LJ, Demartino AM, Brittian KR, Readnower RD, Boakye AA, Zhang D, Hoetker JD, Bhatnagar A, Baba SP and Jones SP. High fat feeding in mice is insufficient to induce cardiac dysfunction and does not exacerbate heart failure. *PLoS One*. 2013;8:e83174.

132.   Condorelli G, Roncarati R, Ross J, Jr., Pisani A, Stassi G, Todaro M, Trocha S, Drusco A, Gu Y, Russo MA, Frati G, Jones SP, Lefer DJ, Napoli C and Croce CM. Heart-targeted overexpression of caspase3 in mice increases infarct size and depresses cardiac function. *Proc Natl Acad Sci U S A*. 2001;98:9977-82.

133.   Jones SP, Greer JJ, van Haperen R, Duncker DJ, de Crom R and Lefer DJ. Endothelial nitric oxide synthase overexpression attenuates congestive heart failure in mice. *Proc Natl Acad Sci U S A*. 2003;100:4891-6.

134.   Greer JJ, Kakkar AK, Elrod JW, Watson LJ, Jones SP and Lefer DJ. Low-dose simvastatin improves survival and ventricular function via eNOS in congestive heart failure. *Am J Physiol Heart Circ Physiol*. 2006;291:H2743-51.

135.   Wysoczynski M, Dassanayaka S, Zafir A, Ghafghazi S, Long BW, Noble C, DeMartino AM, Brittian KR, Bolli R and Jones SP. A New Method to Stabilize C-Kit Expression in Reparative Cardiac Mesenchymal Cells. *Front Cell Dev Biol*. 2016;4:78.

136.   Watson LJ, Facundo HT, Ngoh GA, Ameen M, Brainard RE, Lemma KM, Long BW, Prabhu SD, Xuan YT and Jones SP. O-linked beta-N-acetylglucosamine transferase is indispensable in the failing heart. *Proc Natl Acad Sci U S A*. 2010;107:17797-802.

137.   Muthusamy S, DeMartino AM, Watson LJ, Brittian KR, Zafir A, Dassanayaka S, Hong KU and Jones SP. MicroRNA-539 is up-regulated in failing heart, and suppresses O-GlcNAcase expression. *J Biol Chem*. 2014;289:29665-76.

138.   Dassanayaka S, Brainard RE, Watson LJ, Long BW, Brittian KR, DeMartino AM, Aird AL, Gumpert AM, Audam TN, Kilfoil PJ, Muthusamy S, Hamid T, Prabhu SD and Jones SP. Cardiomyocyte Ogt limits ventricular dysfunction in mice following pressure overload without affecting hypertrophy. *Basic Res Cardiol*. 2017;112:23.

139.   Chen S, Zhou Y, Chen Y and Gu J. fastp: an ultra-fast all-in-one FASTQ preprocessor. *Bioinformatics*. 2018;34:i884-i890.

140.   Dobin A, Davis CA, Schlesinger F, Drenkow J, Zaleski C, Jha S, Batut P, Chaisson M and Gingeras TR. STAR: ultrafast universal RNA-seq aligner. *Bioinformatics*. 2013;29:15-21.

141.   Grillon JM, Johnson KR, Kotlo K and Danziger RS. Non-histone lysine acetylated proteins in heart failure. *Biochim Biophys Acta*. 2012;1822:607-14.

142.   Andrienko TN, Pasdois P, Pereira GC, Ovens MJ and Halestrap AP. The role of succinate and ROS in reperfusion injury – A critical appraisal. *J Mol Cell Cardiol*. 2017;110:1-14.

143.   Lee CF, Chavez JD, Garcia-Menendez L, Choi Y, Roe ND, Chiao YA, Edgar JS, Goo YA, Goodlett DR, Bruce JE and Tian R. Normalization of NAD+ Redox Balance as a Therapy for Heart Failure. *Circulation*. 2016;134:883-94.

144.   Robinson MD, McCarthy DJ and Smyth GK. edgeR: a Bioconductor package for differential expression analysis of digital gene expression data. *Bioinformatics*. 2010;26:139-40.

145.   Howe EA, Sinha R, Schlauch D and Quackenbush J. RNA-Seq analysis in MeV. *Bioinformatics*. 2011;27:3209-10.

146.   Sharma LK, Subramanian C, Yun M-K, Frank MW, White SW, Rock CO, Lee RE and Jackowski S. A therapeutic approach to pantothenate kinase associated neurodegeneration. *Nature Communications*. 2018;9:4399.

147.   Sansbury BE, DeMartino AM, Xie Z, Brooks AC, Brainard RE, Watson LJ, DeFilippis AP, Cummins TD, Harbeson MA, Brittian KR, Prabhu SD, Bhatnagar A, Jones SP and Hill BG. Metabolomic analysis of pressure-overloaded and infarcted mouse hearts. *Circulation Heart failure*. 2014;7:634-642.

148.   Sansbury BE, Cummins TD, Tang Y, Hellmann J, Holden CR, Harbeson MA, Chen Y, Patel RP, Spite M, Bhatnagar A and Hill BG. Overexpression of endothelial nitric oxide synthase prevents diet-induced obesity and regulates adipocyte phenotype. *Circ Res*. 2012;111:1176-89.

149.   Watson LJ, Facundo HT, Ngoh GA, Ameen M, Brainard RE, Lemma KM, Long BW, Prabhu SD, Xuan Y-T and Jones SP. O-linked β-N-acetylglucosamine transferase is indispensable in the failing heart. *Proc Natl Acad Sci U S A*. 2010;107:17797-17802.

150.   Rock CO, Karim MA, Zhang Y-M and Jackowski S. The murine pantothenate kinase (Pank1) gene encodes two differentially regulated pantothenate kinase isozymes. *Gene*. 2002;291:35-43.

151.   Fulghum KL, Rood BR, Shang VO, McNally LA, Riggs DW, Zheng Y-T and Hill BG. Mitochondria-associated lactate dehydrogenase is not a biologically significant contributor to bioenergetic function in murine striated muscle. *Redox Biol*. 2019;24:101177-101177.

152.   Gibb AA, Epstein PN, Uchida S, Zheng Y, McNally LA, Obal D, Katragadda K, Trainor P, Conklin DJ, Brittian KR, Tseng MT, Wang J, Jones SP, Bhatnagar A and Hill BG. Exercise-Induced Changes in Glucose Metabolism Promote Physiological Cardiac Growth. *Circulation*. 2017;136:2144-2157.

153.   Hindi SM, Sato S, Xiong G, Bohnert KR, Gibb AA, Gallot YS, McMillan JD, Hill BG, Uchida S and Kumar A. TAK1 regulates skeletal muscle mass and mitochondrial function. *JCI Insight*. 2018;3:e98441.

154.   McNally LA, Altamimi TR, Fulghum K and Hill BG. Considerations for using isolated cell systems to understand cardiac metabolism and biology. *Journal of Molecular and Cellular Cardiology*. 2021;153:26-41.

155.   Schägger H and von Jagow G. Tricine-sodium dodecyl sulfate-polyacrylamide gel electrophoresis for the separation of proteins in the range from 1 to 100 kDa. *Anal Biochem*. 1987;166:368-79.

156.   Tokita Y, Tang XL, Li Q, Wysoczynski M, Hong KU, Nakamura S, Wu WJ, Xie W, Li D, Hunt G, Ou Q, Stowers H and Bolli R. Repeated Administrations of Cardiac Progenitor Cells Are Markedly More Effective Than a Single Administration: A New Paradigm in Cell Therapy. *Circ Res*. 2016;119:635-51.

157.   Tang XL, Rokosh G, Sanganalmath SK, Yuan F, Sato H, Mu J, Dai S, Li C, Chen N, Peng Y, Dawn B, Hunt G, Leri A, Kajstura J, Tiwari S, Shirk G, Anversa P and Bolli R. Intracoronary administration of cardiac progenitor cells alleviates left ventricular dysfunction in rats with a 30-day-old infarction. *Circulation*. 2010;121:293-305.

158.   Wysoczynski M, Guo Y, Moore JBt, Muthusamy S, Li Q, Nasr M, Li H, Nong Y, Wu W, Tomlin AA, Zhu X, Hunt G, Gumpert AM, Book MJ, Khan A, Tang XL and Bolli R. Myocardial Reparative Properties of Cardiac Mesenchymal Cells Isolated on the Basis of Adherence. *J Am Coll Cardiol*. 2017;69:1824-1838.

159.   Marín-García J, Goldenthal MJ and Moe GW. Abnormal cardiac and skeletal muscle mitochondrial function in pacing-induced cardiac failure. *Cardiovascular Research*. 2001;52:103-110.

160.   Vadvalkar SS, Matsuzaki S, Eyster CA, Giorgione JR, Bockus LB, Kinter CS, Kinter M and Humphries KM. Decreased Mitochondrial Pyruvate Transport Activity in the

Diabetic Heart: ROLE OF MITOCHONDRIAL PYRUVATE CARRIER 2 (MPC2) ACETYLATION. *J Biol Chem*. 2017;292:4423-4433.

161. Wagner GR and Payne RM. Widespread and enzyme-independent Nε-acetylation and Nε-succinylation of proteins in the chemical conditions of the mitochondrial matrix. *J Biol Chem*. 2013;288:29036-45.

162. Baeza J, Smallegan MJ and Denu JM. Site-specific reactivity of nonenzymatic lysine acetylation. *ACS Chem Biol*. 2015;10:122-8.

163. Lantier L, Williams AS, Hughey CC, Bracy DP, James FD, Ansari MA, Gius D and Wasserman DH. SIRT2 knockout exacerbates insulin resistance in high fat-fed mice. *PLOS ONE*. 2018;13:e0208634.

164. Hirschey Matthew D, Shimazu T, Jing E, Grueter Carrie A, Collins Amy M, Aouizerat B, Stančáková A, Goetzman E, Lam Maggie M, Schwer B, Stevens Robert D, Muehlbauer Michael J, Kakar S, Bass Nathan M, Kuusisto J, Laakso M, Alt Frederick W, Newgard Christopher B, Farese Robert V, Kahn CR and Verdin E. SIRT3 Deficiency and Mitochondrial Protein Hyperacetylation Accelerate the Development of the Metabolic Syndrome. *Molecular Cell*. 2011;44:177-190.

165. Jing E, Emanuelli B, Hirschey MD, Boucher J, Lee KY, Lombard D, Verdin EM and Kahn CR. Sirtuin-3 (Sirt3) regulates skeletal muscle metabolism and insulin signaling via altered mitochondrial oxidation and reactive oxygen species production. *Proceedings of the National Academy of Sciences*. 2011;108:14608-14613.

166. Davies MN, Kjalarsdottir L, Thompson JW, Dubois LG, Stevens RD, Ilkayeva OR, Brosnan MJ, Rolph TP, Grimsrud PA and Muoio DM. The Acetyl Group Buffering Action of Carnitine Acetyltransferase Offsets Macronutrient-Induced Lysine Acetylation of Mitochondrial Proteins. *Cell Rep*. 2016;14:243-54.

167. Davidson MT, Grimsrud PA, Lai L, Draper JA, Fisher-Wellman KH, Narowski TM, Abraham DM, Koves TR, Kelly DP and Muoio DM. Extreme Acetylation of the Cardiac Mitochondrial Proteome Does Not Promote Heart Failure. *Circ Res*. 2020;127:1094-1108.

168. Murashige D, Jang C, Neinast M, Edwards JJ, Cowan A, Hyman MC, Rabinowitz JD, Frankel DS and Arany Z. Comprehensive quantification of fuel use by the failing and nonfailing human heart. *Science*. 2020;370:364-368.

169. Carley AN, Maurya SK, Fasano M, Wang Y, Selzman CH, Drakos SG and Lewandowski ED. Short-Chain Fatty Acids Outpace Ketone Oxidation in the Failing Heart. *Circulation*. 2021;143:1797-1808.

170. Goldenberg JR, Carley AN, Ji R, Zhang X, Fasano M, Schulze PC and Lewandowski ED. Preservation of Acyl Coenzyme A Attenuates Pathological and Metabolic Cardiac Remodeling Through Selective Lipid Trafficking. *Circulation*. 2019;139:2765-2777.

171. Biernacka A, Dobaczewski M and Frangogiannis NG. TGF-β signaling in fibrosis. *Growth Factors*. 2011;29:196-202.

172. Hanna A and Frangogiannis NG. The Role of the TGF-β Superfamily in Myocardial Infarction. *Frontiers in Cardiovascular Medicine*. 2019;6.

173. Lok SI, Winkens B, Goldschmeding R, van Geffen AJ, Nous FM, van Kuik J, van der Weide P, Klöpping C, Kirkels JH, Lahpor JR, Doevendans PA, de Jonge N and de Weger RA. Circulating growth differentiation factor-15 correlates with myocardial fibrosis in patients with non-ischaemic dilated cardiomyopathy and decreases rapidly after left ventricular assist device support. *Eur J Heart Fail*. 2012;14:1249-56.

174. Bouzeghrane F, Reinhardt DP, Reudelhuber TL and Thibault G. Enhanced expression of fibrillin-1, a constituent of the myocardial extracellular matrix in fibrosis. *Am J Physiol Heart Circ Physiol*. 2005;289:H982-91.

175.   Imanaka-Yoshida K, Tawara I and Yoshida T. Tenascin-C in cardiac disease: a sophisticated controller of inflammation, repair, and fibrosis. *Am J Physiol Cell Physiol*. 2020;319:C781-c796.

176.   Wallner K, Li C, Shah PK, Fishbein MC, Forrester JS, Kaul S and Sharifi BG. Tenascin-C is expressed in macrophage-rich human coronary atherosclerotic plaque. *Circulation*. 1999;99:1284-9.

177.   Heymans S, Schroen B, Vermeersch P, Milting H, Gao F, Kassner A, Gillijns H, Herijgers P, Flameng W, Carmeliet P, Van de Werf F, Pinto YM and Janssens S. Increased cardiac expression of tissue inhibitor of metalloproteinase-1 and tissue inhibitor of metalloproteinase-2 is related to cardiac fibrosis and dysfunction in the chronic pressure-overloaded human heart. *Circulation*. 2005;112:1136-44.

178.   McKenzie M, Lazarou M, Thorburn DR and Ryan MT. Mitochondrial Respiratory Chain Supercomplexes Are Destabilized in Barth Syndrome Patients. *Journal of Molecular Biology*. 2006;361:462-469.

179.   Jain-Ghai S, Cameron JM, Al Maawali A, Blaser S, MacKay N, Robinson B and Raiman J. Complex II deficiency--a case report and review of the literature. *Am J Med Genet A*. 2013;161a:285-94.

CURRICULUM VITAE

Timothy N. Audam, MS.

Diabetes and Obesity Center
University of Louisville School of Medicine
580 S Preston Street
Delia Baxter II Building, Room 326
Louisville, KY, 40202
Mobile: 423-676-8382
Email: tnauda01@louisville.edu, timothyaudam@yahoo.com

EDUCATION

2012 **BS in Microbiology, University of Abuja,** Abuja, Nigeria (GPA: 3.73/4)

2016 MS in Biology, East Tennessee State University, Johnson City, TN (GPA: 3.83/4)

2018 **MS in Biochemistry and Molecular Genetics**, University of Louisville, Louisville, KY (GPA: 3.8/4)

2021 **PhD in Biochemistry and Molecular Genetics**, University of Louisville, Louisville, KY (Expected August 2021)

RESEARCH EXPERIENCE

2014-2016 **MS Candidate/Research Assistant.** Department of Biology, East Tennessee State University, Johnson City, TN

2016-2018 **MS Candidate/Research Assistant.** Department of Medicine, University of Louisville, Louisville, KY

2018-2021 **PhD Candidate/Research Assistant.** Diabetes and Obesity Center, University of Louisville, Louisville, KY

TEACHING EXPERIENCE

2014-2016 **Teaching Assistant.** Department of Biology, East Tennessee State University, Johnson City, TN

2016-2018 **Teaching Assistant.** Department of Biochemistry and Molecular Genetics, University of Louisville, Louisville, KY

CERTIFICATION

2019 KBRIN next-generation sequencing (NGS) workshop certification.

PROFESSIONAL MEMBERSHIP AND ACTIVITIES

Memberships
Sigma Xi, The Scientific Research Honor Society
American Heart Association (Basic Cardiovascular Sciences Council)
International Society for Heart Research
American Society for Biochemistry and Molecular Biology

HONORS AND AWARDS

2014	Graduate Assistantship Scholarship, East Tennessee State University
2016	Frank and Mary Loewus Student Travel Award (PSNA Conference)
2016	William Harvey Fraley and Nina M. Fraley Memorial Research Award (East Tennessee State University)
2016	Integrated Program for Biomedical Science Research Fellowship (IPIBS), University of Louisville
2018	Graduate Student Council Travel Award, University of Louisville
2018	Alfred and Iva Homberger Travel Award, Department of BMG, University of Louisville
2018	American Heart Association BCVS Abstract Travel Grant
2019	Certificate of Excellence (Celebration of Excellence in Graduate Diversity), School of Interdisciplinary and Graduate Studies, University of Louisville
2019	Cardiovascular Outreach Award (Basic Cardiovascular Sciences Council, American Heart Association)

RESEARCH GRANTS AND FUNDING

2016	Sigma Xi Grant in Aid of Research (GIAR). October 15, 2015, Grant cycle.
2018-2020	American Heart Association Predoctoral Fellowship AHA Award number: 19PRE34380003 Role: Principal Investigator Sponsor: Steven P Jones, PhD

ABSTRACTS

1. **Audam, T.N.** *et al*., "Characterization of SIP470, a Family 1 Lipid Transfer Protein and its Role in Plant Stress Signaling". Phytochemical Society for North America (PSNA) Conference, August 2015, University of Illinois, Urbana Champagne, Abstract #P3

2. **Audam, T.N.** *et al.* "Macrophage Polarization Modulates Expression of Hyaluronan Metabolizing Enzymes." Biochemistry & Molecular Genetics Research Retreat, August 2017 University of Louisville

3. **Audam T.N.** *et al.* "Hyaluronan Composition Guides Macrophage Function: Potential Role in Ventricular Remodeling. "American Hearts Association Annual Meeting, November 2018

4. **Audam T.N.** "Metabolic Regulation of cardiac extracellular matrix." Cardiovascular Symposium, University of Louisville, April 2019 (Oral presentation).

5. **Audam T.N.** *et al.* "The Extracellular Matrix Component, Hyaluronan, Provokes a Pro-Inflammatory Phenotype in Macrophages." Basic Cardiovascular Sciences Scientific Meeting, July 2019.

6. Audam T.N. *et al.* "Hyaluronan Interacts and Suppresses Macrophage Phagocytosis." Biochemistry & Molecular Genetics Research Retreat, August 2019. (Oral and Poster presentation).

7. **Audam T.N.** *et al.* "The Extracellular Matrix Component, Hyaluronan, Suppresses Macrophage Phagocytosis Independently of the Hyaluronan Receptor, CD44" Southeast regional (IDeA) conference, November 2019.

8. **Audam T.N.** *et al.* "Characterization of Cardiac Mesenchymal Cells from Non-failing and Failing Hearts. American Hearts Association Annual Meeting, November 2019.

9. **Audam T.N.** *et al.*" Coenzyme A (CoA) Depletion Exacerbates Cardiac Dysfunction and Fibrosis During Pressure Overload. International Society for Heart Research (ISHR), North American Section, October 2020 (Oral presentation).

PEER REVIEWED PUBLICATION

1. Dassanayaka S., Brainard R.E., Watson L.J, Long B.W., Brittian K.R., DeMartino A.M., Aird A.L., Gumpert A.M., **Audam, T.N**., Kilfoil, P.J., Muthusamy S., Hamid T., Prabhi S.D. and Jones S.P. (2017) Cardiomyocyte Ogt limits ventricular dysfunction in mice following pressure overload without affecting hypertrophy. *Basic Res Cardiol*.123 (3): 23.

2. Dassanayaka S., Zheng Y., Gibb A.A., Cummins T.D., McNally L.A, Brittian K.R, Jagaseethan G., **Audam T.N**., Long B.W., Brainard R.E., Jones S.P., and Hill B.G (2018) Cardiac-specific overexpression of aldehyde dehydrogenase 2 exacerbates cardiac remodeling in response to pressure overload. *Redox Biol.* 17:440-449.

3. Dassanayaka S, Brittian K.R., Jurkovic A., Higgins L.A., **Audam T.N**., Long B.W., Harrison L.T., Militello G., Riggs D.W., Chitre M.G., Uchida S., Muthusamy S., Gumpert A.M, and Jones S.P (2019). E2f1 Deletion Attenuates Infarct-Induced Ventricular Remodeling without Affecting O-GlcNAcylation. *Basic Res Cardiol*. 114 (4):28.

4. **Audam T.N**., Nong Y., Tomlin A., Jurkovic A., Li H., Zhu X., Long B.W., Zheng Y.W., Weirick T., Brittian K.R., Riggs D.W., Gumpert A., Uchida S., Guo Y., Wysoczynski M., and Jones S.P. (2020). Cardiac Mesenchymal

Cells Isolated from Failing Hearts Limit Ventricular Dilation when Administered Late after Infarction. *Am J Physiol Heart Circ Physiol*. 319 (1):H109-H122.

5. Dassanayaka S., Brittian K.R., Long B.W., Higgins L.A., Bradley J.A., **Audam T.N**., Jurkovic A., Hartyánszky I., Perge P., Merkely B., Radovits T., Hanover J.A., and Jones S.P. (2020). Cardiomyocyte Oga haploinsufficiency increases O-GlcNAcylation but hastens ventricular dysfunction following myocardial infarction. *PLoS One*. 15 (11):e0242250.

6. **Audam T.N.,** Howard M.C., Garrett L.F., Zheng Y., Bradley J.A., Brittian K.R., Frank M.W., Fulghum K.L., Polos M., Herczeg S., Merkely B., Radovits T., Uchida S., Hill B.G., Dassanayaka S., Jackowski S., and Jones S.P. Coenzyme A (CoA) Depletion Exacerbates Cardiac Dysfunction and Fibrosis During Pressure Overload. *Manuscript under review*.

7. Fulghum K.L., **Audam T.N**., Lorkiewicz P.K., Zheng Y., Merchant M.,Cummins T.D., Dean W.L., Cassel T.A., Higashi R.M., Fan T.W.M., and Hill B.G. *In vivo* deep network tracing reveals phosphofructokinase-mediated coordination of biosynthetic pathway activity in the myocardium. *Manuscript under review*